Title
Molecular Simulations of the Effect of Cholesterol on Membrane-Mediated Protein-Protein Interactions

Author
de Meyer, Frédérick Jean-Marie

Publication Date
2010

Peer reviewed|Thesis/dissertation

Molecular Simulations of the Effect of Cholesterol on Membrane-Mediated Protein-Protein Interactions.

by

Frédérick Jean-Marie de Meyer

A dissertation submitted in partial satisfaction of the
requirements for the degree of
Doctor of Philosophy

in

Chemical Engineering

in the

GRADUATE DIVISION
of the
UNIVERSITY OF CALIFORNIA, BERKELEY

Committee in charge:
Professor Berend Smit, Chair
Professor Alexis Bell
Professor Jhih-Wei Chu
Professor David Chandler

Fall 2010

Molecular Simulations of the Effect of Cholesterol on Membrane-Mediated Protein-Protein Interactions.

Abstract

Molecular Simulations of the Effect of Cholesterol on Membrane-Mediated Protein-Protein Interactions.

by

Frédérick Jean-Marie de Meyer

Doctor of Philosophy in Chemical Engineering

University of California, Berkeley

Professor Berend Smit, Chair

In this work we use molecular simulations to investigate how cholesterol affects membrane-mediated protein-protein interactions. We consider a typical hydrated biological model membrane containing saturated phospholipids (for example, dimyristoylphosphatidylcholine or DMPC), cholesterol, and trans-membrane proteins. We introduce a model in which the different molecules are coarse-grained, retaining their hydrophobic and hydrophilic properties together with their main structure and flexibility. The system is studied using a hybrid Monte-Carlo dissipative particle dynamics method.

First we study lipid-mediated protein-protein interactions in a pure hydrated saturated phospholipid bilayer. The potential of mean force between the proteins show that hydrophobic forces drive long-range lipid-mediated protein-protein interactions and that the nature of these interactions depends on the length of the protein hydrophobic segment, on the three-dimensional structure of the protein and on the properties of the lipid bilayer. The concept of hydrophilic shielding is introduced to gain insight into the nature of the computed potentials of mean force.

To study the effect of cholesterol on the properties of a membrane, we extend our model to cholesterol. Structural and mechanical properties of the hydrated bilayer containing a saturated lipid and cholesterol are studied at various temperatures and cholesterol concentrations. The properties studied are the area per lipid, condensation, bilayer thickness, tail order parameters, bending modulus, and area compressibility. The model quantitatively reproduces most of the experimental effects of cholesterol on these properties and reproduces the main features of the experimental temperature-composition phase diagram. Based on the changes in structural properties a temperature-composition structure diagram is proposed, which is compared with the experimental phase and structure diagrams. The lateral organization

of cholesterol in the bilayer is also discussed. In a second part, modifications of the cholesterol model are made to allow a better understanding of the cholesterol condensation effect. This condensation effect is further discussed in relation to the DMPC-cholesterol phase behavior.

Finally, the effect of cholesterol on lipid-mediated protein-protein interactions is investigated. This is done in accordance with the results concerning the effect of cholesterol on the phase behavior of lipid bilayers. The calculations of the potential of mean force between proteins and protein clusters show that the addition of cholesterol gradually reduces repulsive lipid-mediated interactions between certain proteins. At a given cholesterol concentration, the interactions even become attractive. Hence, cholesterol significantly promotes protein aggregation. The role of protein-induced dynamical cholesterol-enriched and cholesterol-depleted shells in these effects is discussed in detail.

Professor Berend Smit
Dissertation Committee Chair

To my lovely wife
Anne-Laure

Contents

List of Figures

Acknowledgments

None of this work would have been possible had it not been for the advice and support of my advisor, colleagues, friends and family.

I am very grateful for the advice, support and scientific intuition provided by my advisor, Prof. Berend Smit. I very much appreciate the opportunity he gave me to perform doctoral research in the very interesting area of biological membranes, the guidance he has provided me during this research and his genuine concern for the well-being of the members of our lab. I greatly value the freedom he has given me to work out my ideas.

I would also like to thank Prof. Alexis Bell, Prof. Jhih-Wei Chu and Prof. David Chandler for accepting of being a member of my dissertation committee.

I am very much indebted to Dr. Maddalena Venturoli and Dr. Jocelyn Rodgers, with whom I worked during my Ph.D. Maddalena and Jocelyn have spent hours at a time providing advice of all kinds and sharing their appreciation for rigorous analysis. Both have been dedicated supervisors and have pushed me to set high standards.

I also would like to thank the undergraduate and graduate students with whom I have had the pleasure to work during the summers: Thomas, Jonathan, Winnie, Sereina, Yannick, Jesper, and Sheeva.

I owe much to the all the people who helped me with the administration and with computer-related stuff: Emmanuelle, Emilie, Jordi, Kristin, Rocio, Drew, and John. Thank you for your invaluable help.

During this Ph.D., I have met the most wonderful friends. I am thinking about Serguei, Galina, Manolis, Marianna, Leopoldo, Veronique, Luca, Ayelet, Roberta, An and Joe. I hope to meet you again soon.

Finally I would like to thank my family, which is a constant source of inspiration. It is thanks to the supportive, patient and loving environment in which I grew up that all this has been possible.

Chapter 1

Introduction

1.1 Biological and Model Membranes

All known living organisms are made of cells, which are the smallest units of life classified as living. Eukaryotic cells contain membrane-bound compartments, or organelles, the most important of which is the nucleus. Not only are the different organelles surrounded by membranes, but the cell itself is also enclosed by a membrane called the plasma or the cell membrane. The biological membranes act as a selective permeable structure and thus regulate the in- and outflow of molecules in the cell or in the different compartments. The cell membrane anchors the cytoskeleton which provides the shape of the cell. It is also involved in cell adhesion, in endo- and exocytosis, in signaling, in maintaining a membrane potential, etc.

Biological membranes have a very diverse and complex composition. They mainly contain a wide variety of lipids and proteins. The lipids most often form a lipid bilayer. Different classes of membranes span a wide gamut of lipid variety, with each class containing many derivatives. Membrane proteins, involved in a variety of cellular processes such as cell adhesion, ion channel conductance, signal transduction, cytoskeleton contact and cell signaling, make up to 50 mass% of the cell membrane (1).

One of the main challenges of biological membrane research is to relate the functioning of the membrane to its structure and dynamics. For this purpose, and because biological membranes are too complex, simple model membranes are often studied, both experimentally and with molecular simulations, as a first approach (see Fig. 1.1). Those model membranes are typically lipid bilayers consisting of one to three types of lipids, eventually containing a real or synthesized transmembrane protein (see Fig. 1.1 a, d).

Two of the most common lipid classes are phospholipids and sterol lipids. A major derivative of phospholipids is phosphatidylcholine. A common example of

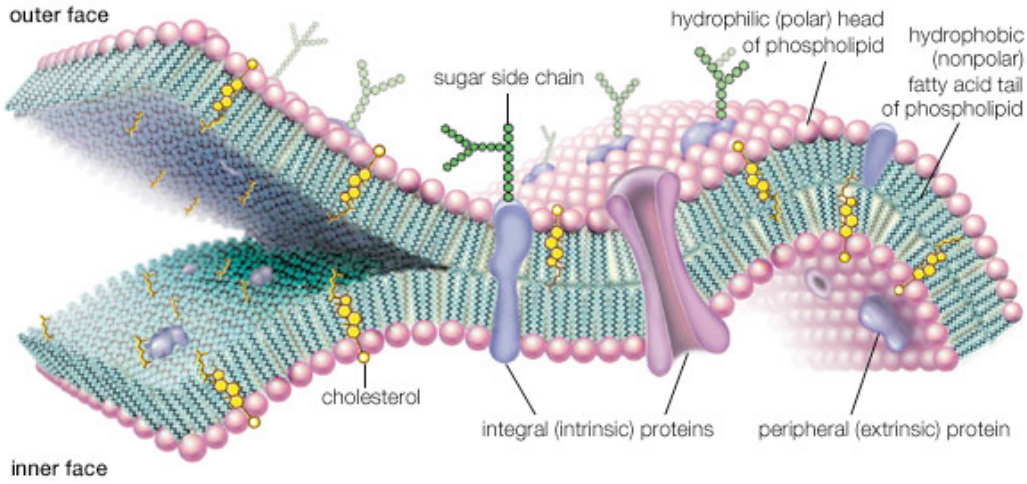

(a)

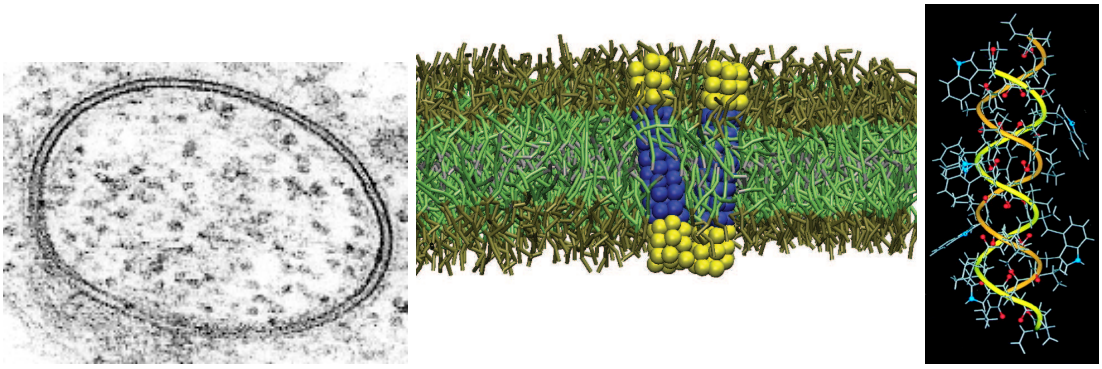

(b) (c) (d)

Figure 1.1: (a) cartoon of a model membrane (*Encyclopedia Britannica*). (b) transmission electron microscopy image of a lipid bilayer vesicle. The dark lines are the head groups of the lipids. (c) coarse-grained model of a lipid bilayer containing two peptides. The hydrophilic lipid and protein groups are depicted in brown and yellow, respectively, while the hydrophobic lipid and protein segments are colored green and blue, respectively. Water is not shown. (d) atomistic representation of gramicidin, a small membrane protein. The ribbon is added to accentuate the helical structure. The structure was derived from solid-state NMR (2).

phosphatidylcholine is shown in Fig. 1.2; dimyristoylphosphatidylcholine (DMPC). Cholesterol, the most common sterol, is also presented.

DMPC contains a choline, which is a quaternary saturated amine, to which a phosphatidic acid is attached. This phosphatidic acid consists of an electron-rich phosphate group, a glycerol backbone and two esters containing each a myristoyl

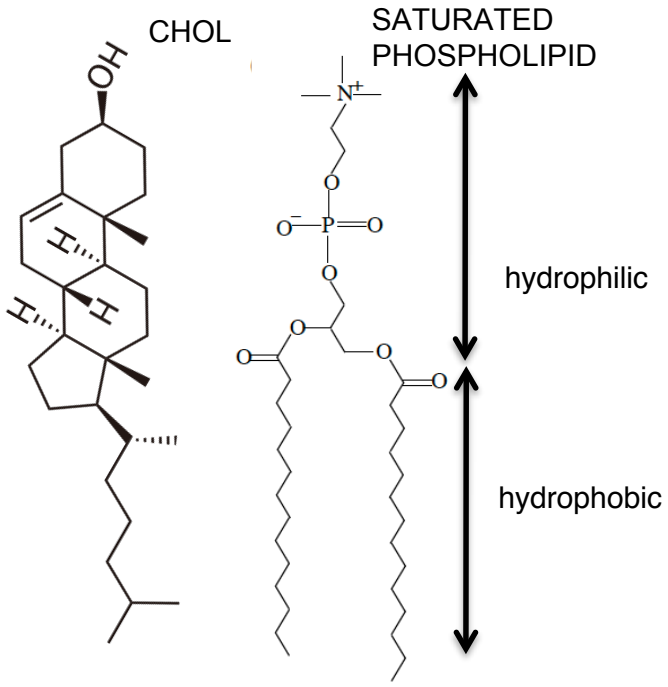

Figure 1.2: Structure of cholesterol and DMPC

tail of 14 carbon atoms. The phosphatidylcholine group is called the headgroup of the lipid, and is zwitterionic, with a positively charged amine and a negatively charged phosphatidic acid. The headgroup is hydrophilic, while the two tails are hydrophobic. Cholesterol consists of a relatively stiff hydrophobic tetrameric ring, to which a hydrophilic hydroxyl group is attached and a hydrophobic iso-octyl chain.

Lipids are thus amphiphilic molecules, as they contain a part which is hydrophobic and another part which is hydrophilic. Due to their amphiphilic nature, phospholipids spontaneously form a more complex structure when exposed to water in order to minimize the contact between water and the hydrophobic parts. The formation of, for example, lipid bilayers, is a manifestation of the hydrophobic effect. The hydrophobic effect is the experimentally-observed tendency for water and non-polar and uncharged (hydrophobic) molecules to segregate as a result of the low solubility of the latter in water (3–6). The discovery of the bilayer structure dates back to the 1920s (7). It was not before 1963 that it was experimentally observed that a dispersion of phospholipids and cholesterol in water spontaneously forms a bilayer to minimize the contact between the hydrophobic parts and water (8). Cholesterol does not form a bilayer on its own, but it precipitates. Today, this self-assembly property is relied upon to obtain model lipid bilayers for experimental use.

One of the challenges of modern biophysics is to obtain reliable experimental data of the bilayer properties. This is not straightforward because the bilayer is a only a

few nanometers thin (to see a membrane one needs a transmission electron microscope (see Fig. 1.1 b)) and extremely fragile. Chapter 2 delves into how estimates of several bilayer properties are obtained using different, often indirect, experimental methods.

Proteins (or polypeptides) are macromolecules as they are a sequence of amino acids (see Fig. 1.1 d). The amino acids in a polymer are joined together by the peptide bonds between the carboxyl and amino groups of adjacent amino acid residues. There exist 20 standard amino acids. The amino acids span a wide range of hydrophobicity and, as a result, some segments of the protein are hydrophobic while other segments are hydrophilic. The hydrophobic effect, among others, thus also plays a crucial role in the organization of a protein.

The insertion of a protein in a membrane is mostly done with the help of a translocon and, to a lesser extent, spontaneously. Both experiments and thermodynamic considerations lead to the conclusion that an increasing side chain hydrophobicity of a membrane protein drives the equilibrium towards a bilayer insertion (9). Once inserted, the proteins fold and associate in a certain topology. The driving force behind the first step of the protein folding, i.e. from an unfolded protein towards a more compact, sometimes helical, molten globule, consists in the hydrophobic effect. Although the translocon plays an important role in determining the protein topology, it is observed that the length of the protein hydrophobic segment could partly determine the topology and hence the function of the membrane protein (3, 9, 10).

1.2 Membrane-Mediated Protein-Protein Interactions

In Fig. 1.3, a simplified representation of a model membrane is shown. An important property we will frequently invoke in this work is hydrophobic mismatch (11), defined as the difference, d, between the length of the hydrophobic region of the protein, h_P, and the bilayer hydrophobic thickness, h_L. If $d = h_P - h_L = 0$ one says that the protein matches the bilayer. If $h_P > h_L$ the protein has a positive hydrophobic mismatch with respect to the bilayer, while $h_P < h_L$ implies a negative mismatch.

Most membrane proteins have one or more hydrophobic segments that span the bilayer in an α-helical conformation. The interactions between these transmembrane helices, which determine the structure of multispanning membrane proteins and might result in the assembly of membrane proteins into oligomeric structures, are a major field of study. Membrane proteins like G-protein-coupled receptors (GPCR) are a primary drug target and currently the drugs are developed assuming that these transmembrane proteins are monomeric (12, 13). A more fundamental insight into protein-protein interactions and into protein oligomerization will certainly contribute to a more optimal drug development. Factors identified to affect the protein-protein interactions include surface complementarity, the presence of hydrophilic residues in the transmembrane region and certain specific motifs (sequences of residues). These

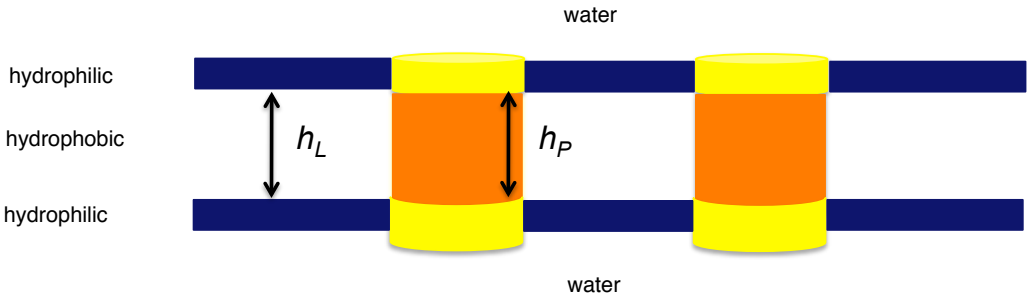

Figure 1.3: Simplified representation of a model membrane containing two transmembrane proteins. h_L and h_P are the hydrophobic thickness of the lipid bilayer and the length of the protein hydrophobic segment, respectively.

factors are related to direct interactions between the proteins. However, in an increasing number of experiments it appears that interactions between the helices and the surrounding lipids also play a role in the organization of transmembrane proteins. Hydrophobic mismatch, for example, is a property that is known to affect helix-helix association (11). This factor is related to indirect, or lipid-mediated, interactions between the proteins. It is likely that several factors act in concert resulting in the effective interaction between proteins. Contrary to molecular simulations, in experiments it is difficult to distinguish between the different factors and to quantify their respective contributions.

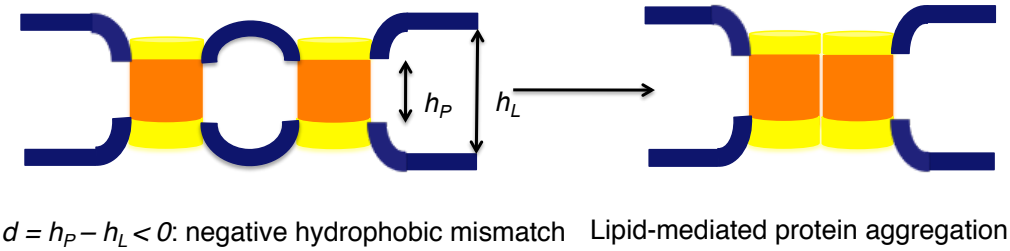

Figure 1.4: Lipid-mediated protein-protein aggregation induced by negative hydrophobic mismatch.

In Fig. 1.4 an example of lipid-mediated protein-protein aggregation induced by negative hydrophobic mismatch is shown. Let us consider two proteins in a membrane. The proteins have a hydrophobic segment that is smaller than the hydrophobic thickness of the bilayer. As a result of this negative hydrophobic mismatch, the membrane surrounding the proteins is perturbed. This perturbation might be lowered if the proteins form a dimer. If this is the case, the proteins spontaneously aggregate. This aggregation is not the result of a direct attractive interaction between the proteins, but is indirect or lipid-mediated.

The presence of lipid-mediated protein-protein interactions results from the lipid-protein interactions (14–18). Experimentally, it was observed that lipid-protein interactions affect the protein configuration (and thus protein activity) but also, and this should be stressed, the properties of the bilayer itself (11, 19–30). Therefore, one speaks of a collective behavior of all components: lipids, proteins, and water.

To experimentally study the indirect protein-protein interactions, transmembrane proteins have been designed without specific helix-helix recognition motifs, without hydrophilic residues in the transmembrane region and showing no surface complementarity. Another reason why membrane proteins have been synthesized is because, although an estimated 30 to 40 % of all proteins are membrane proteins, only 1% of the proteins of which the structure is known are membrane proteins. This is because X-ray crystallography, the usual method to study protein structure, is more difficult to apply to a protein embedded in the membrane. Today one often unravels the structure of a membrane protein with solid-state NMR.

In experimental studies, an increase in FRET (Fluorescence Resonance Energy Transfer) efficiency (see Chapter 2) for synthetic proteins with hydrophobic mismatch with respect to the FRET efficiency for synthetic proteins matching the same bilayer has been measured (31), suggesting an increase in attractive protein-protein interactions. The experiments do not tell us, however, where the increase in FRET efficiency comes from. For example, do the proteins form one cluster or do they form different small oligomers?

Instead of modifying the hydrophobic length of synthetic peptides, one can also insert real proteins in lipid bilayers with varying tail length in order to study the effect of hydrophobic mismatch on protein aggregation. From FRET experiments it has again been concluded that hydrophobic mismatch induces (lipid-mediated) protein-protein aggregation (32–35).

Other experimental techniques are applied to study lipid-mediated protein-protein interactions. For example, a two-dimensional model of a membrane has been fitted to the structure factor of oriented bilayers containing proteins, obtained with X-ray diffraction. In this model, the proteins are modeled as interacting hard disks confined in the plane. Only pairwise (two-body) interactions are considered. From the fitting the parameters of the protein-protein interaction potential are obtained. For example, between alamecithin pores, which have a positive mismatch in a DMPC bilayer (this was concluded from the tilt from ^{2}H NMR experiments), a lipid-mediated soft repulsive interaction of $2.5k_BT$ was found (36, 37). A similar conclusion was obtained for gramicidin pores (38, 39).

With AFM it has been shown that gramicidin A clusters in saturated lipid bilayers under negative mismatch conditions (40). Recently, high-speed AFM has been used to provide a measure of the membrane-mediated protein-protein interaction potential between two large proteins with positive mismatch (41). An unresolved challenge is the bad sampling of rare configurations, and thus a very poor estimate of protein aggregation barriers. The same issues occur in molecular simulations where they can,

however, be addressed with appropriate simulation techniques.

In a freeze fracture experiment bacteriorhodopsin was observed to remain dispersed except under very large mismatch conditions (42). For a review on the membrane proteins which appear to be regulated by changes in lipid bilayer thickness we refer to (43).

Understanding indirect protein-protein interactions has thus been studied in different experiments. The experimental observations can be explained with lipid-mediated interactions, but do not unambiguously show the existence of lipid-mediated interactions. In this work we will use molecular simulations to study lipid-mediated protein-protein interactions.

1.3 Effect of Cholesterol on Membrane-Mediated Protein Interactions

Cholesterol is an essential component of the membranes in eukaryotic cells. The cholesterol to lipid ratio typically ranges from 0.1 to 0.6 in the various membranes found in the cell. The exact role of cholesterol in a membrane is still under investigation. Cholesterol has been observed to condense the membrane and hence has been considered important to regulate the permeability of the membrane (44).

A wide range of independent experiments also indicate that cholesterol is intimately related to the oligomerization of transmembrane proteins in both model and real biological membranes (31, 33, 45–50). These protein clusters are often enriched in cholesterol and a prerequisite for other important biological processes to occur. For example, SNARE protein clusters are indispensable for exocytosis. In the absence of cholesterol the SNARE proteins are dispersed in much smaller clusters and no exocytosis takes place (46). On the other hand, similar cholesterol effects are intimately related to various diseases (51).

Several theoretical mechanisms have been proposed to explain the formation of cholesterol-enriched protein clusters in the presence of cholesterol. Experiments on model lipid bilayers have shown that cholesterol regulates the membrane properties. For example, the addition of cholesterol might increase the bilayer hydrophobic thickness and the bending modulus. A mechanism often mentioned in the literature invokes this property of cholesterol: a change in bilayer hydrophobic thickness might result in hydrophobic mismatch between proteins and bilayer and lead to membrane-mediated protein aggregation. This mechanism is shown in Fig. 1.5.

However, recent experiments show that cholesterol does not regulate the hydrophobic thickness of real biological membranes (19) while the effect of cholesterol on the clustering of transmembrane proteins has been observed in both model and real biological membranes. Questions related to the exact role of cholesterol thus remain unanswered.

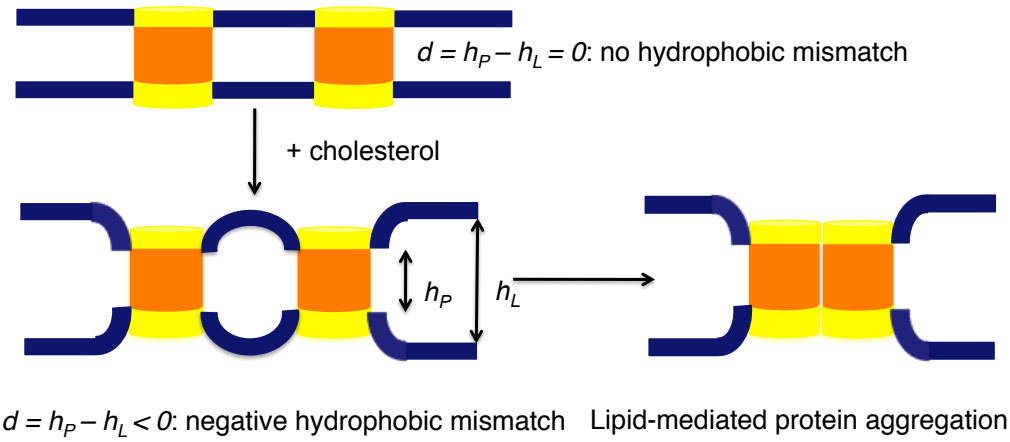

Figure 1.5: Simplified representation of the effect of cholesterol on a model membrane containing two proteins. h_L and h_P are the hydrophobic thickness of the lipid bilayer and the length of the protein hydrophobic segment, respectively. Cholesterol increases the bilayer hydrophobic thickness as a result of which the proteins have a negative hydrophobic mismatch. This leads to a lipid-mediated protein aggregation.

1.4 Overview of this Work

In this work we develop a coarse-grained model of a hydrated DMPC-cholesterol bilayer in which proteins are embedded and use this model to investigate wether the organization of membrane proteins in cholesterol-enriched clusters might be understood from indirect protein-lipid and protein-protein interactions, i.e., from the point of view of a collective behavior of all the membrane components. The basic question is the following: can the presence of a second component like cholesterol modify the nature of membrane-mediated protein interactions? For example, could it be that membrane-mediated protein interactions are repulsive in the absence of cholesterol, but become attractive in the presence of cholesterol? To answer this question we proceed in three steps. First we quantitatively study lipid-mediated protein interactions in a hydrated saturated phospholipid bilayer. Secondly, we study the effects of cholesterol on the properties of this bilayer. Finally, we study the effect of cholesterol on lipid-mediated protein interactions.

In Chapter 2, the coarse-grained model (see Fig. 1.1 c) and the hybrid dissipative particle dynamics-Monte Carlo simulation method are described in detail. Also covered are the model potentials and parameters, the relation between simulation and physical units and the details of the simulations. We close this chapter with an overview of the experimental and simulation techniques used to obtain the relevant bilayer properties.

In Chapter 3, the model and simulation method is used to calculate the potential of mean force between transmembrane proteins. These calculations show that hy-

drophobic forces might drive long-range lipid-mediated protein-protein interactions and that the nature of these interactions depends on the length of the protein hydrophobic segment, on the three-dimensional structure of the protein and on the properties of the lipid bilayer. The concept of hydrophilic shielding is introduced to gain insight into the nature of the computed potentials of mean force. Within this concept, the observed protein interactions are interpreted as resulting from the dynamic reorganization of the system to maintain an optimal hydrophilic shielding of the protein and lipid hydrophobic parts, within the constraint of the flexibility of the components.

This chapter has been published in: F. de Meyer, M. Venturoli, B. Smit, *Molecular simulations of lipid-mediated protein-protein interactions*, in Biophys. J., Vol. 95, Pages 1851-1865 (2008). Part of the work presented in this chapter has served as a basis for the discussion on the calculation of potential of mean forces between membrane proteins (see: F. de Meyer, B. Smit, *Comment on Cluster formation of transmembrane proteins due to hydrophobic mismatching*, in Phys. Rev. Lett. Vol. 102 (2009)) and on many-body interactions to describe protein-protein interactions in a 2-D model (see: M. Yiannourakou, L. Marsella, F. de Meyer, B. Smit, *Towards an understanding of membrane-mediated protein-protein interactions*, in Faraday Discuss. Vol. 144, Pages 359-367 (2010)).

In Chapter 4, the coarse-grained model of a hydrated lipid bilayer is extended to cholesterol. Structural and mechanical properties of the hydrated bilayer containing a saturated lipid and cholesterol are studied at various temperatures and cholesterol concentrations. The properties studied are the area per lipid, condensation, bilayer thickness, tail order parameters, bending modulus, and area compressibility. The model quantitatively reproduces most of the experimental effects of cholesterol on these properties and reproduces the main features of the experimental temperature-composition phase diagram. Based on the changes in structural properties a temperature-composition structure diagram is proposed, which is compared with the experimental phase and structure diagrams. The lateral organization of cholesterol in the bilayer is also discussed. In a second part, modifications of the cholesterol model are made to allow a better understanding of the cholesterol condensation effect. This condensation effect is further discussed in relation to the DMPC-cholesterol phase behavior.

The simulation of the DMPC-cholesterol phase diagram has been published in: F. de Meyer, A. Benjamini, J. Rodgers, Y. Mistelli, B. Smit *Molecular simulation of the DMPC-cholesterol phase diagram*, in J. Phys. Chem. B, Vol. 114, Pages 10451-10461 (2010). The mechanism of the cholesterol condensation effect and its relation to the DMPC-cholesterol phase diagram is summarized in the research paper: F. de Meyer, B. Smit. *Effect of cholesterol on the structure of a phospholipid bilayer*, in Proc. Natl. Aca. Sci. USA. Vol. 106, Pages 3654-3658 (2009).

In Chapter 5, the effect of cholesterol on lipid-mediated protein-protein interactions described in Chapter 3 is investigated. This is done in accordance with the re-

sults obtained in Chapter 4 concerning the effect of cholesterol on the phase behavior of lipid bilayers. The calculations of the potential of mean force between proteins and protein clusters show that the addition of cholesterol gradually reduces repulsive lipid-mediated interactions between certain proteins. At a given cholesterol concentration, the interactions even become attractive. Hence, cholesterol significantly promotes protein aggregation. The role of protein-induced dynamical cholesterol-enriched and cholesterol-depleted shells in these effects is discussed in detail.

This part has been published in: F. de Meyer, J. Rodgers, T. Willems, B. Smit *Molecular simulation of the effect of cholesterol on lipid-mediated protein-protein interactions*, in Biophys. J., Vol. 99 (2010).

In Chapter 6 we briefly bundle the main conclusions of this work and discuss interesting perspectives.

Chapter 2

Mesoscopic Model, Simulation Method and Simulation and Experimental Techniques

In this chapter we introduce the mesoscopic model that we use to represent a membrane. We describe the hybrid Monte Carlo (MC) - Dissipative Particle Dynamics (DPD) simulation technique that we have applied to study the mesoscopic model membrane. We finally close this chapter with a detailed overview of the experimental and simulation techniques used to obtain the relevant bilayer properties.

2.1 Motivation for a Coarse-Grained Model

Over the last three decades, several research groups have developed all-atom simulation packages to study lipid bilayers with proteins (52, 53). The main aim of these studies on lipid and protein models is to deepen our understanding of the experimental bilayers and to access information on the systems that is very difficult to obtain from experiements.

In these models all atoms of the lipid and water molecules are considered. Water molecules are explicitly represented. A critical component has been the development of a reliable force field or potential energy function (53). Over the years the force fields have been continuously improved using quantum mechanical calculations and comparisons with experimental data.

The following intramolecular interactions are considered: harmonic bond potentials to model chemical bonds, harmonic bending potentials for the angles between two consecutive bonds, and a torsion potential modeling the torsion of a chain segment of four atoms. The intra-molecular interactions are: van der Waals interactions, modeled by Lennard-Jones potentials and the electrostatic Coulomb interactions.

On the current computers, one can typically perform a simulation of a bilayer

containing between 100 and 200 lipids for 200 ns within a reasonable simulation time (several months). There are still serious doubts whether this is enough to just equilibrate the bilayer. Although the size of this bilayer is probably sufficient to study structural properties of the bilayer (at least for a bilayer in the liquid phase), it is certainly too small to study bilayer mechanical properties (bending modulus, etc.). For example, to calculate the bending modulus, one needs long simulations to fully sample the bilayer undulation modes and sufficiently large membrane patches to observe the membrane thermal undulations. Properties related to phase transitions and phase behavior require simulations of many points in state space and are therefore unaccessible with all-atom simulations today. Almost all simulations have been performed at a specific temperature in the liquid phase, some in the gel and ripple phase (54–57). For similar reasons, quantitative atomistic simulations of bilayers containing more than two small proteins have not been reported (58).

The force fields of the simplest and most studied lipid bilayers are still continuously optimized. The force fields have long been validated by comparison of highly non accurate experimental values like the area per lipid. Recently, a new strategy has been proposed: a direct comparison with the most accurate part of the experimental data (data for which the least assumptions and fitting to models have been made). For example, the form factor of the simulated bilayer has been directly compared to the experimental form factor obtained from X-ray diffraction (37, 59). Additionally, the simulations have been used to interpret the form factor. Similar comparisons have been made with NMR experiments (53, 60).

To allow for simulations of the cooperative behavior between lipids, water and peptides at longer time and length scales within a reasonable simulation time, coarse-grained models have been developed (61). Groups of atoms are lumped into beads which interact via effective potentials. Water may or may not be coarse-grained. One can apply classical molecular dynamics simulations on a coarse-grained model, or more sophisticated simulation methods like dissipative particle dynamics. The same formulas to calculate bilayer properties apply as for all-atom simulations.

The main difference between the different course-grained models of lipids is the force field for the interactions. One can distinguish three different approaches:

A first approach is called the reverse Monte Carlo method (62). After empirically selecting an appropriate functional form for the effective interaction potentials, the force fields are fitted such that the radial distribution functions obtained from coarse-grained simulations resemble those obtained from all-atom simulations. The radial distribution function, g(r), describes how the density of a group varies as a function of the distance of one particular group. The major disadvantage of this approach is that the potentials are not transferable to other systems.

A second approach is the force matching scheme (63–66). In the conventional force matching method, the classical forces $\mathbf{F}_i^p$ of a preselected analytical form, which are dependent on a set of parameters, are optimized by minimizing the average over the

whole configuration data functional, $\left|\mathbf{F}_i^{ref} - \mathbf{F}_i^p\right|^2$, where $\mathbf{F}_i^{ref}$ is the reference force supplied by atomistic simulations. The basic idea is thus that the forces acting on a bead in the coarse-grained model should be similar to the force obtained from the coarse-grained atomistic simulations. Again the potentials are not transferable to other systems.

A third approach is to empirically use a selected functional form and to parametrize it by fitting certain thermodynamic properties (61, 67, 68). This approach was the first used for coarse-grained models of lipids and is followed in this work. It will be worked out in detail below.

All approaches are based on the fitting of one or several particular properties, for example, the radial distribution function, at one specific condition and, as a result, those models often fail to predict many other properties. One should particularly be careful with properties at different conditions.

Although the use of coarse-grained models to study collective phenomena at mesoscopic length- and time-scales in lipid bilayers is barely a decade old, there have been considerable achievements, which are reviewed in (61). Major results include the self-assembly of micelles and bilayers (69), the reproduction of parts of the experimental qualitative phase behavior of pure saturated lipids (70–73), of mixed saturated bilayers (74) and of saturated lipids containing small alcohols (75), the simulation of water pore formation in lipid bilayers (76), the study of structural properties of saturated lipids as function of the tail length (69, 71, 75), and the study of vesicle fusion and fission (77–79). Simple peptide models have been developed to investigate the collective response of membrane and peptides to hydrophobic mismatch (80), to study the effect of peptides on the lipid phase behavior (81), the spontaneous adsorption of peptides into a membrane (82) and the qualitative self-assembly of α-helices (83).

2.2 Coarse-Grained Model of a Model Membrane

Within the mesoscopic approach, each molecule of the system is coarse-grained by a set of beads. In this work we consider 4 types of beads (69):

1. A water-like bead, denoted as w, which models water.

2. An hydrophilic bead, denoted as h, which models a section of the hydrophilic phospholipid and cholesterol headgroup and of the protein hydrophilic parts.

3. A first hydrophobic bead, denoted as t (sometimes t_L), which models the hydrophobic segments of the phospholipid hydrocarbon tail and of cholesterol.

4. A second hydrophobic bead, denoted as t_P, which models a segment of the hydrophobic part of the peptides.

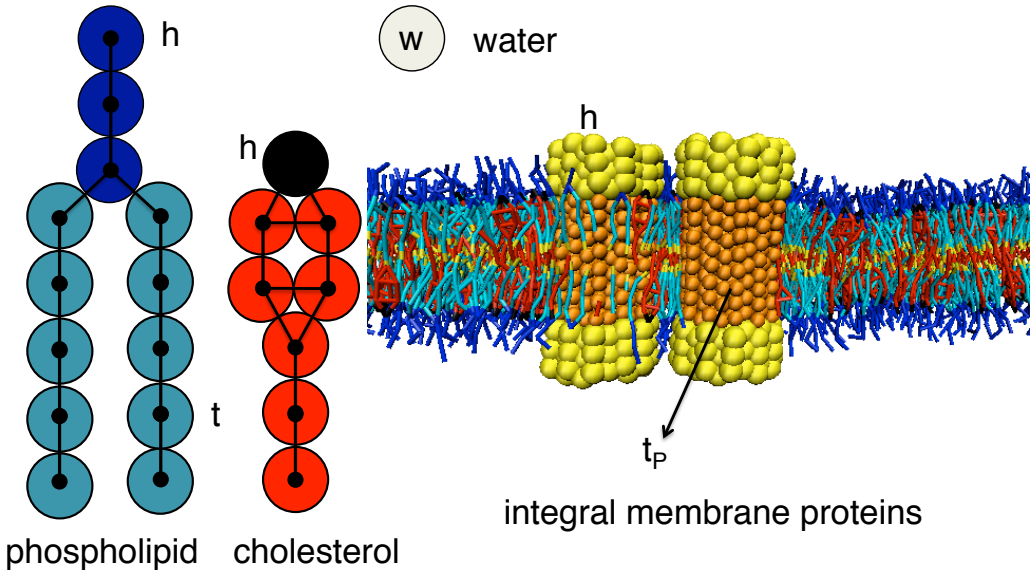

Figure 2.1: (left) Coarse-grained model of a phospholipid and cholesterol. Lipid hydrophilic head beads (type h) are depicted in dark blue, while the hydrophobic tail beads (type t) are depicted in light blue. Cholesterol hydrophilic (type h) and hydrophobic (type t) beads are depicted in black and red, respectively. (right) Snapshot of a model bilayer containing phospholipids and cholesterol and in which two proteins are embedded. Water (type w) is not shown for clarity. The protein hydrophilic (type h) and hydrophobic (type p) beads are depicted in yellow and orange, respectively.

A snapshot of the model is shown in Fig. 2.1. In our model, a water bead comprises three water molecules. A lipid is constructed by connecting head- and tail-beads with springs. The phospholipid lipid consists of a headgroup containing three hydrophilic beads (one for the glycol, one for the phosphorous group and one for the choline group) to which two tails of X hydrophobic beads (of type t, t_L) are attached. A hydrophobic tail bead comprises 3 to 4 $-CH_2-$ groups. In this work we will consider lipid tails containing X=4 and 5 hydrophobic beads. We will often denote the lipids $h_3\,(t_x)_2$. Cholesterol consists of a single hydrophilic bead, representing the hydroxyl group, which, together with 5 hydrophobic beads forms a stiff ring, representing the tetrameric ring, and to which a tail of two hydrophobic beads is attached, which represents the iso-octyl tail. The cholesterol coarse-grained model is introduced in more detail in Chapter 4. A transmembrane protein is modeled by linking together N_p amphiphatic chains into a cylindrical bundle. The N_p amphiphatic chains are linked to the neighboring ones by springs, thus forming a relatively rigid object with no appreciable internal flexibility. Each amphiphatic chain consists of n_{tp} hydrophobic beads t_P, to the ends of which are attached three headgroup h beads. The distance spanned by a bead is approximately equal to that spanned by a helix turn. By

varying N_P and n_{tp} one can model proteins with different diameters and hydrophobic thickness. In this work we consider peptides with N_P=4, 7, and 43 and with n_{tp} ranging from 4 to 10.

In our model we use bonded and non-bonded interactions to describe the main structure and flexibility of the molecules and the inter- and intra-molecular interactions.

2.2.1 Bonded Interactions

The bonded interactions contain an elastic contribution

$$\mathbf{F}_{\text{spring}} = -K_r \left(r_{ij} - r_{\text{eq}}\right) \mathbf{e}_{ij}, \tag{2.1}$$

which describes the harmonic force used to tie two consecutive beads i and j in a chain, and a bond-bending force

$$\mathbf{F}_{\theta} = -\nabla \left(\frac{1}{2} K_{\theta} \left(\theta - \theta_o\right)^2 \right), \tag{2.2}$$

between consecutive bonds, to control the chain flexibility.

The parameters of the bonded interactions were obtained from all-atom molecular simulations (84). The criterium is that the probability distribution function of r_{ij} and θ obtained from mesoscopic simulations should be reasonably similar to the corresponding probability distribution functions obtained from coarse-grained all-atom molecular simulations.

The parameters for the elastic contribution to the interaction energy (Eq. 2.1) have the values r_{eq}=0.7 R_c and K_r=100 for the lipids, cholesterol and the proteins and the parameters for the bond-bending force (Eq. 2.2) are K_θ=6 and θ_o=180^o for the angle formed by consecutive bonds in the lipid and cholesterol tails, K_θ=3 and θ_o=90^o for the angle between the bonds connecting the last head-bead to the first beads in the lipid tails and K_θ=100 and θ_o=180^o for each consecutive pair of bonds in the protein (80). K_θ=100 and θ_o=150^o for the angles forming the stiff cholesterol ring. The units of K_r and K_θ are E_0/R_C^2 and E_0/rad^2, respectively, where E_0 is the reduced energy unit.

2.2.2 Non-Bonded, Soft-Repulsive Interactions

The non-bonded interactions between a bead of type i and a bead of type j is assumed to be soft-repulsive:

$$\mathbf{F}_{ij}^{C} = \begin{cases} a_{ij} \left(1 - r_{ij}/R_{\text{c}}\right) \mathbf{e}_{ij} & (r_{ij} < R_{\text{c}}) \\ 0 & (r_{ij} \geq R_c) \end{cases} \tag{2.3}$$

where R_c is the cut-off diameter. The corresponding potential energy function (within an additive constant) is then given by:

$$V_{ij}^{C} = \begin{cases} \frac{1}{2} a_{ij} R_c \left(1 - r_{ij}/R_c\right)^2 & (r_{ij} < R_c) \\ 0 & (r_{ij} \geq R_c) \end{cases} \tag{2.4}$$

In these equations, $r_{ij} = |\mathbf{r}_i - \mathbf{r}_j|$ and $\mathbf{e}_{ij} = (\mathbf{r}_i - \mathbf{r}_j)/r_{ij}$ is a unit vector pointing from particle j to particle i. In our simulations R_c is the unit of length, and has the value 1.

The effective interactions computed from coarse-grained atomistic simulation are found to be soft-repulsive, in the sense that they do not contain the steep repulsive interaction of the Lennard-Jones potential used in all-atom simulations, but a softer repulsive interaction (85). This can be understood, noting that atoms cannot physically overlap, but that beads might overlap. As a result of this, one can use much longer time steps in the integration method, and thus allow for a much faster exploration of configuration space. DPD is estimated to be a 1000 times faster than conventional molecular dynamics (86).

In the next section, we explain how the soft-repulsive parameters, a_{ij}, are related to experimental thermodynamical properties (86–90).

2.2.3 Soft-Repulsive Parameters $\mathbf{a}_{ij}$

Water: $\mathbf{a}_{ww}$ According to Groot and Warren (87) we make a link between the soft-repulsive parameters and experimental thermodynamic properties. Let us first have a look at a liquid of a single component. The system contains N water molecules in a volume V at temperature T. In our model, the parameter of the water model a_{ww} is fitted such that the fluctuations in the number density $\rho = N/V$ at a given temperature, are reproduced. The fluctuations in the number density, $\delta\rho = \rho - \langle\rho\rangle$, are related to the compressibility of water, κ_T, which is defined as:

$$\kappa_T = \frac{1}{\rho}\left(\frac{\partial\rho}{\partial P}\right)_T \tag{2.5}$$

Indeed:

$$\left\langle (\delta\rho)^2 \right\rangle = \frac{1}{V}\rho^2 k_B T \kappa_T \tag{2.6}$$

To solve Eq. 2.5, the equation of state should be known. There are two possible ways to compute the pressure as function of the number density. The first possibility is by using the Clausius' virial theorem which states that if the scalar moment of inertia of N particles about an origin has no acceleration (in other words, if the particles hang together) the total kinetic energy of the system relates to the forces acting on the particles:

$$2E_{Kin} = -\sum_i \langle \mathbf{F}_i \mathbf{r}_i \rangle \tag{2.7}$$

This equation follows directly from $d^2I/dt^2 = 0$, with $I = \sum_i m_i \mathbf{r}_i^2$ the scalar moment of inertia of N particles about the origin. Indeed:

$$\frac{d^2I}{dt^2} = \frac{d}{dt}\left(\sum_i \langle \mathbf{p}_i \mathbf{r}_i \rangle\right) = \sum_i \frac{\langle \mathbf{p}_i^2 \rangle}{m_i} + \sum_i \langle \mathbf{F}_i \mathbf{r}_i \rangle \tag{2.8}$$

Let us note that $\mathbf{F}_i = \sum_{j \neq i} \mathbf{F}_{ji}$ is defined as the total force acting on particle i.

Now, for a system of N particles, its kinetic energy is $E_{Kin} = 3/2 N k_B T$ as defined by the equipartition theorem. For an ideal gas of N particles ($PV = Nk_BT$) the only forces are between particles and container wall and the virial theorem rewrites:

$$\sum_i \langle \mathbf{F}_i \mathbf{r}_i \rangle = -3PV \tag{2.9}$$

For a real gas or liquid one needs to take the particle-particle interactions into account as well. If pairwise interactions are assumed ($\mathbf{F}_{ji} = \mathbf{F}_{ij}$):

$$\sum_i \langle \mathbf{F}_i \mathbf{r}_i \rangle = -3PV + \sum_i \sum_{j>i} \langle \mathbf{F}_{ij} \mathbf{r}_{ij} \rangle = -3Nk_BT \tag{2.10}$$

From this equation one obtains directly the pressure as function of the number density:

$$P = \rho k_B T + \frac{1}{3V} \sum_i \sum_{j>i} \langle \mathbf{F}_{ij} \mathbf{r}_{ij} \rangle \tag{2.11}$$

A second possibility to calculate the pressure as a function of the number density is by using the radial distribution function $g(r)$. Take a particle at the center of N particles. Consider an infinitesimal spherical shell of volume $4\pi r^2 \delta r$, which contains $4\pi r^2 \delta r \rho g(r)$ particles at a distance r from this particle. The total pressure is the sum of the ideal gas pressure and the pressure due to the interactions between the particles in the shell and the central particle:

$$PV = Nk_BT + \frac{1}{3V}\frac{N}{2}\int_0^\infty 4\pi r^2 \rho g(r) r \frac{-dV(r)}{dr} dr \tag{2.12}$$

The factor $N/2$ finds its origin from the fact that N particles could be in the center, and that every interaction should be counted only once. This equation can be rewritten as:

$$P = k_B T \rho + \frac{2\rho^2 \pi}{3}\int_0^\infty g(r) r^3 F(r) dr \tag{2.13}$$

The radial distribution function can be determined experimentally using X-ray scattering techniques. This provides an important link between experiments and simulations.

In dissipative particle dynamics, the force acting on a particle is $F(r) = a(1-r)$. The cut-off diameter is $r = 1$. Thus, the pressure can be written as:

$$P = k_B T\rho + \frac{2\rho^2\pi}{3}\int_0^1 g(r)a(1-r)r^3dr = k_B T\rho + \alpha a\rho^2 \tag{2.14}$$

Via molecular simulations it can be shown that for densities $\rho > 2$ the factor $\alpha = \frac{2\pi}{3}\int_0^1 g(r)(1-r)r^3dr$ goes to a constant value of 0.101 ± 0.001 (87). Thus, if for a constant a-value, the bead density would increase by a factor n, the pressure would adapt such that the radial distribution function (defined only between $r = [0, 1]$) would not change significantly.

Combining Eq. 2.14 and Eq. 2.5 gives:

$$\frac{1}{\rho k_B T\kappa_T} = 1 + \frac{2\alpha a\rho}{k_B T} \tag{2.15}$$

Experimentally the dimensionless left part of Eq. 2.15 equals 16 for water at a temperature of 300 K. From this and taking α=0.101, we obtain $a\rho/k_B T = 75$. In our simulations ρ=3, and thus $a_{ww} = 25k_B T/R_c$.

Flory-Huggins Model for Polymer Solutions The other soft-repulsive interaction parameters are derived from the Flory-Huggins parameters (87). The Flory-Huggins model for polymer solutions and its connection with experiments via the Hildebrand solubility parameter is first worked out here. Thereafter, the link is made with the soft-repulsive parameters.

The Flory-Huggins theory is a theory for the free-energy of mixing of polymer solutions based on a statistical approach on a regular lattice. Working out the theory would lead us too far. In short, let us consider a small molecule of type 1, which is the solvent (in our case, water) and a macromolecule of type 2, which is the solute (in our case, a lipid, which is not a macromolecule). Let the system consist of N_1 solvent molecules, each occupying a single site on the lattice, and N_2 solute molecules, each occupying n lattice sites. The total number of sites is $N=N_1+nN_2$. The free energy of mixing can then be written as:

$$\Delta G_m = \Delta H_m - T\Delta S_m = k_B TN\phi_1\phi_2\chi + k_B T\left(x_1 ln\phi_1 + x_2 ln\phi_2\right) \tag{2.16}$$

where x_1, x_2 are the fractions of component 1 and 2, respectively, $\phi_1 = N_1/N$, $\phi_2 = nN_2/N$ and χ is the Flory-Huggins interaction parameter.

To understand the Flory-Huggins interaction parameter, consider the following physical reorganization of solvent (1) and solute (2): (1,1)+(2,2) $\rightarrow$ 2(1,2). The

change in interaction energy per (1,2) pair is then given by (if one takes only two-body interactions into account) (89):

$$\frac{1}{2}\Delta w = \frac{1}{2}\left[2w_{12} - w_{11} - w_{22}\right] \cong \frac{1}{2}\left[2\sqrt{w_{11}w_{22}} - w_{11} - w_{22}\right] = \frac{1}{2}\left[\sqrt{w_{11}} - \sqrt{w_{22}}\right]^2 \tag{2.17}$$

with w_{ij} the interaction energy between i and j. The simplification (geometric mean mixing rule) is most accurate when the interactions are soft (e.g., London dispersion forces or dipole-dipole interactions), and breaks down for hydrogen bonding, and certainly for strong specific interactions. The Flory-Huggins interaction parameter is defined as:

$$\chi = \frac{1}{2}\frac{Z\Delta w}{k_B T} \tag{2.18}$$

where Z is the average number of neighbors. For $\chi = 0$, the mixing is athermal, for $\chi < 0$, the mixing is exothermic and for $\chi > 0$, the mixing is endothermic. Because the sign of the entropy of mixing is always negative, the sign of the free energy of mixing, and thus the phase behavior of the binary mixture, strongly depends on the value of χ.

Hildebrand Solubility Parameters For systems in which $\Delta H_m > 0$ (no enthalpy-driven mixing), it is common to express ΔH_m in terms of the cohesive energy density or solubility parameter. The change in internal energy of vaporization of one molecule (removing one molecule) of type i is:

$$\Delta E_{v,i} = \frac{1}{2} Z w_{ii} \tag{2.19}$$

Combining Eq. 2.19, Eq. 2.18 and Eq. 2.17 and rewriting everything on a per unit volume basis gives:

$$\chi = \frac{ZV}{2k_B T}\left[\left(\frac{\Delta E_{v,1}}{V_1}\right)^{\frac{1}{2}} - \left(\frac{\Delta E_{v,2}}{V_2}\right)^{\frac{1}{2}}\right]^2 \tag{2.20}$$

The Hildebrand solubility parameter of component i is defined as the square root of the cohesive energy density:

$$\delta_i = \left(\frac{\Delta E_{v,i}}{V_i}\right)^{\frac{1}{2}} \tag{2.21}$$

and thus Eq. 2.20 can be rewritten as:

$$\chi = \frac{ZV}{2k_B T}\left[\delta_1 - \delta_2\right]^2 \tag{2.22}$$

This important equation relates the theoretical Flory-Huggins interaction parameter to the tabulated Hildebrand parameters of the interacting components. This equation, together with the Flory-Huggins expression of the free energy of mixing, allows thus to make predictions concerning the miscibility of two components, based on their respective solubilities. For example, components having a similar solubility parameter will likely be miscible, while components having very different solubility parameters, are likely to segregate. Solubility parameters of solvents can be obtained from their heat of vaporization, while the parameters of solutes can be obtained indirectly.

Link between Flory-Huggins Model and DPD Model with Soft-Repulsive Interactions There are several similarities between the DPD model and the Flory-Huggins model. In the DPD model all beads have the same volume and in the Flory-Huggins model all lattice sites have the same dimensions. Both systems are rather incompressible. The most interesting similarity is the expression for the free energy of mixing. This is worked out below.

For incompressible fluids one can neglect the ideal gas part in the equation of state. The virial part of the equation of state for a one component system is, from Eq. 2.14:

$$P_{virial} = \alpha a \rho^2 \tag{2.23}$$

Similarly, one can derive an equation of state for a two component system (90). The virial part of the pressure is now:

$$P_{virial} = \left[\alpha_{11} a_{11} \phi_1^2 + \alpha_{22} a_{22} \left(1-\phi_1\right)^2 + 2\alpha_{12} a_{12} \phi_1 \left(1-\phi_1\right)\right] \rho^2 \tag{2.24}$$

where ϕ_1 is the volume fraction of bead-type one, ρ the average number density of the beads and $\alpha_{XY} = \frac{2\pi}{3} \int_0^1 g_{XY}(r)(1-r)r^3 dr$. If now one assumes that all α values go to the same constant value (this assumption holds if both components are miscible (89, 90)), one can simplify Eq. 2.24 to:

$$P_{virial} = \left[a_{11} \phi_1^2 + a_{22} \left(1-\phi_1\right)^2 + 2a_{12} \phi_1 \left(1-\phi_1\right)\right] \alpha \rho^2 \tag{2.25}$$

From Eq. 2.25 one can calculate the virial Helmholtz free energy F (we are in an NVT ensemble) using the relation $P = \left(-\partial F/\partial V\right)_{T,N}$ and keeping in mind that ρ is a function of V:

$$F_{virial}\left(N, \phi_1\right) = \left[a_{11} \phi_1^2 + a_{22} \left(1-\phi_1\right)^2 + 2a_{12} \phi_1 \left(1-\phi_1\right)\right] \alpha \rho N \tag{2.26}$$

The virial contribution of the free energy of mixing is given by:

$$\Delta F_{m,virial} = F_{virial}\left(N, \phi_1\right) - F_{virial}\left(N_1, 1\right) - F_{virial}\left(N_2, 0\right) \tag{2.27}$$

which, using Eq. 3.3, becomes,

$$\Delta F_{m,virial} = 2N\alpha\rho \left[a_{12} - \frac{a_{11} + a_{22}}{2} \right] \phi_1 \phi_2 \tag{2.28}$$

Comparison with the virial part of the Flory-Huggins free energy of mixing (Eq. 2.16) gives:

$$\chi = \frac{2}{k_B T} \alpha\rho \left[a_{12} - \frac{a_{11} + a_{22}}{2} \right] \tag{2.29}$$

Now, in a two component mixture with a Flory-Huggins parameter leading to segregation in equilibrium (let us note that the assumption in Eq. 2.25 is not valid then), the mechanical equilibrium at the interface requires that the pressure in each species, given by Eq. 2.14, must be equal, and thus that $a_{11} = a_{22}$ ($\rho_1 = \rho_2$ is imposed). This relation can easily be extended to multicomponent systems. Therefore:

$$\chi = \frac{2}{k_B T} \alpha\rho \left[a_{12} - a_{11} \right] \tag{2.30}$$

Combining Eq. 2.30 and Eq. 2.22 gives a direct relation between the soft-repulsive interaction parameter between beads of different types and the tabulated Hildebrand solubilities:

$$a_{12} = a_{11} + \frac{Z V_{bead}}{4\alpha\rho} \left[\delta_1 - \delta_2 \right]^2 \tag{2.31}$$

Values of soft-repulsive Parameters Let us now apply the above derived relations to our coarse-grained model. We derived $a_{ww} = 25 k_B T / R_c$. We showed that $a_{ww} = a_{tt} = a_{hh}$. Now we need to calculate the cross terms: a_{wh}, a_{wt} and a_{ht}.

Let us consider for the lipid head group only the glycerol, which has a solubility δ_{glyc}=21.1 $(\mathrm{cal/cm^3})^{1/2}$ at a temperature of 300 K. Water has a solubility of δ_{wat}=23.4 $(\mathrm{cal/cm^3})^{1/2}$. Glycerol and water have very similar solubility parameters and are thus expected to be miscible. Applying formula 2.31 with ρ=3, Z=4, α=0.1, V_{bead}=90Å^3 and converting to the right units gives $a_{wh}=a_{ww}+1.6\ k_B T/R_c$.

Let us consider polyethylene for the tail, the solubility of which is 8.2 $(\mathrm{cal/cm^3})^{1/2}$. This gives $a_{wh}=a_{ww}+69.3\ k_B T/R_c$, and $a_{th}=a_{tt}+50\ k_B T/R_c$.

The soft-repulsive parameters (in $k_B T/R_c$) are summarized in the following table:

a_{ij}	w	h	t
w	25	26.6	94.3
h	26.6	25	75
t	94.3	75	25

The lipid head group is zwitterionic, and as a result there will be an extra repulsive interaction between two head groups. A second consequence of this is an even more favorable water-headgroup interaction. To account for these effects, we modified the parameters. We also put $a_{ht}=a_{wt}$=80 to simplify the parameter set.

The resulting soft-repulsive parameters (in k_BT/R_c), which are used in our simulations, are summarized in the following table:

a_{ij}	w	h	t
w	25	15	80
h	15	35	80
t	80	80	25

For the protein and cholesterol hydrophilic parts, we use, as a first approach, the same bead-type as for the lipid hydrophilic part. For the cholesterol hydrophobic part we use the same bead-type as for the lipid tails. For the hydrophobic part of the proteins, we introduce a new bead type, which is strongly hydrophobic, to ensure that the protein remains in the lipid bilayer. All the soft-repulsive parameters (in k_BT/R_c), which are used in our simulations, are summarized in the following table:

a_{ij}	w	h	t_L	t_P
w	25	15	80	120
h	15	35	80	80
t_L	80	80	25	25
t_P	120	80	25	25

The parameters of this model have been derived at a temperature of 300 K. One should derive them for different temperatures if one wants to simulate this system at other temperatures. However, in this work, as a first approach, we kept the parameters constant as function of the temperature. One thus expects the simulations to be most accurate around room temperature.

This model has been validated in many ways. First of all, we could simulate the self-assembly of the lipids into a lipid bilayer (91). Secondly, the lipid model correctly predicts the experimental phase behavior of a saturated phosphatidylcholine bilayer as a function of temperature (71, 92, 93). Third, this model correctly reproduced the experimentally observed response of bilayer and protein in case of hydrophobic mismatch (80). The validation of the coarse-grained model of hydrated phospholipid-cholesterol is the subject of Chapter 4.

2.3 Dissipative Particle Dynamics

2.3.1 Dissipative Particle Dynamics

To simulate coarse-grained models efficiently, dissipative particle dynamics (DPD) has been introduced by Hoogerbrugge and Koelman (94). DPD can be seen as an improved method with respect to Brownian dynamics. The statistical mechanics of DPD have been worked out by Español and Warren (95).

In DPD, the total force balance on a given particle i is written in the form:

$$m_i \frac{\partial \mathbf{u}_i}{\partial t} = \sum_{i \neq j} \mathbf{F}_{ij}^C + \sum_{i \neq j} \mathbf{F}_{ij}^D + \sum_{i \neq j} \mathbf{F}_{ij}^R \tag{2.32}$$

with $\mathbf{F}_{ij}^C$ a conservative force deriving from a potential exerted on particle i by particle j, $\mathbf{F}_{ij}^D$ is a dissipative force and $\mathbf{F}_{ij}^R$ is a random force. It is important to note that pair additivity has been assumed. The conservative and the dissipative force satisfy certain requirements:

1. Gallilean invariance, which states that Newton's second law should be applicable in every reference, requires that both forces $\mathbf{F}_{ij}^R$ and $\mathbf{F}_{ij}^D$ depend only on relative distances and velocities, namely the combinations $\mathbf{r}_{ij} = \mathbf{r}_i - \mathbf{r}_j$ and $\mathbf{u}_{ij} = \mathbf{u}_i - \mathbf{u}_j$.

2. Isotropy, which implies that the forces should transform under rotations as vectors, or, in other words, that the magnitude of the forces should not change when the particles are rotated.

3. The dissipative forces are linear on the momentum and the random forces are independent of the momentum (just as in classical Langevin dynamics).

Points 1 and 2 should be seen as an improvement over Lattice-Gas and Lattice-Boltzmann dynamics where spurious dynamics were introduced due to the absence of isotropy and Gallilean invariance.

A simple form of the forces that satisfy these hypotheses is:

$$\mathbf{F}_{ij}^D = -\gamma \omega_D (\mathbf{e}_{ij} \mathbf{u}_{ij}) \mathbf{e}_{ij} \tag{2.33}$$

$$\mathbf{F}_{ij}^R = \sigma \omega_R \zeta_{ij} \mathbf{e}_{ij} \tag{2.34}$$

In these equations, ω_D and ω_R are both a function of $r_{ij} = |\mathbf{r}_i - \mathbf{r}_j|$ solely, and $\mathbf{e}_{ij} = (\mathbf{r}_i - \mathbf{r}_j)/r_{ij}$ is a unit vector pointing from particle j to particle i. The term ζ_{ij} is a Gaussian white noise term with the following stochastic properties:

$$\langle \zeta_{ij}(t) \rangle = 0 \tag{2.35}$$

$$\langle \zeta_{ij}(t) \zeta_{i'j'}(t') \rangle = (\delta_{ii'}\delta_{jj'} + \delta_{ij'}\delta_{ji'})\delta(t - t') \tag{2.36}$$

The latter equation is basically saying that at every fixed time, the only correlation is $\zeta_{ij} = \zeta_{ji}$ and that in all other cases ζ_{ij} and $\zeta_{i'j'}$ are completely uncorrelated. ω_D and ω_R provide the range of interaction for the dissipative and the random forces. γ and σ are interpreted as the friction coefficient and the amplitude of the noise. The total force balance on a given particle is thus:

$$m_i \frac{\partial \mathbf{u}_i}{\partial t} = \sum_{i \neq j} \mathbf{F}_{ij}^C + \sum_{i \neq j} -\gamma \omega_D (\mathbf{e}_{ij} \mathbf{u}_{ij}) \mathbf{e}_{ij} + \sum_{i \neq j} \sigma \omega_R \zeta_{ij} \mathbf{e}_{ij} \tag{2.37}$$

Without the dissipative and the random force the system would evolve from a given initial condition towards a dynamical equilibrium, as in classical MD in a microcanonical ensemble. Because the molecules were lumped into beads, the dissipation of energy during the collisions between beads should be specifically accounted for.

The physical interpretation of the dissipative force is as follows. If $(\mathbf{e}_{ij}\mathbf{u}_{ij}) > 0$, it means that particle i is moving apart from particle j, and, therefore, it feels a viscous force towards j. If it moves towards j, the viscous (dissipative) force is in the opposite direction.

To include the continuous thermal fluctuations that keep the system dynamic the random force was added in the force balance. The result is conventional Langevin dynamics. However, the difference between conventional Langevin dynamics and DPD is that in Langevin dynamics only the number of particles is conserved, and, therefore, the only macroscopic behavior will be diffusive. In Langevin dynamics the total momentum is not conserved, or, in other words, the Navier-Stokes equation does not hold, and thus the macrosopic behavior is not hydrodynamic. In DPD, however, the total momentum is conserved ($d(\sum_{i=1}^{N} m_i\mathbf{u}_i)/dt = d(\sum_{i=1}^{N} \mathbf{p}_i)/dt = 0$), and, therefore, the macroscopic behavior is both diffusive and hydrodynamic.

Total momentum is automatically conserved if Newton's third law (action=reaction) is satisfied. The following aspects of DPD conserve the total momentum:

1. The conservative forces are pairwise additive and symmetric ($\mathbf{F}_{ij}^{C} = \mathbf{F}_{ji}^{C}$). This is a simplification if many-body interactions are important.

2. The dissipative and the conservative forces are pairwise additive and symmetric ($\mathbf{F}_{ij}^{D} = \mathbf{F}_{ji}^{D}, \mathbf{F}_{ij}^{R} = \mathbf{F}_{ji}^{R}$, because $\zeta_{ij} = \zeta_{ji}$)

DPD can be seen as a simulation method to solve the conservation of mass equation coupled to the conservation of momentum equation at constant temperature. For an incompressible (constant density), isotropic, single phase fluid these equations are:

$$\nabla\mathbf{u} = 0 \tag{2.38}$$

$$\rho\frac{\partial\mathbf{u}}{\partial t} = -\nabla P + \sum \mathbf{F}_i \tag{2.39}$$

Let us note that in this equation $\sum \mathbf{F}_i$ is the sum of the external forces acting on the fluid, like e.g. gravitation or external stress.

Contrary to momentum and mass, total energy is not conserved in DPD. In DPD, as in classical Langevin dynamics, the dissipative and the random forces act as a thermostat. Simulations of a constant number of particles using DPD are thus always in an NXT ensemble, with X=P or X=V.

2.3.2 Fluctuation Dissipation Theorem

Let us first consider some basic aspects of stochastic methods before applying them to DPD. Let us consider a stochastic process described by the following equation, called Ito stochastic differential equation:

$$d\mathbf{x}(t) = A(\mathbf{x},t)dt + \sqrt{B(\mathbf{x},t)}d\mathbf{W}(t) \tag{2.40}$$

with $d\mathbf{W}(t) = \zeta dt$, an increment of the Wiener process. Consider now a distribution function $f(\mathbf{x},t)$, which is related to the probability of finding the system in a state $\mathbf{x}$ at time t. The time evolution of this distribution, $\partial f(\mathbf{x},t)/\partial t$, given that at a time t' the system was in state $\mathbf{x}'$ (which is an N-dimensional vector) is given by the differential Chapman-Kolmogorov equation, which, in case jump probabilities are zero, reduces to the Fokker-Planck equation, which describes a purely diffusive process:

$$\frac{\partial f(\mathbf{x},t)}{\partial t} = -\sum_{i=1}^{N}\frac{\partial}{\partial x_i}\left[A(\mathbf{x},t)f(\mathbf{x},t)\right] + \frac{1}{2}\sum_{i=1}^{N}\sum_{j=1}^{N}\frac{\partial^2}{\partial x_i \partial x_j}\left[B(\mathbf{x},t)f(\mathbf{x},t)\right] \tag{2.41}$$

One can show that the stochastic process described by a conditional probability satisfying the Fokker-Planck equation is equivalent, but complementary, to the Ito stochastic differential equation.

Let us again consider the DPD system. The DPD Langevin equations can be written in the form of stochastic differential equations:

$$d\mathbf{r}_i = \frac{\mathbf{p}_i}{m_i}dt \tag{2.42}$$

$$d\mathbf{p}_i = \sum_{j\neq i}\mathbf{F}_{ij}^{C}dt + \sum_{j\neq i} -\gamma\omega_D(\mathbf{e}_{ij}\mathbf{u}_{ij})\mathbf{e}_{ij}dt + \sum_{j\neq i}\sigma\omega_R\mathbf{e}_{ij}\zeta_{ij}dt \tag{2.43}$$

which can be rewritten as two Ito stochastic differential equations:

$$d\mathbf{r}_i = \frac{\mathbf{p}_i}{m_i}dt + 0dW \tag{2.44}$$

$$d\mathbf{p}_i = \left[\sum_{j\neq i}\mathbf{F}_{ij}^{C} + \sum_{j\neq i} -\gamma\omega_D(\mathbf{e}_{ij}\mathbf{u}_{ij})\mathbf{e}_{ij}\right]dt + \sum_{j\neq i}\sigma\omega_R\mathbf{e}_{ij}dW_{i,j} \tag{2.45}$$

Let us now consider the distribution function $\rho(\mathbf{r},\mathbf{p},t)$, which is related to the probability of finding the system in a state where the particles have positions $\mathbf{r}$ and momenta $\mathbf{p}$, at any particular time t. The time evolution of this distribution, $\partial\rho/\partial t$, given that at a time t' the system was in state $(\mathbf{r}',\mathbf{p}')$ is given by the differential Chapman-Kolmogorov equation, which, in case jump probabilities are zero, reduces to the Fokker-Planck equation, which describes a purely diffusive process:

$$\frac{\partial \rho(\mathbf{r},\mathbf{p},t)}{\partial t} = -\sum_i \frac{\partial}{\partial \mathbf{r}_i}\left[\frac{\mathbf{p}_i}{m_i}\rho(\mathbf{r},\mathbf{p},t)\right]$$
$$-\sum_i \frac{\partial}{\partial \mathbf{p}_i}\left[\sum_{j\neq i}\mathbf{F}^C_{ij}\rho(\mathbf{r},\mathbf{p},t) - \sum_i\sum_{j\neq i}\gamma\omega_D(\mathbf{e}_{ij}\mathbf{u}_{ij})\mathbf{e}_{ij}\rho(\mathbf{r},\mathbf{p},t)\right]$$
$$+\frac{1}{2}\sum_i\sum_j \frac{\partial^2}{\partial \mathbf{p}_i\partial \mathbf{p}_j}\left[\sum_{k\neq i}\sum_{l\neq j}\sigma^2\omega_R^2(\delta_{ik}\delta_{jl}+\delta_{il}\delta_{jk})\mathbf{e}_{ik}\mathbf{e}_{jl}\rho\left(\mathbf{r},\mathbf{p},t\right)\right]$$

Let us note that the term $\delta_{ik}\delta_{jl}+\delta_{il}\delta_{jk}$ originates from the definition of the stochastic noise. The last term can be simplified towards:

$$\frac{1}{2}\sigma^2\omega_R^2\sum_i\sum_{k\neq i}\mathbf{e}_{ik}\mathbf{e}_{ik}\left(\frac{\partial^2}{\partial {\mathbf{p}_i}^2} - \frac{\partial^2}{\partial \mathbf{p}_i\partial \mathbf{p}_k}\right)\rho\left(\mathbf{r},\mathbf{p},t\right) \tag{2.46}$$

The Fokker-Planck equation has the form:

$$\frac{\partial \rho}{\partial t} = \mathcal{L}^C\rho + \mathcal{L}^{D,R}\rho \tag{2.47}$$

where $\mathcal{L}^C$ and $\mathcal{L}^{D,R}$ are the Liouville evolution operators of the Hamiltonian system interacting with conservative forces, and of the dissipative and the random noise forces, respectively. The Liouville operators are defined as:

$$\mathcal{L}^C \equiv -\sum_i\left[\frac{\mathbf{p}_i}{m_i}\right]\frac{\partial}{\partial \mathbf{r}_i} - \sum_i\left[\sum_{i\neq j}\mathbf{F}^C_{ij}\right]\frac{\partial}{\partial \mathbf{p}_i} \tag{2.48}$$

$$\mathcal{L}^{D,R} \equiv \sum_i \frac{\partial}{\partial \mathbf{p}_i}\left[\sum_{j\neq i}\gamma\omega_D(\mathbf{e}_{ij}\mathbf{u}_{ij})\mathbf{e}_{ij}\right] + \frac{1}{2}\sigma^2\omega_R^2\sum_i\sum_{k\neq i}\mathbf{e}_{ik}\mathbf{e}_{ik}\left(\frac{\partial^2}{\partial {\mathbf{p}_i}^2} - \frac{\partial^2}{\partial \mathbf{p}_i\partial \mathbf{p}_k}\right) \tag{2.49}$$

The operator $\mathcal{L}^C$ is the usual Liouville operator of a Hamiltonian system interacting with conservative forces. The $\mathcal{L}^C$ operator takes into account the effects of the dissipative and the random forces. Consider now the case for which the equilibrium distribution ρ^{eq}, which is the steady state solution $\partial\rho/\partial t$=0, is the Gibbs canonical ensemble. In the Gibbs canonical ensemble the probability to find the system in a given microstate is given by the Boltzmann distribution:

$$\rho^{eq}(\mathbf{r},\mathbf{p},t) = \frac{1}{Z}\exp\left[-H(\mathbf{r},\mathbf{p})/k_BT\right] = \frac{1}{Z}\exp\left[\left(-\sum_i\frac{p_i^2}{2m_i} + V(r)\right)/k_BT\right] \tag{2.50}$$

where H is the Hamiltonian of the system, V is the potential related to the conservative forces and Z is the partition function. The canonical ensemble is always the equilibrium solution for the conservative system, i.e., $\mathcal{L}^C\rho^{eq} = 0$. To have the canonical ensemble as equilibrium solution for the entire system, $\mathcal{L}^C\rho^{eq} + \mathcal{L}^{D,R}\rho^{eq} = 0$, $\mathcal{L}^{D,R}\rho^{eq} = 0$ should be zero. This requirement is satisfied if:

$$\omega_R = \omega_D^{1/2} \tag{2.51}$$

$$\sigma = \sqrt{2k_BT\gamma} \tag{2.52}$$

Indeed, inserting these relations in the dissipative and random Liouville operator gives, after rearranging:

$$\mathcal{L}^{D,R}\rho^{eq}(\mathbf{r},\mathbf{p},t) = \gamma\omega_D \sum_i \sum_{j\neq i} \frac{\partial}{\partial \mathbf{p}_i}\left[(\mathbf{e}_{ij}\mathbf{u}_{ij})\mathbf{e}_{ij} + k_BT\mathbf{e}_{ij}\mathbf{e}_{ij}\left(\frac{\partial}{\partial \mathbf{p}_i} - \frac{\partial}{\partial \mathbf{p}_j}\right)\right]\rho^{eq}(\mathbf{r},\mathbf{p},t) \tag{2.53}$$

Because:

$$\frac{\partial}{\partial \mathbf{p}_i}\rho^{eq}(\mathbf{r},\mathbf{p},t) = -\beta\mathbf{u}_i\rho^{eq}(\mathbf{r},\mathbf{p},t) \tag{2.54}$$

The above equation reduces to:

$$\mathcal{L}^{D,R}\rho^{eq}(\mathbf{r},\mathbf{p},t) = \gamma\omega_D \sum_i \sum_{j\neq i} \frac{\partial}{\partial \mathbf{p}_i}\left[(\mathbf{e}_{ij}\mathbf{u}_{ij})\mathbf{e}_{ij} + \mathbf{e}_{ij}\mathbf{e}_{ij}(\mathbf{u}_i - \mathbf{u}_j)\right]\rho^{eq}(\mathbf{r},\mathbf{p},t) \tag{2.55}$$

which reduces to zero because $\mathbf{u}_i - \mathbf{u}_j = -\mathbf{u}_{ij}$.

The recovery of the Gibbs canonical ensemble as equilibrium solution of the DPD system implies that all thermodynamic properties can be calculated using only the conservative forces.

Let us note that the condition $\sigma = \sqrt{2k_BT\gamma}$ is the same condition in Brownian dynamics. Brownian motion is the motion of a macroscopically small, but microscopically large particle that is subject only to collisional forces exerted by the molecules of a surrounding fluid. Conservative forces are absent. Newton's second law equation on the particle gives:

$$m\frac{du}{dt} = -\gamma u + \sigma\zeta \tag{2.56}$$

The physical interpretation is that the particle is subject to two kinds of forces: a steady dissipative drag force and a zero-mean temporally uncorrelated fluctuating force. On can show that in order to satisfy the equipartition of energy condition $mu^2 = k_BT$, $\sigma = \sqrt{2\gamma k_BT}$.

This requirement is the so-called dissipation-fluctuation theorem, which implies that dissipation and fluctuation are not independent, but intimately related.

2.3.3 Integration Method

To advance the set of positions and velocities, a modified (because the force depends on the velocities) version of the velocity-Verlet algorithm is used (96).

$$\mathbf{r}_i\left(t+\Delta t\right)=\mathbf{r}_i\left(t\right)+\Delta t\mathbf{v}_i\left(t\right)+\frac{1}{2}\left(\Delta t\right)^2\mathbf{f}_i\left(t\right) \tag{2.57}$$

$$\tilde{\mathbf{v}}_i\left(t+\Delta t\right)=\mathbf{v}_i\left(t\right)+\lambda\Delta t\mathbf{f}_i\left(t\right) \tag{2.58}$$

$$\mathbf{f}_i\left(t+\Delta t\right)=\mathbf{f}_i\left(\mathbf{r}\left(t+\Delta t\right),\tilde{\mathbf{v}}\left(t+\Delta t\right)\right) \tag{2.59}$$

$$\mathbf{v}_i\left(t+\Delta t\right)=\mathbf{v}_i\left(t\right)+\frac{1}{2}\Delta t\left(\mathbf{f}_i\left(t\right)+\mathbf{f}_i\left(t+\Delta t\right)\right) \tag{2.60}$$

A detailed discussion on the order of this algorithm and on other integration algorithms used for dissipative particle dynamics can be found elsewhere (87). Recently a complex integration scheme for DPD using the stochastic Trotter formula has been derived (97).

2.3.4 Dissipative and Random Forces and Integration Parameters

We impose that the dissipative and the random forces have the same functional dependence on the interparticle distance. Therefore the the function ω_R has the following form:

$$\omega_R=\begin{cases}\left(1-r_{ij}/R_{\mathrm{c}}\right)\mathbf{e}_{ij} & \left(r_{ij}<R_{\mathrm{c}}\right)\\ 0 & \left(r_{ij}\geq R_c\right)\end{cases} \tag{2.61}$$

and, as explained in Sec. 2.3.2, $\omega_D=\omega_R^2$.

The parameters of the integration method and of the dissipative and the random forces are intimately related (87). The timestep size has to be chosen as a compromise between fast simulations and the amount of artificial temperature increase one is willing to allow. In our simulations we put λ=0.65. The integration timestep is Δt=0.03. The value of σ is 3, the value of η is related to σ via the dissipation fluctuation theorem (see Sec. 2.3.2).

2.4 Hybrid DPD-MC Simulation Method

Because unconstrained lipid bilayers are essentially in a tensionless state (98), we reproduced this condition by simulating the system in the $NV\gamma T$ or in the $NP_\perp\gamma T$ ensemble, where γ is the surface tension of the lipid bilayer.

We simulate in the $NP_\perp\gamma T$ ensemble via a hybrid Monte Carlo (MC) and dissipative particle dynamics (DPD) approach (69, 99, 100). Each cycle of the simulation consists of one of the following possible moves: (1) a DPD trajectory of 1 to 50 steps which applies a thermostat to the dynamics, (2) a constant surface tension MC move, and (3) a constant normal pressure MC move. These moves are chosen with a likelihood of 60% - 20% - 20%. Simulations in the $NV\gamma T$ ensemble are similar, but contain only move (1) and (2), chosen with a likelihood of 60% - 40%.

The Monte Carlo moves are carried out in order to allow relevant degrees of freedom to relax during simulations as temperature varies. These relevant degrees of freedom include the density of the box and the surface area of the lipid bilayer. As such, in the following discussions, the particle positions are described via the scaled coordinates $\mathbf{s}^N$ where any position $\mathbf{r}$ of a particle may be obtained via $\mathbf{r} = (L_x s_x, L_y s_y, L_z s_z)$ and the x-direction is chosen to be perpendicular to the lipid bilayer surface.

Surface area is allowed to vary via the constant surface tension MC move because lipid bilayer areas are known to vary with the temperature and the phase of the bilayer. The constant surface tension MC move alters the lateral surface area of the lipid bilayer while maintaining a constant volume in order to do no work against external pressure (75). The moves are executed in order to sample from the following partition function, expressing particle positions in terms of reduced positions $\mathbf{s}$:

$$Z_{NV\gamma T} = \frac{V^N}{\Lambda^{3N} N!} \frac{1}{L_0} \int_0^\infty dL_y \int dL_z \delta(L_y - L_z) e^{\beta\gamma L_y L_z} \times \int dL_x \delta\left(L_x - \frac{V}{L_y L_z}\right) \int d\mathbf{s}^N \exp\left(-\beta E(\mathbf{s}^N; L_y)\right). \quad (2.62)$$

A random step in the box length L_y is chosen and L_z is changed identically while L_x is changed in order to maintain a constant volume. The surface tension γ is set to zero. A detailed description on the computation of the surface tension in coarse-grained lipid bilayers can be found in (69).

We also maintain a constant pressure applied normal to the lipid bilayer via an additional MC move. Application of the constant normal pressure allows for varying degrees of lipid head group hydration from the water molecules while maintaining a well-defined bulk water reservoir. In reduced units, $P_\perp = 22.5$, the pressure of bulk water (see Sec. 2.5). Constant pressure moves were chosen to sample from the

partition function:

$$Z_{NP_\perp AT} = \frac{1}{\Lambda^{3N} N!} \frac{1}{V_0} \int_0^\infty dV V^N e^{-\beta p_\perp V} \int dL_x \delta \left(L_x - \frac{V}{A} \right) \times \int d\mathbf{s}^N \exp\left(-\beta E(\mathbf{s}^N; L_x) \right). \tag{2.63}$$

A random step in the box volume V is chosen and then solely the simulation box length L_x is varied. This approach ensures that no work is done relative to the surface tension during the constant pressure simulation moves. For a transformation from V_o to V_n, the acceptance probability is defined as

$$acc\left(V_o \rightarrow V_n\right) = \min \left[1, \left(\frac{V_n}{V_o} \right)^N \exp\left(-\beta p_\perp \Delta V - \beta \Delta E \right) \right]. \tag{2.64}$$

In this acceptance probability, the volume ratio is raised to the total number of molecules (not individual beads) because during the constant pressure moves all relative intramolecular coordinates are held constant.

2.5 Reduced Simulation Units and Simulation Parameters

Usually, within the DPD approach, one uses reduced units for the length, mass, energy, time, pressure, and temperature (87).

Length The cut-off diameter R_c is the simulation unit for the distance. In our simulations R_c=1. To relate this distance with a physical distance, we use the coarse-grained model of water. If N_w is the number of water molecules per water bead, v_w the volume of a water molecule, then ${\mathrm{R}_c}^3 = v_w \mathrm{N}_w \rho$. For N_w=3, v_w=30Å^3, ρ=3 beads per R_c^3, we obtain R_c=6.46Å.

Mass The unit of mass is the mass of one bead, thus m_{bead}=1. It is assumed that all beads have the same mass.

Time The DPD simulation method loses track of the physical unit of time because of the coarse-graining (86). The time is introduced in the integration method via the dimensionless time step of the integration Δt. One could, however, match the simulated self-diffusion coefficient of water with the physical self-diffusion coefficient:

$$\tau = \frac{N_w D^{sim}_{waterbead} R_c^2}{D^{exp}_{watermolecule}} \tag{2.65}$$

where τ is the physical time corresponding to Δt=1. The value for τ is around 5ps. The total physical simulation time is then given by: number of DPD steps x Δ t x τ. One could also use the self-diffusion of a lipid as reference, which gives a slightly different value for τ (69). Due to the coarse-graining the beads interact via soft-repulsive potentials. The absence of the strong repulsive interactions (Lennard-Jones potentials) used to model interactions between atoms leads to a significant increase of the simulated time. The diffusion of the particles is typically increased by a factor of 1000 (86).

Energy, temperature, and pressure In our simulations we use a reduced unit of energy, E_0. The reduced temperature and pressure are T^* and P^*. k_BT^* is expressed in units of E_0. Typical simulation values for k_BT^* range from 0.1 to 1.0.

One can estimate the values of the reduced temperature, T^*, in terms of a physical temperature, T, by assuming a linear relation between both:

$$T = aT^* + b \tag{2.66}$$

The values of the coefficients a and b can be found by the system of linear equations obtained by substituting in this relation the reduced and physical values of the main- and pre-transition temperatures of the bilayer.

One can calculate the values of the pressure in reduced units using the model equation of state derived for water given in Eq. 2.14, rewritten in reduced units:

$$P^* = k_BT^*\rho + \alpha a_{ww}\rho^2 \tag{2.67}$$

As for a liquid the virial part is much bigger than the ideal gas contribution, one finds that $P^* \cong 0.1\text{x}25\text{x}9 = 22.5$. This is the pressure we impose if we perform calculations at constant water bulk pressure.

Surface tension There are strong reasons to believe that an unconstrained flat lipid bilayer is in a tensionless state (98, 101). Therefore we simulate the bilayer at a constant surface tension γ=0.

2.6 Experimental Characterization of Model Lipid Bilayers

One of the challenges of modern biophysics is to obtain reliable experimental data of the bilayer properties. This is not straightforward because the bilayer is a only a few nanometers thin and extremely fragile. In this dissertation we often refer to experimental data. This section delves into how estimates of several bilayer properties are obtained using different, often indirect, methods. This is a vast research

area and we will limit ourselves to the most current methods and to the bilayers of interest for this work, namely, bilayers containing saturated (e.g., DMPC, DPPC) and unsaturated (e.g., DOPC) phospholipids and cholesterol. The main purpose is to give a general overview of these methods, and to make clear that the extraction of experimental data is often complicated and based on several assumptions. One of the purposes of molecular simulations is to check the assumptions and to refine the models used to extract experimental data. Here we will expatiate on thermal properties (phase behavior), structural, mechanical and dynamical properties and the lateral organization (phase separation) of a bilayer. Other important bilayer properties, for example: hydration (102), permeability (103), lateral pressure profile (69), partial molecular volumes of lipids and cholesterol (104), thermal expansion and contraction parameters (105) etc, are not delved into.

2.6.1 Thermal Studies

One of the most widely used methods to measure the order or melting transitions of lipid membranes is differential scanning calorimetry. A calorimeter records the heat capacity of a sample by measuring the heat uptake upon temperature increase. A calorimeter consists of a sample cell containing the lipid membrane and the solvent, and of a reference cell containing the solvent, which is mostly water. Both cells are heated in such a way that the rate of the temperature increase is constant, typically around 0.1-1 Ks^{-1}, and that both cells are always in thermal equilibrium. The heat absorbed by both the sample cell and the reference cell is measured as a function of the temperature. In a melting transition, the sample cell absorbs more heat which is compensated by an increase in heat transfer Q that keeps the temperature rate in the sample cell constant and equal to the reference cell. As a result, the heat transfer versus temperature curve will show a sharp increase around the lipid melting transition. If this process takes place at constant temperature, the heat capacity is defined as:

$$C_p(T) = \left(\frac{dQ}{dT}\right)_P = \left(\frac{dH}{dT}\right)_P \tag{2.68}$$

Thus, by differentiating the Q(T) curves one obtains $C_p^{ref}(T)$ and $C_p^{sam}(T)$, in JK^{-1}, for the reference cell and the sample cell, respectively. $C_p^{sam}(T)$ shows a peak at the phase transition. $C_p^{ref}(T)$ is called the baseline. The deviation of $C_p^{sam}(T)$ from the baseline can be measured directly as a function of temperature. Making several assumptions it is possible to obtain the molar heat capacity of the lipid bilayer $c_{p,m}^{l}(T)$ (in $\mathrm{JK}^{-1}\mathrm{mol}^{-1}$) from $C_p^{sam}(T) - C_p^{ref}(T)$ (106–109).

For some lipids like DOPC the phase transitions take place below the melting temperature of water, which freezes during the DSC experiment (110). In many experiments anti-freeze molecules are added.

The main advantage of differential scanning calorimetry over other experimental techniques to study phase transitions, like spectroscopy, is that important thermodynamic parameters related to the phase transition can directly be extracted from the experiment. For example, the surface under the peak of the lipid heat capacity profile is related to the membrane molar melting free energy, as it is defined (if reversibility is assumed) :

$$\Delta G_m^l = \Delta H_m^l - T\Delta S_m^l = \int_{T_m-\Delta T_1}^{T_m+\Delta T_2} c_{p,m}^l(T) - T \int_{T_m-\Delta T_1}^{T_m+\Delta T_2} \frac{c_{p,m}^l(T)dT}{T} \tag{2.69}$$

The melting temperature T_m is usually determined as the temperature at which $c_{p,m}^l(T)$ has a maximum. However, this implies a symmetric $c_{p,m}^l(T)$ curve around T_m, which is generally not true. ΔT_1 is mostly different from ΔT_2. It would be more correct to define T_m as the temperature where the excess enthalpy is 50% of the total melting enthalpy. ΔT_1 and ΔT_2 are chosen with help of the baseline. If $C_p^{sam}(T)$ and $C_p^{ref}(T)$ are superimposed on each other, then ΔT_1 is the temperature where the $C_p^{sam}(T)$ curve starts deviating from the $C_p^{ref}(T)$ curve, and ΔT_2 is the temperature where the $C_p^{sam}(T)$ curve starts rejoining the baseline again, after having been through a maximum. It is clear that incorrect baseline determinations and a somewhat arbitrary choice of ΔT_1 and ΔT_2 are a significant source of error.

The narrower the temperature range over which $c_{p,m}^l(T)$ shows a peak, the more the phase transition is cooperative, or in other words, the more the lipids melt all together, at the same temperature. If the transition width becomes infinitely small, the transition becomes first-order.

For example, the heat capacity profiles of DMPC has a small peak around 15 °C, attributed to the pre-transition from the gel phase to the ripple phase and a sharp second peak around 24 °C, attributed to the main transition from the ripple phase to the fluid phase (109, 111). The excess heat capacity of the first peak is lower than 5 kJmol^{-1}K^{-1}, while the excess heat capacity of the second peak is around 200 kJmol^{-1}K^{-1}. Remembering that the thermal energy unit is k_BT=2.47 kJmol^{-1}, one immediately sees that it is very unlikely that the main phase transition can take place due to thermal fluctuations.

For many systems, for example, for phospholipid-cholesterol mixtures, the peaks in the heat capacity are not always narrow and sharp and, as a result, the interpretation of those DSC experiments is still subject to much debate. For the experimental data we refer the reader to (111–120). Not only model lipid bilayers, but also real biological membranes (containing proteins) show a liquid-gel phase transition (121). The experimental phase behavior of DMPC and cholesterol and of the binary mixtures will be discussed in more detail in Chapter 4.

2.6.2 Structural and Mechanical Properties

Diffraction For a long time, due to the presence of intrinsic fluctuations, the quantitative experimental uncertainty of bilayer structural parameters was too large to be of interest for practical applications (122). Today diffraction measurements provide the best estimates of structural properties. But, some quantities, like the area per lipid, are still subject to errors of 10 %.

One of the main difficulties doing diffraction experiments on a lipid bilayer is that the bilayer is not a crystal, not even when the bilayer is in the gel phase. This is mainly because strong fluctuations occur due to the presence of water. Fully hydrated liquid bilayers are generally assumed to best mimic physiologically relevant conditions.

However, the scattering patterns from the thermally fluctuating (undulating) bilayers contain diffuse scattering which can be successfully analyzed to obtain information regarding bilayer structure and interactions.

Because of the absence of a the crystal structure one cannot determine the exact position of every atom. The description of the position of the atoms in the lipid is a broad statistical distribution function. As a result, properties like hydrophobic thickness and bilayer thickness cannot be defined as a simple distance between two atoms.

X-ray scattering experiments can be performed on unilamellar or multilamellar vescicles, or, more recently, on oriented multilamellar samples. The most common method for the fabrication of oriented samples containing approximately 2000 bilayers is evaporation of the organic solvent from a concentrated membrane solution deposited either on a flat or a cylindrical solid support (123). For binary or ternary mixtures it is assumed that the composition of each individual bilayer fluctuates around the average value.

During an X-ray scattering experiment the amount of x-rays scattered (i.e. the intensity) from the bilayers can be measured. The scattering curves are continuous in scattering vector $\mathbf{q}\left(q_r, q_z\right)$, with $|\mathbf{q}| = 4\pi/\lambda \sin(\theta/2)$, where λ is the wavelength of the X-ray and θ is the scattering angle. The intensity is made up of scattering from the bilayer itself (from factor), as well as scattering from the interbilayer contributions (structure factor). In $\mathbf{q}$ space, q_r (in Å^{-1}) is in the plane of the bilayers and q_z (in Å^{-1}) is normal to the stack of bilayers.

The scattering intensity can be written as:

$$I\left(\mathbf{q}\right) = \frac{S\left(\mathbf{q}\right)\left|F\left(q_z\right)\right|^2}{f\left(q_z\right)} \tag{2.70}$$

where $S\left(\mathbf{q}\right)$ is the structure factor and $F\left(q_z\right)$ is the form factor. The form factor contains the information about the bilayer structure. The structure factor contains the information about the bilayer material properties. $f\left(q_z\right)$ is the Lorentz correction factor, a correction due to the random orientation of the bilayer.

$I\left(\mathbf{q}\right)$ is known from the experiment. $S\left(\mathbf{q}\right)$ can experimentally be obtained from

the q_r dependence on the background subtracted diffuse scattering intensity. A theoretical expression for $S(\mathbf{q})$, where $S(\mathbf{q})$ is written as function of, among other parameters, the bending modulus κ_C, can be derived from smectic liquid crystalline theory. By fitting the theoretical expression to the experiment, one can extract κ_C (124, 125). Extracting material properties from x-ray diffraction experiments is relatively new. The traditional method to obtain κ_C, area compressibility κ_A, surface tension γ and relative area per lipids was pipette aspiration of bilayer vesicles (126, 127).

The form factor $|F(q_z)|$ (in e/Å^2) can now be calculated using Eq. 2.70, after the intensity $I(\mathbf{q})$ has been corrected for various effects (128). The form factor is the Fourier transform of the electron density profile $\rho(z)$, with z the coordinate perpendicular to the bilayer plane:

$$|F(q_z)|^2 = \left(\int_{-D/2}^{D/2} (\rho(z) - \rho_w) \cos(q_z)\, dz \right)^2 + \left(\int_{-D/2}^{D/2} (\rho(z) - \rho_w) \sin(q_z)\, dz \right)^2 \quad (2.71)$$

where D represents the average distance spanning a single bilayer plus half the water space on each side of the bilayer (i.e. the unit cell periodicity or the lamellar repeat distance) and ρ_w is the water density. For a symmetric bilayer the second part of Eq. 2.71 is zero. From an inverse Fourier transform of the form factor one could extract the electron density profile. But because the phasing is not known, one cannot do this.

Two methods have been used. A first possibility is to obtain an estimate of the phasing and to perform the inverse Fourier transformation to obtain the electron density profile. The thickness of the bilayer, PtP (in Å), is then readily obtained as it is defined as the distance between the two peaks in the electron density profile corresponding with the electron-rich phosphorous atoms. The area per lipid, A_L (in Å^2), is obtained using the formula $A_L = 2V_c/(PtP - 10\ \text{Å})$, where V_c is the volume of the lipid chains, obtained from independent volumetric experiments (104, 129), and where the thickness of the hydrocarbon region is PtP minus twice the length of the glycerol region, estimated to be close to 10 Å (from the phosphate to the first methylene of the hydrocarbon chains) (44).

A second possiblity is to make a model of the density distributions of the various structural groups of the lipid(s) and of the water. For example, the choline group is assumed to have a Gaussian distribution, with two fitting parameters. From this, and using independent experimental estimates of the volumes of those groups (104, 129), the total electron density distribution, and thus the form factor, can be calculated. The parameters of the various distributions can be fitted in order to reproduce the experimental form factor. The best fit also gives the density distribution functions of the structural groups automatically. It should be noted that the form factor is very sensitive to changes in bilayer structure, so the fit should be optimal. The area

per lipid is one of the parameters to be fitted, as part of the constraint: $2D_c = 2V_c/A_L$ (130). For a membrane containing a single component the definition of the area per lipid is somewhat straightforward. For membranes consisting of mixtures, experimentalists recently introduced a partial-specific-area formalism (131).

The hydrophobic thickness of the bilayer is defined starting from the probability distribution of all methylenes (the carbonyl carbon is thus not included). The hydrophobic thickness, D_c (in Å) roughly corresponds to the distance between the two outer inflection points of this curve. A more accurate definition makes use of a dividing surface criterion (122).

Both methods give similar results for pure lipid bilayers, but for mixtures of DOPC and cholesterol, for example, there are differences significant enough to make opposite conclusions concerning DOPC-cholesterol interactions.

X-ray diffraction studies exist for DMPC bilayers (128, 130), DOPC bilayers (105, 132), DMPC-cholesterol bilayers (44, 133, 134), and DOPC-cholesterol bilayers (44, 133–135).

One can also perform the same experiment with neutrons instead of X-rays. Structural parameters obtained from x-ray or neutron scattering should ideally be the same. However, this is not the case because of the various assumptions that are made, and one of the main challenges of experimentalists is to close this gap. Similarly, there are deviations between data obtained from low and wide angle X-ray diffraction. For example, at 30 °C, the area obtained for a DOPC molecules is 67.4 Å^2 from neutron scattering (132), 72 Å^2 from low angle X-ray scattering (LAXS) and 74 Å^2 from wide angle X-ray scattering (WAXS) (134). This is a very important challenge because, for example, force fields used in atomistic simulations are validated with the area per lipid.

Recently, an analytical model has been developed to describe the relationship between the chain orientational distribution function and wide angle x-ray scattering data from oriented liquid phase membranes. This was used to obtain an average orientational lipid tail order parameter S_{X-ray} (136).

X-ray diffraction experiments are not constrained to structural and material properties. There have also been several approaches to determine properties of the bilayer ripple phase, like the repeat distance, from diffraction (137, 138), or even to identify new phases based on a different diffraction pattern (139). Previously, the ripple phase was studied with freeze fracture experiments (140). As will be discussed in Sec. 2.6.4, X-ray diffraction is also often used to prove the existence of phase coexistence or small domains within the bilayer.

Nuclear Magnetic Resonance When magnetic nuclei, i.e., nuclei with a non-zero magnetic moment $\mu = \gamma S$ (γ is the gyromagnetic ration, S the spin quantum number), are in a magnetic field, they might absorb energy from an electromagnetic pulse (e.g., a radio frequency pulse) and radiate this energy back out. This effect is called nuclear magnetic resonance. Resonant absorption by nuclear spins occurs only

when the electromagnetic radiation of the correct frequency is being applied to match the energy difference between the nuclear spin levels in a constant magnetic field of the appropriate strength.

All nuclei of the same nuclide do not resonate at the same frequency. Moreover, because of the electrons of surrounding atoms, perturbations occur of the NMR frequency. The latter is called the shielding effect and allows to determine whether a nucleus is in a specific chemical group. The shielding depends on the orientation of the molecule with respect to the magnetic field. Thus, because of those properties, NMR can be used to obtain chemical and structural information data in relation to interatomic distances and nuclear orientation.

One can only apply NMR to identify nuclei with a non-zero magnetic moment, or, in other words, with a non-zero spin. This is for example the case for H (S=1/2). In lipid bilayers the hydrogens are often deuterated (replaced by D=^{2}H, with spin S=1) to avoid interactions from the hydrogens in water or to study one specific region of the lipid. Deuterium exhibits an NMR absorption spectrum characteristic of a quadrupolar nucleus of spin 1, which is distinct from the NMR spectrum of H.

Deuterium NMR is often used to obtain information about the ordering of lipid tails. Typically, the absorption spectrum of a quadrupolar nucleus like D contains two doublet lines. The frequency difference between these two doublet lines, $\Delta\nu\left(\theta\right)$, is, for a homogeneously oriented bilayer, related to the orientation of the C-D bond (141, 142):

$$\Delta\nu\left(\theta\right) = \frac{3QSC}{4} S_{CD}\left(3\cos^2\theta - 1\right) \tag{2.72}$$

where θ is the orientation between the normal to the bilayer and the magnetic field, QSC is the quadrupole splitting constant and the order parameter S_{CD} is defined as:

$$S_{CD} = \frac{1}{2}\left\langle 3\cos^2\gamma - 1\right\rangle \tag{2.73}$$

where γ is the instantaneous angle between the C-D bond and the normal to the bilayer. The $\langle\rangle$ brackets denote an average orientation over time, to allow for rotations around the bilayer normal and thus obtain an average over all the chain conformations. A segmental order parameter, often called local molecular order parameter, S_{mol}, defined as $S_{mol} = \frac{1}{2}\left\langle 3\cos^2\alpha - 1\right\rangle$ can be calculated from S_{CD} from the relation $S_{mol} = -1/2 S_{CD}$ (142, 143). Here α is the angle between the segment direction and the bilayer normal and the $\langle\rangle$ brackets denote an average orientation over time. The segment direction is normal to the plane defined by the two C-D bonds of a $-CD_2-$ group of the lipid tail. S_{mol} is thus a measure of the average orientation of the chain segment to which the two deuterium atoms are attached.

A value of $\langle S_{CD}\rangle$, where the $\langle\rangle$ brackets denote an average over all the C-D bonds of the lipid tail, can be directly obtained from a ^{2}H NMR experiment where all the acyl-chain protons have been replaced by deuterions, from the first moment M_1 of the

^{2}H NMR spectrum with lineshape $g(\omega - \omega_0)$ (ω is frequency, ω_0 is Larmor or central frequency) (141, 143, 144):

$$M_1 = \frac{\int_{-\infty}^{+\infty} (\omega - \omega_0)\, g\,(\omega - \omega_0)\, d\omega}{\int_{-\infty}^{+\infty} g\,(\omega - \omega_0)\, d\omega} = A_1\,(2\pi)\,\langle(\delta\nu)\rangle = A_1\,(2\pi\nu_q)\,\langle S_{CD}\rangle \qquad (2.74)$$

where A_1 is a constant and $\langle(\delta\nu)\rangle$ is the average quadrupole splitting.

The order parameters of the lipid tails are intimately related to the thermodynamic phase of the lipid. Bilayer phase transitions take place with structural changes that often include a change in lipid tail order parameters, and thus of $\langle S_{CD}\rangle$, $\langle(\delta\nu)\rangle$ or M_1. Thus, the different phases should have a distinct ^{2}H NMR spectrum. Therefore, ^{2}H NMR is often applied to determine phase boundaries in phase diagrams (143–145). As will be discussed in Sec. 2.6.3 and Sec. 2.6.4, NMR is also frequently used for obtaining dynamical properties of lipids or to identify phase coexistence in bilayers. Another relevant application of ^{2}H NMR is the study of cholesterol orientation in a bilayer (146).

2.6.3 Dynamical Properties

The two most frequently used experimental methods to determine lipid lateral self-diffusion coefficients are FRAP (Fluorescence Recovery After Photobleaching) and, more recently, pfg-NMR (pulsed field gradient NMR).

In FRAP all lipids are first labeled with a fluorescent tag. A small group of the lipids are then photobleached (photochemical destruction of the fluorophore) with a light pulse. As a result, the fluorescence intensity of the group of photobleached lipids is zero. The fluorescing lipids (those that were not photobleached) diffuse throughout the sample and replace the non-fluorescent probes in the bleached region until eventually uniform fluorescence intensity is restored. One can demonstrate that under certain assumptions the lipid lateral self-diffusion constant is proportionate to $R^2/\tau_{1/2}$, where R is the radius of the photobleached group of lipids and $\tau_{1/2}$ is the time required for the bleach spot to recover half of its initial integrated intensity.

The pfg-NMR technique is comparatively more intricate. In short, during the NMR experiment the magnetic field is not kept uniform in the bilayer, but pulses continuously induce opposite magnetic field gradients. As a result, spins are constantly dephased and rephased. The bilayer is oriented with respect to the magnetic field such that the $3\cos^2\theta - 1$ term in Eq. 2.72 is zero. When this is the case, the line broadening disappears and the spin echo of the rephased transverse magnetization can be precisely observed. Due to translational diffusion the spin echo is attenuated. One can prove that the spin echo amplitude displays a mono-exponential decay with respect to the self diffusion coefficient of the lipids (147, 148).

The diffusion of DMPC, CHOL, and DOPC in single-component, binary and ternary bilayers has been studied using FRAP, pfg-NMR, or both (149–153). When the different experimental techniques are applied, they generally give similar results within the same order of magnitude. From ^{2}H NMR relaxation measurements one can obtain axial rotational diffusion of lipids. As will be discussed in Sec. 2.6.4, diffusion experiments are often used to identify phase coexistence in bilayers.

2.6.4 Lateral Organization

The lateral organization of lipid bilayers has received considerable attention and is a debated topic in the scientific community. The interest for the lateral organization of model lipid bilayers originates from the idea that if lipid bilayers spontaneously organize in coexisting domains (or phases) with different compositions and properties, these domains (phases) might attract specific proteins and interact in a specific way with one another. Even if the relevance of this hypothesis to real biological membranes is unproven, this model is palatable, and has yielded a whole range of experiments to study/proof the lateral heterogeneity of model lipid bilayers, which often lead to very different, sometimes opposite, conclusions (154–159). Apart from this, the issue of lateral organization is important to determine phase diagrams correctly (160).

Two key points are to be considered: when comparing between different experimental techniques one should consider the length and time scales at which they can observe phase coexistence. Secondly, every lipid mixture is different.

Fluorescence-based methods like fluorescence microscopy have often been used to study the lateral organization of binary DMPC-CHOL mixtures (161), DMPC (DPPC)-DOPC mixtures (162) and in ternary mixtures of DPPC-DOPC and CHOL (163–166). In binary mixtures of A and B, fluorescence intensities of a probe C, which resembles B, showing sudden jumps as function of B concentration, has often been interpreted as a sign of a regular distribution of B in A. This method has often been applied to prove the existence of regular cholesterol distributions in DMPC-cholesterol mixtures (167–169). Recently, experiments relying on fluorescence techniques started being used to examine whether proteins would preferentially choose one phase if the bilayer displays phase coexistence (170). The major disadvantage of fluorescence methods is that the lipids need to be labeled with a fluorescent probe, while it has been shown that, for example, the phase coexistence may occur as an artifact caused by the probes. Therefore other methods have been explored.

When, for example, in a binary bilayer two phases X and Y occur, each at given conditions, and when both phases have a ^{2}H NMR spectrum that significantly differ from one another, ^{2}H NMR is often used to study phase coexistence of X and Y. Therefore experimentalists check whether under certain conditions the NMR spectrum contains signatures of both the X and the Y spectrum. If this is the case, they conclude that X coexists with Y. The phase boundaries are detemined by the conditions for which the last tracks of X or Y are present in the NMR signal. Using

this technique, many two-phase regions have been identified in the phase diagrams of binary and ternary bilayers. However, and this is certainly true for binary mixtures, many two-phase regions have not been confirmed with other techniques like diffraction. This is probably because this NMR-based methodology does not distinguish between a phase coexistence and a gradual transition from one phase to another. NMR has been applied on DMPC (DPPC)-CHOL systems (145, 171), DPPC-DOPC systems (172) and DPPC-DOPC-CHOL systems (165, 173–175). The principle of NMR spectrum superposition is also applied to draw the tie lines in the phase coexistence region (174). A similar method to detect phase separation is applied using Raman spectroscopy where the lipid vibrational spectrum is detected, and the results agree well with NMR (176)

When in a pfg NMR experiment the spin echo amplitude attenuation cannot be fitted to a monoexponential decay as function of one diffusion coefficient, but requires a fit to a biexponential decay as function of two diffusion coefficients, then it could indicate that the lipid domain comprises two domains. This has been exploited to study phase coexistence in ternary DPPC-DOPC-CHOL bilayers and to calculate the diffusion coefficients of the lipids in both phases (153).

In the literature, three criteria are instrumental in determining the coexistence of phases using X-ray: 1) the existence of two lamellar repeat spacings D in SAXS 2) two chain-chain correlation spacings in WAXS and 3) possibility to deconvolute the angular distribution of the scattering intensity, which is related to the orientational order parameter of the tails, into scattering from two separate chain distributions. Hence, X-ray diffraction detects phase coexistence of two phases (regions) with different thickness, different packing or different tail tilt, respectively. X-ray has been applied to study phase coexistence in DMPC (DPPC)-CHOL (177, 178) and DPPC-DOPC-CHOL systems (179). This technique was also used to detect cholesterol clusters in biological membranes (180).

Another technique which has been applied to prove the existence and to extract the size of cholesterol clusters in DMPC bilayers is FRET (181, 182), which is explained in more detail in Sec. 2.6.5.

In the final analysis, it is crucial to note that the properties of lipid bilayers are very different from the properties of lipid monolayers. For example, a phase coexistence may exist in a binary lipid monolayer, but not in the corresponding bilayer.

2.6.5 Lipid-Mediated Protein-Protein Interactions

To study the indirect protein-protein interactions, transmembrane proteins have been designed without specific helix-helix recognition motifs, without hydrophilic residues in the transmembrane region and showing no surface complementarity. Another reason why membrane proteins have been synthesized is because, although an estimated 30 to 40 % of all proteins are membrane proteins, only 1% of the known proteins are membrane proteins. This is because X-ray crystallography, the usual

method to study protein structure, cannot be applied to a membrane protein embedded in the membrane. Today one can unravel the structure of a membrane protein with solid-state NMR. Outside the membrane, the protein would have a very different configuration. Without knowing the structure of the membrane proteins it is hard to even find out whether a protein shows mismatch with respect to the bilayer.

As an example, the so-called WALP peptide with the following residue sequence has been synthesized: Acetyl-GWW$(LA)_n$LWWGC-NH_2. The acetyl and amide group are hydrophilic, because they can be involved in hydrogen bonds, while the amino acid residues are all hydrophobic. By varying n, one can vary the hydrophobic length of the peptide. The peptides are synthesized by linking the amino acids in the desired sequence via a condensation reaction (14, 26). Solutions of lipids and peptides are mixed in the desired peptide/lipid ratio, hydrated after evaporation of the solvents, and via the hydrophobic self-assembly process, multilamellar vesicles containing the proteins are formed. Using FTIR (Fourier Transform Infrared Spectroscopy) one can check whether the proteins are effectively in the bilayer in an alpha configuration. Via titration one can add a specific number of proteins to a membrane. The synthetic peptides serve as a model for intrinsic membrane proteins.

A popular method to provide information about intra- (molecular structure) and inter- (molecular complex) molecular distances is Fluorescence (or Förster) Resonance Energy Transfer (FRET). During a FRET experiment, the radiation-less dipole-dipole energy transfer between a donor and an acceptor fluorescent label is analyzed. The proteins are thus first labelled with a donor and an acceptor fluorescent label. Natural amino acid residues of proteins, such as tryptophan (W), can be utilized as fluorescent label. Tryptophan is then used as donor. The advantage of this method is that it doesn't require an extra label which might significantly perturb the system. The peptides also require, however, to be labeled with an acceptor, for example, pyrene. Both acceptor and donor need to be dipoles. During a FRET experiment, the donor is excited with light. Due to the dipole-dipole interaction, an energy transfer takes place from the donor to the acceptor. The efficiency of this transfer, E, can be calculated from quantum theory and is extremely sensitive to the separation distance, R, between the fluorophores:

$$E = \frac{1}{1 + \left(\frac{R_0}{R}\right)^6} = 1 - \frac{\tau_{DA}}{\tau_D} \tag{2.75}$$

where R_0 is the Förster distance. R^6 represents the strength of the dipole-dipole interaction as function of distance. The occurrence of the energy transfer manifests itself through quenching of donor fluorescence and a reduction of the fluorescence lifetime, accompanied also by an increase in acceptor fluorescence emission. By measuring the donor fluorescence lifetime in the presence of an acceptor, τ_{DA}, it is possible to determine the distance separating donor and acceptor molecules. τ_D is the donor fluorescence lifetime in the absence of an acceptor.

In experimental studies, an increase in FRET efficiency for proteins with hy-

drophobic mismatch with respect to the FRET efficiency for proteins matching the bilayer has been measured (32), suggesting an increase in attractive protein-protein interactions. The experiments do not tell us, however, where the increase in FRET efficiency comes from. For example, do the proteins form one cluster or do they all form small oligomers? Therefore, a simulation-based fitting method has been developed for the analysis of the protein association. In this model proteins are considered cylinders. Parameters of this model include tilt and degree of clustering. By fitting the parameters such that the experimental energy transfer as a function of the ratio between labeled and unlabeled proteins is reproduced from the simulation, one can obtain an estimate of the protein tilt and the degree of protein clustering (31, 183).

From FRET experiments it has been concluded that hydrophobic mismatch and/or the addition of cholesterol induces (lipid-mediated) protein-protein aggregation (31–35).

2.7 Simulation Methods to Calculate Membrane Properties

In principle it should be possible to determine all experimental parameters described in Sec. 2.6 from all-atom molecular simulations, and, to a lesser extend from mesoscopic simulations, given the experimental conditions, like bilayer type and composition, hydration level, temperature, pressure, etc., are identical. Indeed, once the bilayer is in equilibrium, the density distribution of every atom (or of every structural group, bead, etc.) can be sampled from which important properties like bilayer thickness (typical values are 25-50 Å), hydrophobic thickness (typical values are 15-40 Å), etc., can directly be calculated. The lipid order parameters can be computed using Eq. 2.73. The average area per lipid of a single-component bilayer (typically between 40 and 75 Å^2) is just the total average area divided by half the number of lipids (provided no lipid flip-flop between bilayer leaflets has taken place).

From the average total area and the fluctuations in the total area one can compute the area compressibility κ_A (often given in dyn/cm with 1JÅ^{-2}= 10^{21}dyn/cm), which is a measure of the energy required to expand the bilayer by a given area, and is intimately related to the permeability of the membrane (103):

$$\kappa_A = k_B T A_t / \left\langle \delta A_t^2 \right\rangle \tag{2.76}$$

with A_t the total bilayer area and $\langle \delta A_t^2 \rangle$ the mean square of the fluctuations in the total area. The molecular origin of this expansion energy comes from the unfavorable contact between water and hydrophobic lipid parts. Typical values for a lipid bilayer vesicle in the liquid phase range from 20 to 2000 dyn/cm, which corresponds to 0.5 to 5 k_BTÅ^{-2} at physiological temperatures. This means that fluctuations in the thermal energy, which are of the order of k_BT, can easily expand the bilayers.

The polymer brush model (127) relates the area compressibility to the bilayer bending (or curvature) modulus, κ_C (in J), which is the energy required to deform the bilayer from its intrinsic curvature to some other curvature:

$$\kappa_C = (1/24)\kappa_A \left(PtP - 10\ \mathring{A}\right)^2 \tag{2.77}$$

In short, one can understand this relation by noting that to bend a bilayer one has to stretch the outer part. Typical values of the bending modulus range between 5 and 30 10^{-20} J (or 10 to 70 k_BT) at physiological temperatures. Assuming the bilayer to be a curved sheet, one can also extract the bending modulus and the surface tensions from the Fourier transform of the bilayer height fluctuations:

$$\left\langle \left| h_F\left(q\right)^2 \right| \right\rangle = \frac{k_BT}{A_t\left(\kappa_C q^4 + \gamma q^2\right)} \tag{2.78}$$

where $h_F\left(q\right)$ can be obtained from simulations by Fourier transforming $h\left(n_x, n_y\right)$, which is the bilayer height function calculated on a grid. The surface tension γ (in J$\mathring{A}^{-2}$), is defined as the change in Gibbs free energy per surface area (the value for an unconstrained bilayer is typically zero) :

$$\gamma = \left(\frac{\partial G}{\partial A}\right)_{P,T,n} \tag{2.79}$$

Let us note that the surface tension, the area compressibility and the bilayer Gibbs free energy are related via:

$$\kappa_A = A_t\left(\frac{\partial \gamma}{\partial A}\right)_{P,T,n} = A_t\left(\frac{\partial^2 G}{\partial A^2}\right)_{P,T,n} \tag{2.80}$$

The pressure tensor can be calculated (69) and from this the bilayer surface tension can again be extracted, as it is defined as the integral of the difference between the normal and the lateral component of the pressure tensor:

$$\gamma = \int_{z_1}^{z_2} \left[P_N\left(z\right) - P_L\left(z\right)\right] dz \tag{2.81}$$

where z_1 and z_2 are positions sufficiently far from the bilayer-water interface. Let us indicate that molecular simulations give a direct access to properties which are difficult to measure experimentally, for example, the lateral pressure profile $P_L(z)$.

The lipid lateral self-diffusion coefficient, D_L (in cm^2s^{-1} (values are typically of the order 10^8 cm^2s^{-1} in the liquid phase), is computed with the Einstein formula expressing that after a certain time, the mean square displacement grows linearly with time:

$$D_L = \lim_{t\to\infty} \frac{1}{2Dt} \left\langle \left|\mathbf{r}\left(t\right) - \mathbf{r}\left(0\right)\right|^2 \right\rangle \tag{2.82}$$

where D is the dimensionality, which is two in the plane of the lipid bilayer, t the time, $\mathbf{r}$ the vector position of the lipid and $\langle \left|\mathbf{r}\left(t\right) - \mathbf{r}\left(0\right)\right|^2 >$ the mean square displacement of a lipid.

Phase transitions can be quantified by simulating the heat capacity as function of the temperature from fluctuations in the enthalpy:

$$C_p(T) = \left(\frac{d\langle H\rangle}{dT}\right)_P = \frac{\langle H^2\rangle - \langle H\rangle^2}{RT^2} = \frac{\left\langle (\delta H)^2 \right\rangle}{RT^2} \tag{2.83}$$

Phase coexistence can be readily observed or simulated using the so-called Gibbs-ensemble method. Alternatively, one can calculate the chemical potential for a series of phase points and determine the phase coexistence by finding the points in state space where two phases have the same chemical potential, pressure and temperature (99).

When proteins are embedded into the bilayer one can observe, or quantify, (preferential) protein-lipid interactions. Lipid-mediated protein-protein interactions can also directly be observed and quantified by analyzing the contributions to the potential of mean force between proteins (184):

$$\mathrm{PMF}\left(\xi\right) = -k_B T \ln\left(P\left(\xi\right)\right) \tag{2.84}$$

where ξ is the distance between the two proteins and $P\left(\xi\right)$ the probability to find the proteins at a given distance. The potential of mean force is the reversible work required to bring two proteins from infinity to a distance ξ.

Chapter 3

Molecular Simulation Study of Lipid-Mediated Protein-Protein Interactions

Recent experimental results revealed that lipid-mediated interactions due to hydrophobic forces may be important in determining the protein topology after insertion in the membrane, in regulating the protein activity, in protein aggregation and in signal transduction. In this chapter, we use a mesoscopic model of a lipid bilayer with embedded proteins, which we study with dissipative particle dynamics, to gain insight into the lipid-mediated interactions between two intrinsic membrane proteins. Our calculations of the potential of mean force (PMF) between transmembrane proteins show that hydrophobic forces drive long range protein-protein interactions and that the nature of these interactions depends on the length of the protein hydrophobic segment, on the three dimensional structure of the protein and on the properties of the lipid bilayer. To understand the nature of the computed PMFs, the concept of hydrophilic shielding is introduced. The observed protein interactions are interpreted as resulting from the dynamic reorganization of the system to maintain an optimal hydrophilic shielding of the protein and lipid hydrophobic parts, within the constraint of the flexibility of the components. The results presented in this chapter could lead to a better understanding of several membrane processes in which protein interactions are involved.

3.1 Introduction

For complex biological systems, questions concerning their functioning should be answered from the principle that their properties are not only related to the individual behavior of each component but also to the interactions between them. This is particularly true for biological membranes and hence it is important to invoke the

collective nature of the system for the study of membrane processes. An important membrane process that received increasing attention over the last years is the lipid-mediated interaction between integral membrane proteins. The results from a number of investigations have pointed out that the composition of the lipid membrane and the hydrophobic matching between the lipid bilayer hydrophobic thickness and the hydrophobic length of the transmembrane proteins are important physical properties that regulate the mechanism of lipid-protein interaction in biomembranes. Moreover, a protein-induced bilayer deformation could interact with a bilayer deformation due to one or several other proteins and this could result in indirect lipid-mediated protein interactions (31). These could play a greater part in protein topology, protein activity and membrane processes than is presently supposed. Proteins or other membrane inclusions, like e.g. cholesterol, affect the lipid metabolism and transport, which have a role in diseases (51). On the other hand, lipids influence the distribution and the function of the proteins (185).

The insertion of a protein in a membrane is mostly done with the help of a translocon and, to a lesser extent, spontaneously. Both experiments and thermodynamic considerations lead to the conclusion that an increasing side chain hydrophobicity of a membrane protein drives the equilibrium towards a bilayer insertion (9). Once inserted, the proteins fold and associate in a certain topology. The driving force behind the first step of the protein folding, i.e. from an unfolded protein towards a more compact, sometimes helical, molten globule, is primarily driven by hydrophobic-hydrophilic interactions. Although the translocon plays an important role in determining the protein topology, it is observed that the length of the protein hydrophobic segment could partly determine the topology and hence the function of the membrane protein (9, 10).

The changing nature of the lipid bilayer in the Golgi apparatus has been proposed as an agent for protein segregation in the membrane so that they are excluded from budding vesicles (186–188). Cornelius et al. (189, 190) report that the hydrophobic matching is a crucial parameter in regulating optimal Na, K-ATPase activity. Moreover, the activation entropy and enthalpy of Na, K-ATPase and Na-ATPase reactions together with the temperature dependence of the Na, K-ATPase activity as well as of the Na-ATPase reactions depend not only on the amount of cholesterol present in the membrane but also on the lipid chain lengths. Hinderliter et al. (191) suggest that the enormous lipid variety present in the eukaryotic membrane could play an important role in signal transduction as proteins are observed to interact preferentially with a specific lipid type. Of particular interest are the G-protein-coupled receptors (GPCR), which are essential components of cellular signaling pathways, as they represent by far the largest class of targets for therapeutic agents. With the help of the fluorescence resonance energy transfer (FRET) technique more and more GPCRs are detected in homo- or heteromeric complexes. Because GPCRs are major pharmacological targets, the existence of oligomers should have important implications for the development of new drugs, which up till now have been designed with

the assumption that these receptors are monomeric (12, 13). Previous studies using electron microscopy have shown that bacteriorhodopsin aggregates in bilayers only when there is a very large hydrophobic mismatch (42). It was also determined by X-ray diffraction that bacteriorhodopsin monomers form a very tight trimeric unit and that the contact between the trimers in the membrane plane is almost exclusively mediated by lipids (192). Botelho et al. (32) showed, using the FRET technique, that the hydrophobic mismatch is the main physical mechanism that regulates the oligomerisation of rhodopsin in membranes and that hydrophobic matching indirectly modulates the activity of rhodopsin. Previously, Brown (193) observed that the lipid bilayer modulates the rhodopsin function because the bilayer has a direct influence on the energetics of the conformational states of rhodopsin. Similar results were obtained by Kota et al. (194) and Mansoor et al. (195).

There is very little information regarding the thermodynamic stability, quantitatively described by the interaction free energy, of transmembrane protein-protein interactions in a biological membrane. Most free energies of helix-helix dissociation have been measured in detergent micelles (e.g. the work of Fisher et al. (196), Fleming et al. (197)), however a first approach that allows quantitative measurements of alpha-helical membrane protein interactions has recently been proposed (198). A method to quantify the helix-helix binding affinities in both micelles and lipid bilayers has been developed by Lomize et al. (199). Several continuous models have been developed to calculate quantitatively the indirect lipid-mediated interactions between intrinsic membrane proteins. Among them are approaches based on statistical mechanics integral equation theories developed for dense liquids (200, 201), chain packing theory (202), elasticity theory (203) and elasticity theory combined with director field theory (204).

In the last decade, the first articles in which molecular dynamics (MD) simulations were applied to better understand the nature of several membrane processes have been published. Petrache et al. (205) performed MD simulations of both the dimer and monomer form of glycophorin A in lipid bilayers with different bilayer thickness, which they found to be the most relevant property on which the helix tilt angle, the helix crossing angle and the helix accessible volume depend. With the help of extended MD simulations, Deol et al. (206) studied the interactions of several membrane proteins with phosphatidylcholine bilayers. Nielsen et al. (81) used MD to study a coarse-grained (CG) model of a protein embedded in a mixed lipid bilayer and found peptide induced lipid domain formation as an effect arising solely from hydrophobic mismatch. The MD simulations of Smeijers et al. (207) showed that coarse-grained membrane proteins with hydrophobic mismatch aggregate and that the size of the aggregates depends both on the hydrophobic mismatch and on the protein shape. Hénin et al. (58) estimated the free energy of alpha-helix dimerization of the transmembrane region of glycophorin A by using MD simulations. The coupling between the retinal conformational change and the large scale rhodopsin conformational change which results in G-protein activation and signal amplification throughout the cell has also

been studied by MD simulation (208). This study points out that the efficiency of the coupling has, most likely, a strong dependence on the nature of the lipid bilayer.

However, because most of the described membrane processes happen at the mesoscopic length and time scale, i.e. more than 1-1000 nm, ns, and involve the collective nature of the system, atomistic simulation methods are still too computationally expensive. Hence mesoscopic models of the phospholipids and the embedded proteins have been developed and studied by molecular dynamics and dissipative particle dynamics (DPD) techniques (reviewed in Venturoli et al. (61)). Venturoli et al. studied the protein induced bilayer deformations and the lipid induced protein tilting for proteins with a different hydrophobic length (80). Their results show that the protein induced bilayer perturbation is a function of the hydrophobic mismatch between the protein hydrophobic length and the pure lipid bilayer hydrophobic thickness and that proteins may tilt when embedded in too thin a bilayer. Recently, Periole et al. (209) developed a mesoscopic model to investigate how the physicochemical properties of a phospholipid bilayer affect the self-assembly of rhodopsin.

We have adopted the DPD simulation method and the previously developed model for lipid bilayers with embedded proteins (80) to study the mechanism by which hydrophobic mismatch induces lipid-mediated protein-protein interactions.

3.2 Model and Simulation Methods

In this work we considered proteins of three different sizes: N_p=4 (diameter D=7.8 Å), N_p=7 (diameter D=13.5 Å) and N_p=43 (diameter D=32.0 Å). The smallest protein could represent an α-helical synthetic peptide (diameter D=4-7 Å), the intermediate one a β-helix protein like gramicidin A (diameter D=11-27 Å) and the biggest one a bacteriorhodopsin protein (consisting of 7 α-helical peptides associated into a bundle, diameter $\approx$ 45 Å).

Fig. 3.1 shows a snapshot of two of the systems we studied: (a) two proteins of size N_p=7 and n_{tp}=8 embedded in the lipid bilayer and (b) two proteins of size N_p=43 and n_{tp}=8 embedded in the lipid bilayer. The water particles are not shown for clarity.

Because we are interested in addressing the question of whether hydrophobic mismatch may induce lipid-mediated protein interactions, we performed simulations with proteins of different hydrophobic length (n_{tp}=4, 6 and 8) with the hydrophobic mismatch, d, defined as:

$$d = h_P - h_L \quad (3.1)$$

where h_P is the protein hydrophobic length and h_L is the mean hydrophobic thickness of the unperturbed pure lipid bilayer. In the bilayer considered here, h_L=(23.6 $\pm$ 0.2) Å and the values of h_p for each value of n_{tp} are reported in Table 3.1, together with the corresponding hydrophobic mismatch d.

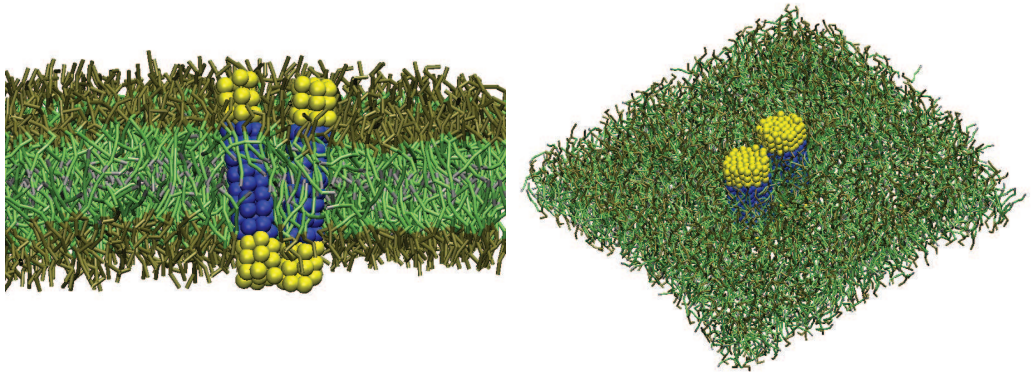

(a) N_p=7 (b) N_p=43

Figure 3.1: Snapshot of the lipid bilayer with two embedded proteins of size $N_p = 7$ (a) and $N_p = 43$ (b). The hydrophilic and the hydrophobic beads of the proteins are depicted in yellow and in blue, respectively. The lipid headgroups are depicted in brown, the lipid tails in green and the terminal beads of the lipid tails in grey.

Table 3.1: Values of the protein hydrophobic thickness h_P and the corresponding mismatch d (Eq. 3.1) for different numbers of protein hydrophobic beads n_{tp} per aliphatic chain.

n_{tp}	h_P (Å)	d (Å)
4	13.6	-10.0 ± 0.2
6	22.6	1.0 ± 0.2
8	31.7	8.1 ± 0.2

The mesoscopic model described is studied with the dissipative particle dynamics (DPD) simulation technique (87). Because unconstrained lipid bilayers are essentially in a tensionless state (98), we reproduced this condition by simulating the system in the NγVT ensemble, where γ is the surface tension of the lipid bilayer. To do so we used a hybrid scheme which combines the DPD and the Monte Carlo (MC) simulation methods. The DPD method is used to evolve the positions of the beads and the MC method to impose a given value to the surface tension of the bilayer (61, 91), and in particular the value $\gamma = 0$. For a detailed description of the model, the simulation method and its applications, we refer to Chapter 2 and to relevant articles (71, 80, 210).

To avoid finite size effects, a sufficiently large bilayer patch should be simulated. Based on the calculation of the decay length of single protein bilayer perturbations (80), we have chosen a bilayer of area 635 nm^2, which contains around 2000 lipids. To assure sufficient hydration, 25 water beads per lipid were considered, for a total of 50000 water beads. The volume of the simulation box is chosen such that the

overall bead density is ρ=3. The simulations were performed at the dimensionless temperature of 0.7 (approximately 60°C), i.e. when the hydrated phospholipid bilayer is well in the fluid phase (80).

3.2.1 Influence of Hydrophobic Mismatch

To investigate whether hydrophobic mismatch can induce lipid-mediated protein-protein interactions, DPD simulations of three different bilayer systems with two embedded proteins, both of size N_p=7 (D=13.5 Å), at negative, d=(-10±0.2) Å, negligible, d=(1±0.2) Å, and positive, d=(8±0.2) Å, mismatch conditions were performed. The two proteins were initially inserted in the membrane at the maximum distance (126 Å) from each other.

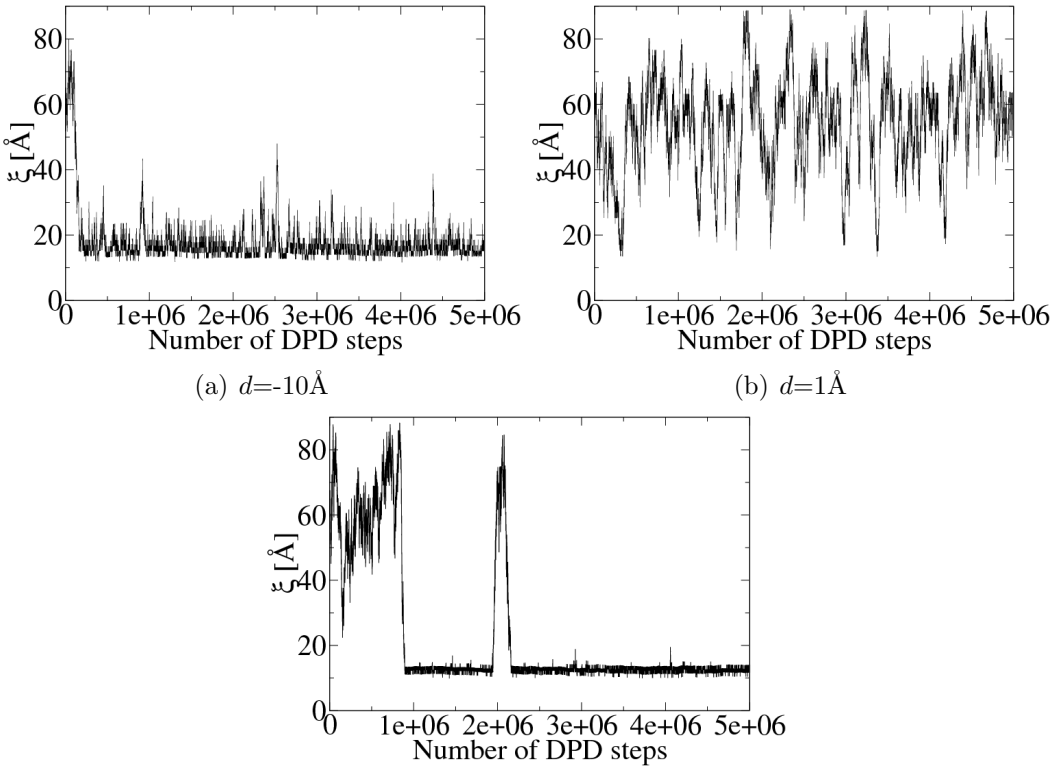

(a) d=-10Å (b) d=1Å

(c) d=8.1Å

Figure 3.2: Time-series (in DPD-steps) of the distance between two proteins with size $N_p = 7$ with negative (a), zero (b) and positive (c) mismatch.

Fig. 3.2 shows the time evolution of the distance between the protein centers of mass during the simulation. Fig. 3.2(a), which represents the time evolution of the distance between two proteins with negative mismatch, suggests that both proteins freely diffuse in the lipid bilayer until they are at a distance of 40-45 Å from each

other. From this point, they appear to be strongly attracted to each other, and, once together, they remain in each other's neighborhood, without forming a stable physical dimer. Here we use the term stable physical dimer to indicate that the proteins are at close contact, i.e., no lipids are present between the proteins. Fig. 3.2(b) shows that the motion of proteins with zero mismatch is a free diffusion in the lipid bilayer, and no attraction is observed. Proteins with positive mismatch (Fig. 3.2(c)), diffuse freely up to a distance of 35-40 Å after which they are strongly attracted to each other and form a stable dimer. Since the cut-off R_c of all acting forces is set to 6.64 Å in the model, no direct interaction can take place between the proteins if they are located at a distance larger than 6.64 Å. Moreover, since the degree of protein mismatch is the only difference between the three systems described, these results suggest that hydrophobic mismatch is a major driving force in lipid-mediated protein-protein interactions.

3.2.2 Potential of Mean Force Calculation

To quantitatively describe the lipid mediated interactions between the proteins we performed free energy calculations, focusing on the interaction between two equal proteins embedded in the lipid bilayer. We express the free energy of protein-protein interactions with respect to the collective variable $\xi(X_p, Y_p)$, which represents the distance in the xy-plane (i.e. the plane parallel to the lipid bilayer) between the centers of mass of the proteins. X_p and Y_p are the coordinates of the centers of mass of the proteins in the bilayer plane. Since the motion of the proteins in the direction perpendicular to the membrane plane is small and supposed not to be important in the description of protein-protein interactions, it is reasonable to restrict the collective variable to the membrane plane. The potential of mean force was computed in two steps.

First, an initial guess of the PMF as function of $\xi(X_p, Y_p)$ was obtained using umbrella sampling with a harmonic biasing potential centered on different values of the collective variable. The data generated by umbrella sampling calculations were unbiased and combined using the weighted histogram analysis method (WHAM) (211, 212). According to Roux (213) this is the most accurate approach for calculating free energy curves from biased distribution functions. During the umbrella sampling, simulations were performed in windows centered around N_W successive values of the reaction coordinate ξ_i (i=1,$\cdots$,N_W; ξ=$i\Delta\xi$) with the potential of the unbiased system $V_0(R)$ replaced by a modified potential $V_i(R)$ of the form:

$$V_i(R) = V_0(R) + V_i(\xi) = V_0(R) + \frac{1}{2}K_\xi \left(\xi - \xi_i\right)^2 \tag{3.2}$$

where R represents the coordinates of all the beads in the system. These simulations were performed in the NVT ensemble. To correctly recombine the different windows, the values of ξ_i and of the harmonic constant K_ξ should be chosen in such a way that

consecutive windows overlap. We found that the values K_ξ=10 k_BT/R_c^2 and $\Delta\xi_i$=0.2 R_c satisfy this requirement. The average unbiased total distribution function, $P^{\mathrm{ub}}(\xi)$, is obtained by solving the coupled WHAM equations:

$$e^{-\beta f_i} = \int P^{\mathrm{ub}}(\xi) e^{-\beta V_i(\xi)} d\xi \tag{3.3}$$

$$P^{\mathrm{ub}}(\xi) = \frac{\sum_{i=1}^{N_W} n_i P_i^{\mathrm{b}}(\xi)}{\sum_{j=1}^{N_W} n_j e^{-\beta(V_j(\xi)-f_j)}} \tag{3.4}$$

where f_i is the (initially unknown) free energy due to the biasing potential, n_i is the number of samples made in the i^{th} window, $P_i^{\mathrm{b}}(\xi)$ is the biased distribution of ξ in the i^{th} window and β=$1/k_BT$. Eq. 3.3 and 3.4 are solved self consistently, starting from an initial guess of f_i, until convergence is reached.

Because the PMF only provides a measure of the difference in free energy between two states, we imposed the PMF to evolve towards zero at large distances between the proteins.

The potential of mean force was then directly calculated from the reversible work theorem (184):

$$\mathrm{PMF}(\xi) = -k_BT \ln(P^{\mathrm{ub}}(\xi)) \tag{3.5}$$

It should be noted that Eq. 3.5 is only exact in the limit of zero protein density. For a system containing a finite protein density, correction terms should be added (214). However, as we consider only two proteins, Eq. 3.5 should hold.

In the second step of the PMF calculation, we used umbrella sampling during which simulations were performed around N_W successive values of the reaction coordinate ξ_i (i=1,$\cdots$,N_W) with a biasing potential $V_i(\xi)$ of the form:

$$V_i(\xi) = 100\left(1 - \left(\frac{1}{1+e^{-100(\xi-\xi_i+\Delta\xi_i)}} - \frac{1}{1+e^{-100(\xi-\xi_i-\Delta\xi_i)}}\right)\right) - \mathrm{PMF}(\xi)_{\mathrm{prev.it.}} \tag{3.6}$$

The first term in Eq. 3.6 is a deep potential well that forces the system to sample in the distance interval $[\xi_i - \Delta\xi_i, \xi_i + \Delta\xi_i]$ with $\Delta\xi_i = 1.3R_C$, while $\mathrm{PMF}(\xi)_{\mathrm{prev.it.}}$ is the PMF calculated at the previous iteration. By using this approach, we were able to reduce the number of windows by a factor of 10, compared with the harmonic biasing potential case. These simulations were performed in the NγVT ensemble, with γ=0. The unbiased distribution function, from which the PMF is calculated, was again obtained by solving the WHAM equations. This step was repeated, updating the PMF, until all the individual histograms of the windows showed a uniform distribution.

The proteins were manually inserted in the equilibrated pure lipid bilayer. For every protein distance (window), we first performed 20000 DPD-MC cycles in order to equilibrate the system at zero surface tension. In each cycle, it was chosen, with a probability of 70%, whether to perform a number of DPD steps. Otherwise an attempt was made to change the box aspect-ratio according to the imposed surface

tension value (γ=0). Data to calculate the PMF were collected after the equilibration period.

The WHAM equations were solved self-consistently starting from an initial value of the free energy constants $f_i = 0$. The iterations were repeated until:

$$\max_{i=1,N_W} |f_i^{\text{iter}} - f_i^{\text{iter}-1}| \leq 10^{-15}$$

.

3.3 Results and Discussion

3.3.1 Potentials of Mean Force

The PMFs as a function of the distance between the centers of mass of the protein pairs of size N_p=4, N_p=7, and N_p=43 are shown in Fig. 3.3(a), 3.3(b), and 3.3(c), for proteins with negative, d=-10 Å, negligible, d=1 Å, and positive, d=8 Å, hydrophobic mismatch conditions, respectively.

No Mismatch For a protein pair with zero or negligible hydrophobic mismatch (*dot-dashed lines*), the PMF is essentially zero, except at short distances between the two proteins, which means that there are no long range lipid-mediated interactions between the two proteins. At short distance, three minima occur in the free energy profiles of the protein pairs of size N_p=7 and N_p=43. These minima are at distances ξ=D, ξ=D+0.7R_c and ξ=D+1.4R_c (where D is the protein diameter). As 0.7R_c is about the diameter of a coarse grained lipid bead, we can, based on geometric arguments, assign these oscillations in the PMF to the free energy needed to remove the lipids that are in between the two proteins.

Interestingly, the number of minima depends on the diameter of the protein. For the protein pair of size N_p=4 there is only one minimum, at position D, corresponding with the physical dimer configuration. Our results suggest that the bigger the diameter of the protein, the more difficult it becomes to expel the lipid beads from between the two proteins and to form a physical dimer. This effect is comparable with the two-dimensional crystallization of molecules located between two parallel surfaces (215). For the protein pair of size N_p=43, the physical dimer configuration is very unstable and does not correspond to the absolute minimum of the free energy curve, as is instead the case for proteins of size N_p=4 and N_p=7, and a rather high free energy barrier (about $3k_BT$) needs to be crossed to go from the configuration with one lipid in between to the physical dimer. From this analysis of the PMF curves we can conclude that two proteins with zero mismatch diffuse randomly in the lipid bilayer and that, when they approach each other, they temporarily associate, but only if their size is sufficiently small (N_p=4 and N_p=7). However, the free energy in this dimer configuration is not sufficiently low to stabilize the dimer against thermal fluctuations (see also Fig.3.2(b)).

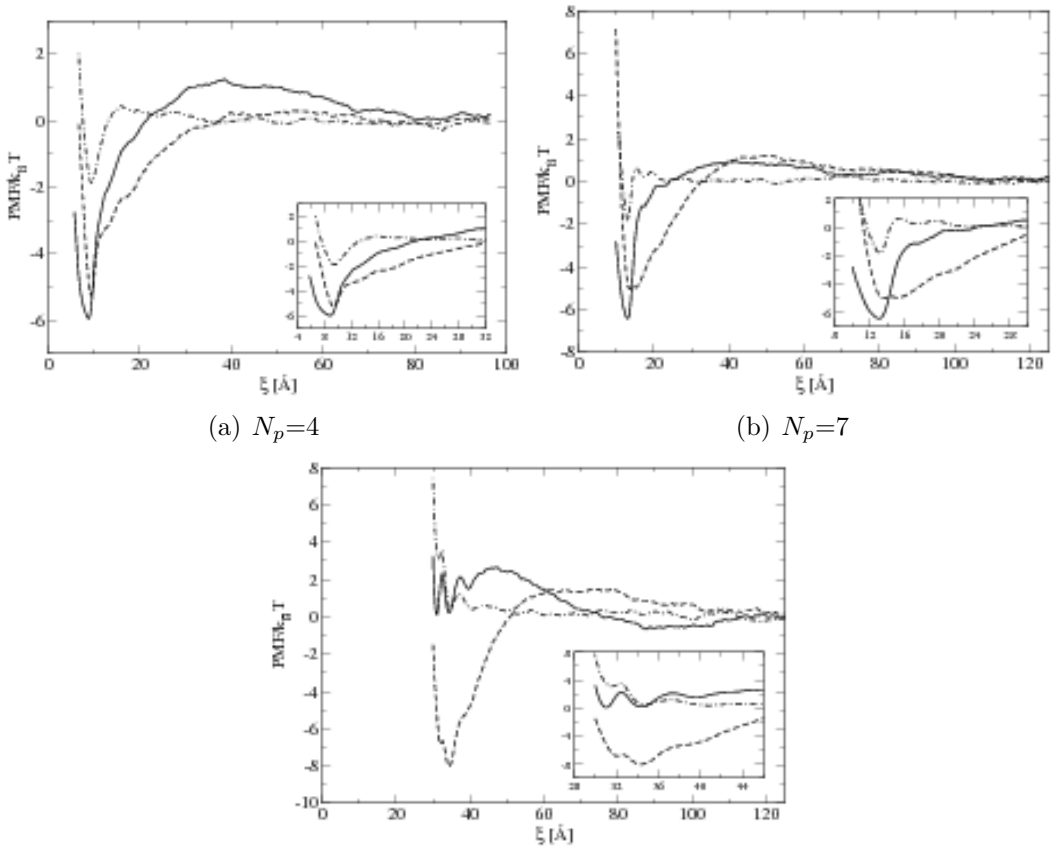

(a) N_p=4 (b) N_p=7

(c) N_p=43

Figure 3.3: Potential of mean force as a function of the distance between two proteins of size $N_p = 4$ (a), $N_p = 7$ (b) and $N_p = 43$ (c) with negative (*dashed line*), zero (*dot-dashed line*) and positive (*full line*) mismatch.

Negative Mismatch Proteins with negative mismatch interact with each other over a broad range of distances, with their PMFs (*dashed lines*) displaying a repulsive barrier at intermediate interprotein distances, followed by a broad and deep attractive minimum as the proteins get closer (but still at several R_c apart). At this point it is important to recall that there are no long range interactions explicitly included in the direct protein-protein interaction potential. In fact, all interactions are short range and repulsive. Comparison with the case of zero hydrophobic mismatch shows that the long range attractive interactions observed in the PMF are therefore induced solely by the hydrophobic mismatch. The negative mismatch causes a perturbation of the lipid bilayer. If the proteins are close to each other, the net perturbation of the surrounding lipids is less than the corresponding perturbation when the proteins are far from each other, explaining the long-range attractions between the proteins. Interestingly, the deformation of the lipid membrane at intermediate distances between the proteins

results in an unfavorable configuration. In section 3.3.3 we discuss the nature of these interactions in more detail as we introduce the concept of hydrophilic shielding. The height of the repulsive barrier increases slightly with increasing protein diameter ($\approx 0.2 k_B T$ for N_p=4, $\approx 1 k_B T$ for N_p=7, and $\approx 1.5 k_B T$ for N_p=43) while the range of the attractive interaction does not depend significantly on the protein diameter. This also holds for the range of the repulsive interactions.

The PMF of the protein pair of size N_p=4 is characterized by one absolute minimum of -5.2$k_B T$ corresponding to the dimer configuration, and two "shoulders" at inter-protein distance of D+0.7R_c and D+1.4R_c corresponding to two proteins with respectively one and two lipids in between. The PMF of the protein pair of size N_p=7 displays two local minima of value $\approx$-5.0$k_B T$. The first one corresponds to the physical dimer configuration. The second one most likely corresponds to the two proteins with one lipid bead in between, although this lipid bead cannot be situated on the axis linking the two centers of mass of the proteins because the distance between the two minima is much shorter than 0.7R_c. The separation of these two minima by only a small barrier ($\approx 0.1 k_B T$) and the broadness of the attractive region of the PMF reflect the instability of the physical dimer. Thermal fluctuations are sufficient to allow lipid beads to slip in between the proteins, thus breaking the physical dimer. The same considerations hold for the protein pair of size N_p=43, with the only difference that the absolute minimum (-8.0$k_B T$) does not correspond anymore to the physical dimer configuration and the physical dimer configuration (-6.8$k_B T$) is unstable.

To summarize, our results show that, due to lipid-mediated interactions, two proteins with negative mismatch experience a short and intermediate range strong attraction and a soft repulsion at larger interprotein distance.

Positive Mismatch In the case of positive mismatch, the PMFs (*solid lines*) show that the protein pairs of size N_p=4 and N_p=7 behave completely different than the protein pair of size N_p=43. The PMFs of the protein pairs of size N_p=4 and N_p=7 are both characterized by a long range weak repulsion with a barrier of about 1.0$k_B T$, followed by an intermediate and short range strong attraction towards a very stable physical dimer. The width, relative to the protein diameter, of the attractive part of the PMF decreases as the protein diameter increases. The physical dimer formed by the protein pair of size N_p=7 is slightly more stable than the dimer of the protein pair of size N_p=4, because a higher energy barrier has to be crossed to go from the dimer configuration to the configuration of two proteins with one lipid in between. Furthermore, the minimum corresponding to the physical dimer of the protein pair of size N_p=7 is slightly deeper (-6.5$k_B T$) than the corresponding minimum for the protein pair of size N_p=4.

The PMF curve of the protein pair of size N_p=43 reveals a completely different behavior. A broad attractive region appears at inter-protein distances between 88 and 105 Å, with a depth of about -0.6$k_B T$. This long distance attraction is also present for the protein pair of size N_p=4, albeit much narrower and shallower. A

high repulsive energy barrier is present at inter-protein distances between 47 and 88 Å, followed by an attraction as the distance between the proteins further decreases. The formation of the physical dimer is clearly hindered by the removing of the last two lipids in between the proteins, shown by the three minima at D and D+0.7R_c and D+1.4R_c. Hence, three energy barriers have to be crossed to reach the physical dimer configuration; first, the barrier of height 3.2k_BT, separating the minimum at long distance from the configuration with two lipids in between the proteins, then the barrier between D+1.4R_c and D+0.7R_c of height 0.6k_BT, and finally the barrier between D+0.7R_c and D, of height 2.0k_BT. The three barriers to be crossed for dissociation are 2.2k_BT, 2.0k_BT, and 1.2k_BT, respectively. As these barriers are relatively easy to cross, none of the free energy minima in this region is stable.

From these results, we can conclude that the interaction of a protein pair with positive mismatch strongly depend on the diameter of the proteins. Proteins that are rather small (N_p=4, N_p=7) repel each other slightly before forming a very stable physical dimer. Larger proteins (N_p=43) are slightly attracted when they are relatively far from each other towards an inter-protein distance of 88 Å (i.e. two times the diameter), but a short-distance repulsive interaction hinders the formation of the physical dimer configuration.

3.3.2 Discussion of Previous Models

The free energy profiles shown in Fig. 3.3 clearly indicate the presence of lipid-mediated protein-protein interactions, whose characteristics depend on the degree of mismatch and on the protein diameter. In an attempt to understand the relation between the nature of the protein-protein interactions, the mismatch condition and the protein diameter, it is instructive to compare our results with those obtained by other theoretical models.

Lagüe et al. (200, 201) applied the hypernetted chain integral equation formalism for liquids to different lipid bilayers and studied the lipid-mediated interactions between two hard repulsive cylinders. Their results show that a cylindrical inclusion induces a perturbation of the average radial lipid density over a distance of about 30 Å from the surface of the inclusion and that the characteristics of this perturbation depend on the type of lipid bilayer and on the diameter of the inclusion. For their model of a DMPC lipid bilayer, these authors observed a depletion layer close to the inclusion, where the lipid density is lower than in the bulk, followed by a lipid enriched region. The density in the depleted region decreases with increasing inclusion diameter. In the enriched region, the density increases with increasing inclusion diameter. However, while the relative range of the depletion decreases with increasing inclusion diameter, the absolute range of the perturbation remains the same. By calculating the PMF as a function of the distance between the two inclusions, these authors find that two inclusions first experience a repulsive interaction followed by an attraction at closer distances and that it is the perturbation of the average hydrocarbon density

around the proteins that gives rise to lipid-mediated protein interactions. Although in our simulations the absolute number of lipid beads as a function of the distance from the protein surface shows the presence of a depletion layer, we did not observe a decrease in lipid density since the membrane thickness around the protein is also changing, resulting in a constant density.

According to the theoretical model of Bohinc et al. (204), which combines elasticity theory with director field theory, the deformation of the lipid bilayer due to embedded rigid proteins showing mismatch induces an increase of the membrane elastic energy. The dimerization of two proteins showing positive or negative mismatch leads to a gain in this elastic free energy. Considering only membrane elastic effects leads to a membrane elastic free energy as a function of the distance between the two proteins which depends on the degree of mismatch, but not on the type of mismatch, i.e. PMF(ξ, d)=PMF($\xi, -d$). The PMF then displays only an intermediate distance attraction whose range is independent of the degree of mismatch and with a minimum which becomes deeper with increasing mismatch. Including director field theory in the free energy computation leads to long range interactions characterized by repulsion-attraction for the case of negative mismatch and only attraction for the case of positive mismatch. The proteins studied by Bohinc et al. (204) have a diameter of 14 Å and the cross-sectional area of their model lipids is 32.5 Å^2, hence their results can be compared with our results for N_p=7 (Fig. 3.2B) (although our model lipid gives an area per lipid of 60.4 Å^2 (80)). For proteins with negative mismatch and N_p=7 we also obtain repulsive-attractive interactions. However, according to our simulations, for the case of positive mismatch, the repulsive part, although smaller than in the case of negative mismatch, does not entirely disappear.

3.3.3 Hydrophilic Shielding

In this section we interpret and explain the features of the PMF curves shown in Fig. 3.3 in terms of hydrophobic and hydrophilic interactions. Due to the soft repulsive interactions, whose strength is given by the parameters a_{ij} in our model, the water beads, the lipids and the proteins tend to reorganize so that the hydrophobic beads of the proteins and the lipids are shielded from the water beads by the hydrophilic beads of the proteins and the lipid headgroups in the most optimal way. This regrouping is however constrained by the internal flexibility of the proteins and the lipids, i.e., by their bond bending rigidity.

To characterize the degree of screening of the hydrophobic parts of the lipids and the peptides from the polar environment of the solvent, we introduce the concept of hydrophilic shielding. For this purpose, we define the lipid head fraction as the average number of lipid head beads at a given position in the plane of the lipid bilayer in which the protein is embedded divided by the average number of lipid head beads of a pure bilayer without embedded proteins. The lipid tail fraction is defined in an analogous way for the lipid tail beads. The hydrophilic shielding parameter, defined

at every position in the plane of a lipid bilayer, is the ratio of the lipid head fraction and the lipid tail fraction, and it is a measure for the relative number of hydrophilic beads shielding the hydrophobic tail beads from the water at a given position. This parameter is one at sufficient distances from a protein. When the hydrophilic shielding parameter is bigger than one, the density of the lipid heads shielding the lipid tails present is higher than in the pure lipid bilayer.

Hydrophilic Shielding around one Protein

Fig. 3.4 shows the lipid head and tail fraction and the hydrophilic shielding parameter as a function of the distance from a single protein embedded in the lipid bilayer. Three different proteins were considered, all of size N_p=43, but with negative (Fig. 3.4a), zero (Fig. 3.4b) and positive (Fig. 3.4c) mismatch. In an unperturbed pure lipid bilayer the lipid head and tail fraction and the hydrophilic shielding parameter are on average one at every point in the bilayer plane. Fig. 3.4 shows that the presence of a protein perturbs the surrounding lipid organization and indicates how the lipids reorganize around the protein as function of the hydrophobic mismatch.

Around a protein with negative mismatch (Fig. 3.4a) the lipids reorganize by increasing the density of the lipid heads close to the protein surface, while the lipid tails point away from the protein surface. This region of high lipid head fraction is followed by a region of low lipid head fraction. Because the tails of the lipids close to the protein are pointing away from the protein, the region of low lipid head fraction contains a high lipid tail fraction. This results in a hydrophilic shielding parameter which is high in the vicinity of the protein (up to 1.6 at 5 Å) but which decreases to a minimum value of 0.96 at a distance of 31 Å from the protein surface. The shielding parameter then goes to one at larger distances. Around a protein with positive mismatch (Fig. 3.4c) the lipids reorganize in the opposite way. An undershielded region appears in the vicinity of the protein surface because the lipid heads regroup at a certain distance from the protein surface while the lipid tails point in the direction of the protein surface. The undershielded region of the bilayer is followed by a well-shielded region. The hydrophilic shielding parameter reaches a maximum value of 1.07 at a distance of 20 Å, after which it decreases towards one. When the lipids reorganize around a protein with zero mismatch (Fig. 3.4b), the lipid heads regroup close to the protein, resulting in a higher shielding in the vicinity of the protein. This effect is, however, smaller than in the case of negative mismatch. The overshielded region is not followed by a large undershielded region and the hydrophilic shielding parameter decays to one at shorter distance from the protein.

The reorganization of the lipids also leads to a change of the lipid bilayer thickness (80) and thus of the structure parameter (143). The lipid tail fraction as a function of the distance from the protein surface shows the same trend as the change in hydrophobic bilayer thickness around the protein as calculated in ref. (80). This implies that the reorganization of the lipids around a protein does not result in long

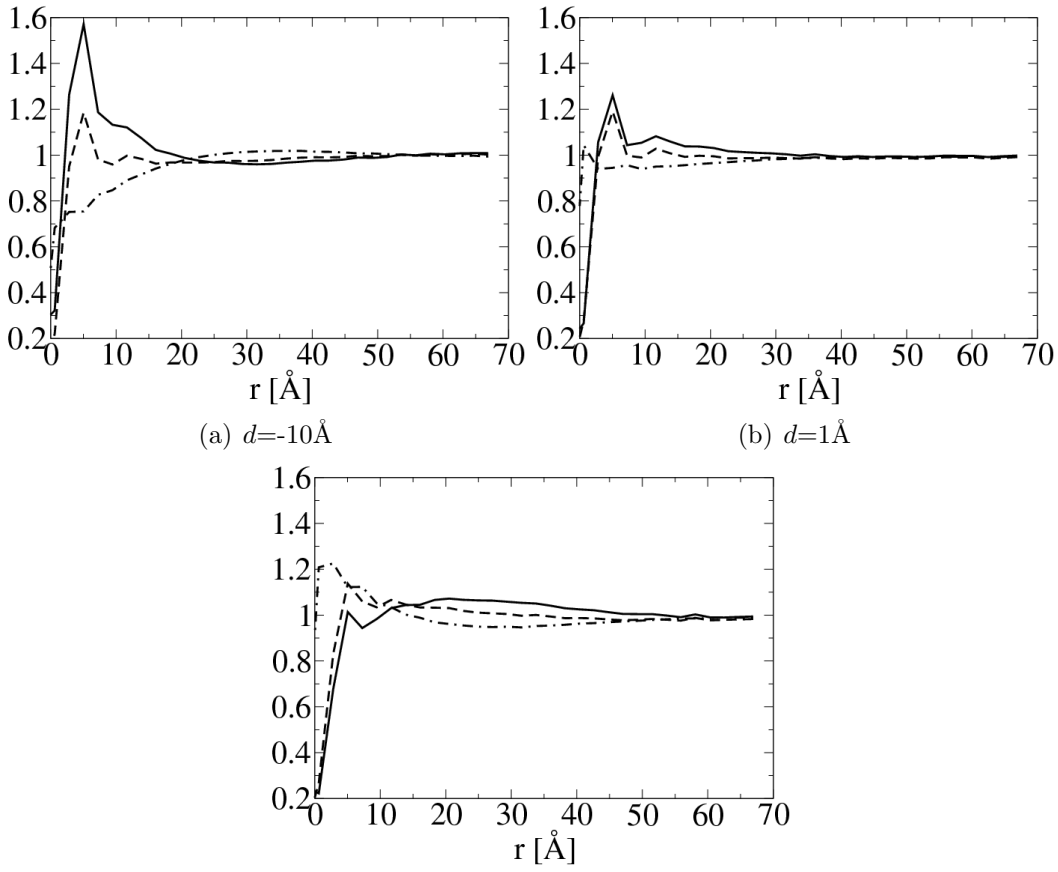

(a) d=-10Å (b) d=1Å

(c) d=8.1Å

Figure 3.4: Lipid tail fraction (*dot-dashed line*), lipid head fraction (*dashed line*) and hydrophilic shielding (*full line*) as a function of the distance from one protein of size $N_p = 43$ with negative (a), zero (b) and positive (c) mismatch.

range lipid tail density fluctuations. This was confirmed by our simulations (data not shown).

It is very important to note that the way the lipids reorganize around a protein in an optimal way may also strongly depend on the three dimensional structure of the protein. Hence, the results presented here are only valid for cylindrical proteins.

Hydrophilic Shielding around two Proteins

In this section we explain how the lipid reorganization around a protein can determine the nature of the interactions between two or more proteins. When the distance between two proteins embedded in a lipid bilayer is decreased from an initial to a final protein-protein distance, three different scenarios may arise. A first possibility is that the approaching of the two proteins allows for a reorganization of the other

components of the system which results in an increase of the hydrophilic shielding. As this is energetically favorable, the free energy curve displays an attractive region over this distance interval, which means that the aggregation process occurs spontaneously. In a second scenario, the position of the proteins within the distance interval does not influence the capability of the system to shield its hydrophobic regions. The total shielding then remains constant, and this is reflected by a flat free energy profile over the distance interval and thus in an absence of lipid-mediated protein-protein interactions. The third possibility is that, as the proteins get closer, the lipids cannot reorganize to optimize the hydrophilic shielding. This then results in a repulsive interaction, which is reflected in the PMF by a barrier in the considered distance interval.

In the following part of this section, we compare the calculated shielding parameter profiles against these three possibilities.

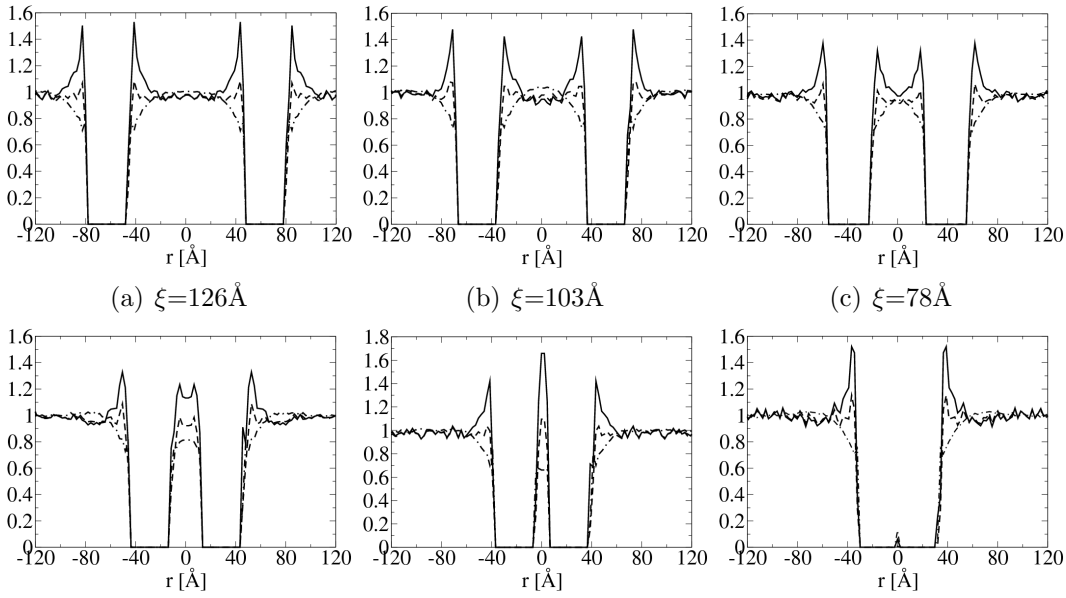

(a) ξ=126Å (b) ξ=103Å (c) ξ=78Å

(d) ξ=58Å (e) ξ=45Å (f) ξ=32Å

Figure 3.5: Lipid head (*dashed line*) and tail (*dot-dashed line*) fraction and hydrophilic shielding parameter (*full line*) along the axis linking the centers of mass of two proteins of size N_p=43 embedded in the lipid bilayer with negative mismatch at different interprotein distances: ξ=126 Å (a), 103 Å (b), 78 Å (c), 58 Å (d), 45 Å (e) and 32 Å (f).

Negative Mismatch Fig. 3.5 shows the lipid head and tail fraction and the hydrophilic shielding parameter along the axis linking the centers of mass of two proteins of size N_p=43 and with negative mismatch, at different distances from each other: ξ=126 Å (a), 103 Å (b), 78 Å (c), 58 Å (d), 45 Å (e) and 32 Å (f). Fig. 3.6 shows,

for the same systems as in Fig. 3.5, the hydrophilic shielding parameter profile in the bilayer plane. From Fig. 3.5a it can be observed that when the two proteins are sufficiently far apart, the lipids regroup around each protein in a similar way as if each protein were isolated, i.e., several lipid heads cluster close to the protein surface while the lipid tails point away from the protein surface (compare with Fig. 3.4a). As the inter protein distance decreases (Fig. 3.5b), the hydrophilic shielding between the two proteins becomes less than one, showing that the lipids cannot rearrange to ensure an optimal shielding. Indeed, a badly shielded hydrophilic region appears (Fig. 3.6b) between the proteins where the hydrophobic tails of the lipids pointing away from one protein meet the lipid tails pointing away from the second protein. Thus, the PMF between ξ=126 Å and ξ=103 Å is repulsive. Further decrease of the inter protein distance to ξ=78 Å involves an important reorganization of the surrounding lipids, whose tails now point away from both proteins, towards the notches in the direction perpendicular to the axis linking the two proteins. This results in an increase of the hydrophilic shielding in the region between the proteins (Fig. 3.5c, 3.6c). Because the lipid heads regroup close to, and the lipid tails point away from, a protein with negative mismatch, a further approach of the proteins increases the inter-protein lipid head fraction and decreases the inter-protein lipid tail fraction, and hence increases the inter-protein hydrophilic shielding (Fig. 3.5d,e and Fig. 3.6d,e). Thus the proteins spontaneously aggregate and the PMF is attractive over this distance interval. Finally, the two proteins from a stable physical dimer (Fig. 3.5f, 3.6f) which allows the most optimal regrouping of the lipids with respect to the hydrophilic shielding, and hence corresponds with the absolute minimum of the PMF curve. The absolute minimum in the PMF is relatively broad compared to the corresponding minima of proteins with positive mismatch because the well shielded region attracts the surrounding lipids.

With this mechanism for protein interactions in mind, one can now make reasonable predictions about many-protein interactions. The aggregation of a third protein to a protein dimer is unlikely in the direction perpendicular to the inter protein axis (Fig. 3.6f) because of the unfavorable interaction with the undershielded regions in the notches of the physical dimer. It is thus more likely that the third protein will approach the dimer along the direction parallel to the inter protein axis. However, because the undershielded notches are energetically unfavorable, the trimer should reorganize such that the number of notches becomes minimal. Hence the optimal final configuration is triangular rather than linear. These predictions are supported by preliminary simulation studies.

Positive Mismatch Fig. 3.7 shows the lipid head and tail fraction and the hydrophilic shielding parameter along the axis linking the centers of mass of two proteins of size N_p=43 and with positive mismatch, at different distances from each other: ξ=126 Å (a), 103 Å (b), 78 Å (c), 58 Å (d), 45 Å (e) and 32 Å (f). For the same system, the average hydrophilic shielding parameter in the bilayer plane is shown in

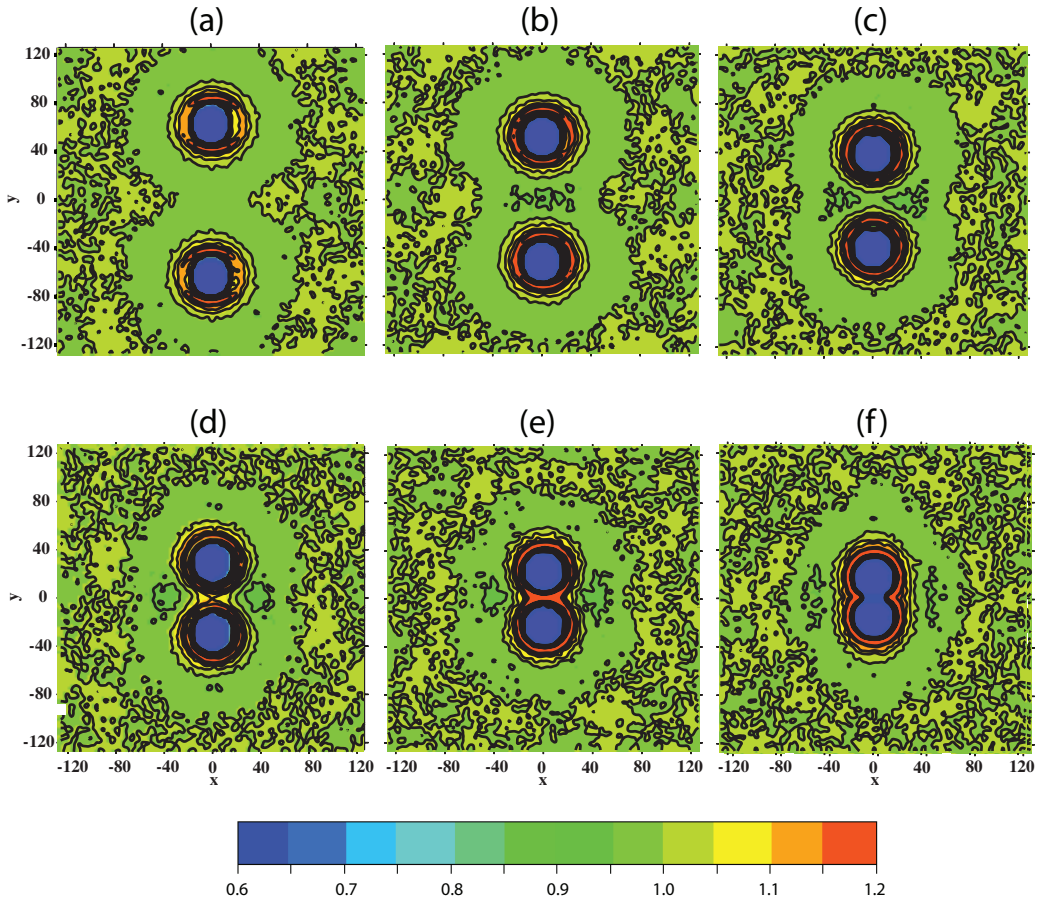

Figure 3.6: Hydrophilic shielding parameter in the plane of the bilayer in which two proteins of size N_p=43 and with negative mismatch are embedded at different interprotein distances: ξ=126 Å (a), 103 Å (b), 78 Å (c), 58 Å (d), 45 Å (e) and 32 Å (f).

Fig. 3.8. Fig. 3.7a shows that at large protein separations the lipids reorganize around each protein in a way similar to the case of one isolated protein of the same size and mismatch (Fig. 3.4c), i.e., by regrouping their heads at a certain distance of, and with the tails pointing towards, the protein surface. When the proteins are at a distance of 103 Å (Fig. 3.7b) a well shielded region forms in between the proteins, due to the interaction of the lipid heads regrouped at a certain distance from both proteins. This explains the attractive region in the PMF between ξ=126 Å and ξ=103 Å. A further approach of the proteins to a distance of ξ=78 Å involves an important reorganization of the inter-protein lipids, whose heads now regroup in the notches between the proteins, while their tails point towards the inter-protein region depleted of lipid headgroups (Fig. 3.7c, 3.8c). Hence, further approach of the proteins decreases the inter-protein lipid head fraction and increases the inter-protein lipid tail fraction, thus

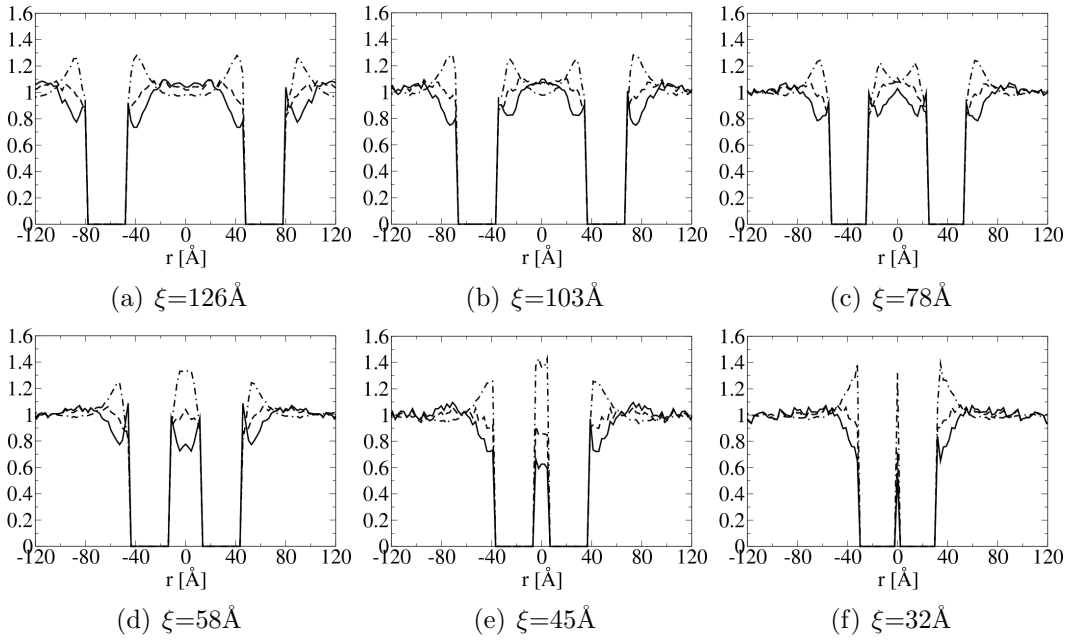

(a) ξ=126Å (b) ξ=103Å (c) ξ=78Å

(d) ξ=58Å (e) ξ=45Å (f) ξ=32Å

Figure 3.7: Lipid head (*dashed line*) and tail (*dot-dashed line*) fraction and hydrophilic shielding parameter (*full line*) along the axis linking the centers of mass of two proteins of size N_p=43 embedded in the lipid bilayer with positive mismatch, at different interprotein distances: ξ=126 Å (a), 103 Å (b), 78 Å (c), 58 Å (d), 45 Å (e) and 32 Å (f).

decreasing the inter-protein hydrophilic shielding (Fig. 3.7d,e, 3.8d,e). As a result, the protein-protein interaction is strongly repulsive over the corresponding distance interval. However, once the repulsive barrier is crossed, the proteins form a physical dimer which allows an optimal regrouping of the lipids with respect to hydrophilic shielding (Fig. 3.8f), and hence corresponds with the absolute minimum of the PMF curve. The stability of the physical dimer is discussed in Sec. 3.3.4.

In Sec. 3.3.3 we noted that the lipid tail fraction follows the same trend as the hydrophobic bilayer thickness. Therefore, the values of the lipid tail fraction between two proteins at different distance, as shown in Fig. 3.5 and in Fig. 3.7, also give us a measure of the corresponding bilayer hydrophobic thickness.

3.3.4 Influence of the Protein Diameter

When a protein with a small diameter, N_p=4 or 7, and subjected to positive mismatch is embedded in the bilayer, the mismatch is compensated for not only by a bilayer deformation, but also by a tilt of the protein, so that its hydrophobic section is shielded from the water (23, 80, 216). Hence, the thickening of the lipid bilayer is not as pronounced as in the case of a protein with a larger diameter (N_p=43), for which

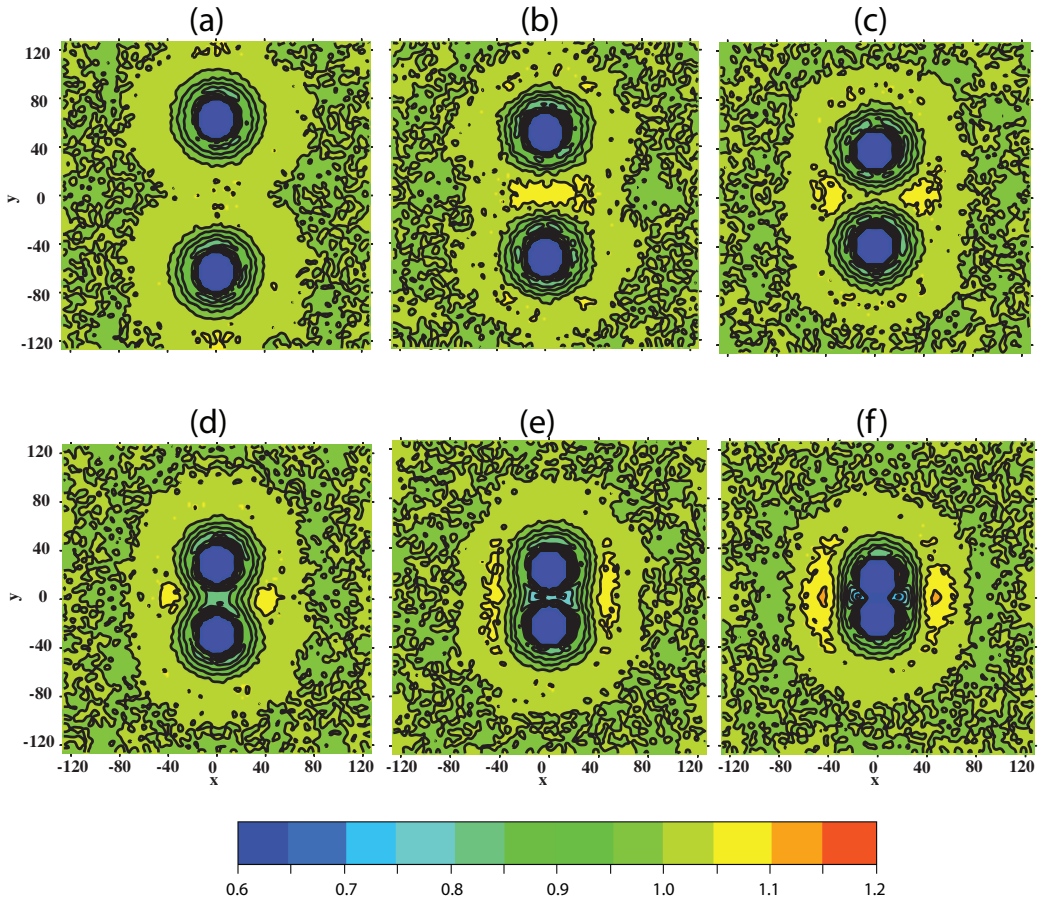

Figure 3.8: Hydrophilic shielding parameter in the plane of the bilayer in which two proteins of size N_p=43 and with positive mismatch are embedded, at different interprotein distances: ξ=126 Å (a), 103 Å (b), 78 Å (c), 58 Å (d), 45 Å (e) and 32 Å (f).

the tilting is instead very small. The different mechanisms of hydrophilic shielding, namely the thickening of the lipid bilayer or the tilt, result in different protein-protein interactions. This explains the difference between the free energy curve for proteins with positive mismatch and of size N_p=43 on the one hand and the free energy curve for proteins with size N_p=4 or 7 on the other hand.

To investigate the influence of tilting on the PMF, we computed the PMF for the protein pair of size N_p=4 and the protein pair of N_p=7 with positive mismatch condition, with the additional constraint that both proteins are not allowed to tilt, and hence remain parallel to the bilayer normal. In Fig. 3.9 we compare the resulting PMFs with the PMFs obtained when the proteins are free to tilt. For both the protein pairs of size N_p=4 and N_p=7, the PMF now shows a shallow and rather broad minimum at large protein separation. At intermediate separation a repulsive

region appears, which is followed by two metastable states and a deep and narrow minimum, corresponding with the two proteins with respectively two and one lipid bead in between and with the physical dimer configuration. A comparison of the PMF obtained when the proteins are not allowed to tilt (Fig. 3.9), with the PMF for the protein pair of size N_p=43 and with positive mismatch (Fig. 3.3c), shows that both have the same characteristics at intermediate and long distance, while they differ at short distance. Our results indicate that, in the case of positive mismatch, the long-range interaction between two proteins is influenced by the degree of protein tilt.

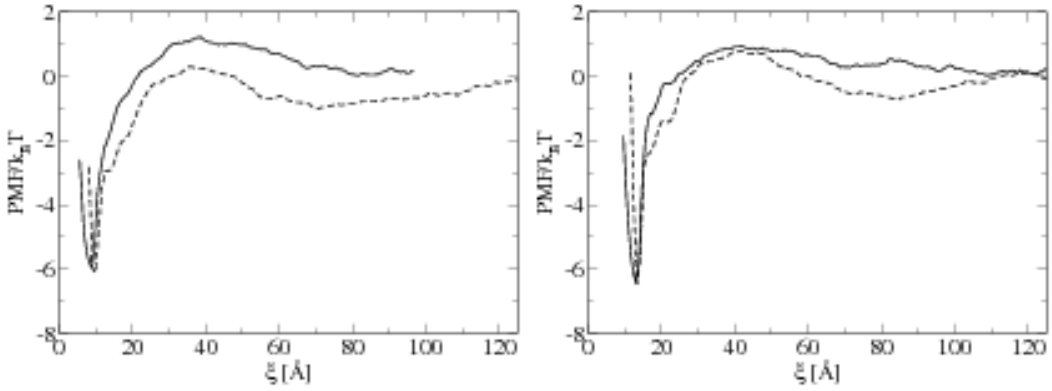

(a) N_p=4 (b) N_p=7

Figure 3.9: Comparison of the potential of mean force as function of the distance between two proteins of size $N_p = 4$ (a) and $N_p = 7$ (b) with positive mismatch in the case when the proteins are allowed (*full line*) or not allowed (*dashed line*) to tilt.

The different shape and depth of the PMF minimum at short distance for the large protein pair (N_p=43) and the small ones (N_p=4,7) at positive mismatch conditions can be explained by looking at Fig 3.8e,f. Indeed, as shown in this figure, the dimerization of two proteins with size N_p=43 reduces the number of badly shielded lipids between the two proteins, but induces two new regions of badly shielded lipids in the notches of the 8-shaped configuration of the dimer. Hence, the dimerization does not bring a significant improvement of the overall hydrophilic shielding. However, when two proteins with a much smaller diameter (N_p=4,7) aggregate, the badly shielded region in between them disappears without the formation of new undershielded regions. This difference can be attributed to the different curvature of the small and large protein. When two large proteins, which have a pronounced curvature, come in close contact, they form an 8-shaped interface with the lipids. This shape creates the very unfavorable undershielded notches, which are not present in the case of smaller proteins, whose physical dimer has a more rectangular shape.

3.4 Comparison with Experimental Observations.

The presence of specific lipid-mediated protein-protein interactions, which depend on the biophysical properties of the lipid bilayer, on the protein diameter, or more generally, on the three dimensional structure of the protein, and on the type and the degree of mismatch, could have several consequences on the stability and the size of protein oligomers, as discussed in the introduction of this chapter. In this section we will attempt to link our simulation results to relevant experimental observations. In making this comparison we have to assume that our model gives a reasonable description of the experimental system. Whereas we can make a very reasonable estimate of the effective sizes of the molecules, we have to assume that the specific nature of, for example, electrostatic interactions or hydrogen bonds, is less important for a general understanding of the protein-protein interactions.

Gramicidin A (D=18 Å, h_P=22 Å) was observed to spontaneously form spherical clusters containing 50-100 proteins when embedded in a DMPC lipid bilayer in the fluid phase (h_L=28 Å) (40). For this system there is a negative hydrophobic mismatch of d=-6 Å. Our results show that for proteins with negative mismatch the nature of the PMF does not significantly depend on the protein diameter. Hence, for the case of negative mismatch our model also predicts clustering of the proteins (i.e. the short-range interaction remains attractive as the cluster size grows).

The aggregation behavior of WALP-23 peptides (D=10 Å, h_P=33 Å) has been investigated in three bilayers with a different hydrophobic thickness: C14:1c-PC (h_L=23 Å), C18:1c-PC (h_L=30 Å) and C22:1c-PC (h_L=37 Å) (31). When embedded in the C18:1c-PC bilayer (d=3 Å), the WALP-23 peptides diffuse randomly in the bilayer without forming stable oligomers. However, aggregation of the WALP-23 peptides was observed when inserted in the C14:1c-PC (d=10 Å) bilayer or in the C22:1c-PC (d=-4 Å) bilayer. Accordingly, for proteins with size N_p=7, our model predicts the attraction between proteins with both positive and negative mismatch conditions, and free diffusion of proteins with negligible mismatch.

Our simulation results support the hypothesis that hydrophobic interactions could influence the protein organization in the bilayer. Indeed, our simulations show that, e.g., for the case of two proteins with positive mismatch, the height of the intermediate range repulsive barrier increases with increasing protein diameter, while the short range attractive minimum deepens with decreasing protein diameter. Hence, it is likely that several smaller proteins could aggregate and form oligomers of increasing size, until the clusters reach a critical size, after which the interactions between the oligomers become dominantly repulsive. Relevant experiments (42) have been performed with bacteriorhodopsin (D=45 Å, h_P=34 Å). Bacteriorhodopsins inserted in bilayers with different hydrophobic thickness, namely lecithins with acyl chains ranging from di-10:0 to di-24:1, were observed to remain dispersed when the bilayer hydrophobic region was less than 4 Å thicker or more than 10 Å thinner than the bacteriorhodopsin hydrophobic length. Aggregation of bacteriorhodopsin was ob-

served when the hydrophobic mismatch was greater than 10 Å or smaller than -4 Å. A related experiment (32) showed organization of bacteriorhodopsin in big clusters when embedded in a bilayer with hydrophobic mismatch d=-5 Å, no aggregation for d=-2 to 2 Å, and the formation of small oligomers for d=5 to 10 Å, with the size of the oligomers slightly increasing with increasing positive mismatch. Considering that the diameter of rhodopsin is comparable to the diameter of our model protein with N_p=43, our results for this protein in the case of negative mismatch also predict clustering. In the case of positive mismatch no aggregation is observed, unless the hydrophobic mismatch is strong. Indeed, strong positive mismatch induces an increase in tilt, which promotes aggregation.

Chapter 4

Molecular Simulation Study of the DMPC-Cholesterol Bilayer

In this chapter we present a coarse-grained model of a hydrated saturated phospholipid bilayer (dimyristoylphosphatidylcholine, DMPC) containing cholesterol that we study using a hybrid dissipative particle dynamics - Monte Carlo method. This approach allows us to reach the time and length scales necessary to study structural and mechanical properties of the bilayer at various temperatures and cholesterol concentrations. The properties studied are the area per lipid, condensation, bilayer thickness, tail order parameters, bending modulus and area compressibility. Our model quantitatively reproduces most of the experimental effects of cholesterol on these properties, and reproduces the main features of the experimental phase and structure diagrams. We also present all-atom simulation results of the system and use these results to further validate the structure of our coarse-grained bilayer. Based on the changes in structural properties we propose a temperature-composition structure diagram, which we compare with the experimental phase and structure diagrams. Attention is paid to the reliability and interpretation of the model and simulation method and of the different experimental techniques. The lateral organization of cholesterol in the bilayer is discussed.

4.1 Introduction

Experiments *in vitro* and *in vivo*, performed to gain insight into the exact role of cholesterol in membranes, revealed its complexity (106). Even for the extensively-studied hydrated bilayer containing solely cholesterol and dimyristoylphosphatidylcholine (DMPC), the effect of cholesterol is not entirely understood (156). In fact, as shown in Fig. 4.1, there is even no consensus on the qualitative form of the cholesterol-DMPC phase diagrams in the literature.

By definition, if a sudden change in the enthalpy of the system takes place, for

example, as a function of temperature at constant pressure, a phase transition occurs. One of the most widely used methods to measure phase transitions of lipid membranes is differential scanning calorimetry (DSC) (109, 111, 119). With DSC, however, it is not possible to characterize the structural, mechanical or dynamical properties of the bilayer in a given phase, or to determine which forces drive the phase transition (109). Several experimental methods to gain information on the structural, mechanical and dynamical properties of a bilayer exist. For example, from NMR and X-ray scattering data, one can extract lipid tail order parameters (136), from X-ray scattering one obtains electron density profiles, bilayer thickness, bending modulus and area per lipid (133, 134) and from fluorescence techniques and NMR diffusion coefficients can be obtained (149, 151, 152). For a more detailed description of the various experimental methods to study the properties of lipid bilayers we refer to Chapter 2.

The available experimental methods can either directly determine the phase boundaries (DSC) or yield information on structural, mechanical or dynamical changes (NMR, X-ray, fluorescence). Therefore, the comparison between the phase diagram and the different diagrams showing structural, mechanical or dynamical changes is not straightforward. Moreover, the different experimental techniques may not be sensitive to all changes that are induced by cholesterol. Molecular simulations should, in principle, allow one to simultaneously obtain information concerning a broad range of bilayer properties.

Using all-atom molecular dynamic simulations, many effects of cholesterol have been studied on several types of lipid bilayers (132, 133, 219–223). The ordering and condensation effects have been observed in simulations of DPPC/Chol and DMPC/Chol mixtures (133, 220–222). The study was extended to different types of sterols and also to bilayers containing sphingomyelin (222, 224). Pandit *et al.* (133) studied the packing of cholesterol around unsaturated lipids. Kucerka *et al.* (132) used molecular simulations to relate the simulated bilayer structure to experimental X-ray results thereby allowing a detailed comparison to the experimental models. Earlier studies (220, 225–231) used a united-atom model to investigate the impact of cholesterol and other sterol molecules on lipid bilayers. These studies use effectively less atoms by grouping a few of the atoms together. Those simulations obtain similar trends for the effect of cholsterol and other sterols. Pasenkiewicz-Gierula *et al.* (220, 227, 228) used those simulations to distinguish between the different types of cholesterol interactions. An extensive study by Hofsass *et al.* (231) followed the effect of cholesterol on the properties of a DPPC bilayer at various concentrations.

Unfortunately, the lengthscales (1-1000 nm) and timescales (1-1000 ns) required to study phase transitions of atomistic lipid models are simply not accessible with current computers. Very extensive simulations are required to reliably determine the phase boundaries and therefore even a single phase point requires much more resources than one has. To access the necessary length- and timescales various coarse-grained models of lipid bilayers have been developed (61). A popular method to study the

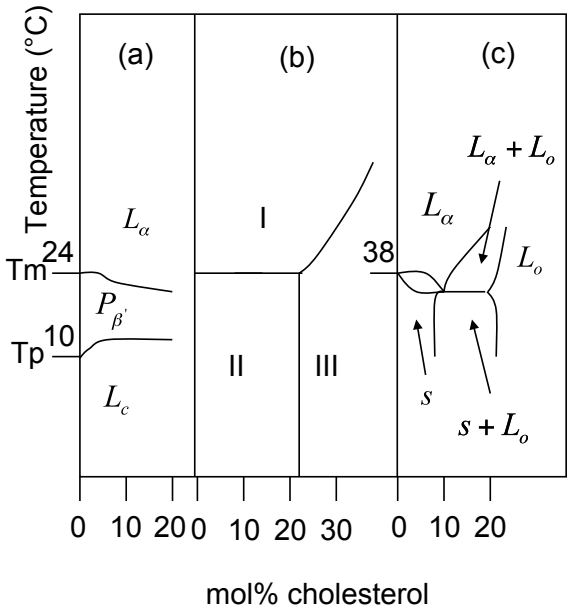

Figure 4.1: Published partial phase diagrams of a hydrated DMPC-cholesterol bilayer. T_M and T_P are the main and the pre-transition temperatures of the pure DMPC bilayer, respectively. In (a), obtained from small-angle neutron scattering experiments which give information on the ripple structure (217), L_α is the liquid phase, $P_{\beta'}$ is the ripple phase and L_c is the gel phase with the lipid tails not tilted. In (b), obtained from differences in membrane fluidity, observed using paramagnetic resonance spectra spin-labels (218), region I denotes the liquid phase which can eventually contain two liquid-liquid immiscible regions, region II denotes a solid phase-fluid phase phase separation and region III denotes a single phase fluid region. In (c), which is a DPPC-cholesterol phase diagram obtained from DSC measurements and NMR (171), s and L_o are the solid phase and the liquid-ordered phase, respectively.

structure, mechanics and dynamics of coarse-grained lipid bilayers is dissipative particle dynamics (DPD) (87). This approach has been successful in reproducing various structural properties of the different phases of a single phospholipid bilayer (61, 73). Recently, coarse-grained models of lipid bilayers containing cholesterol have been developed (47, 65, 68, 232). Murtula *et al.* (47) studied the lateral organization of cholesterol at intermediate cholesterol concentrations, while Marrink *et al.* (68) reproduced the condensation effect of cholesterol.

4.2 Model and Simulation Method

Our mesoscopic model of a hydrated phospholipid-cholesterol is summarized in Fig. 4.2.In our model we explicitly assume that hydrophobic mismatch between the cholesterol and the lipid hydrophobic tails is an important parameter regulating the cholesterol-lipid interactions (119, 233–235). In this cholesterol model we have chosen the parameters and number of beads such that the relative lengths of the different hydrophilic and hydrophobic parts of the cholesterol molecule are consistent with our lipid model.

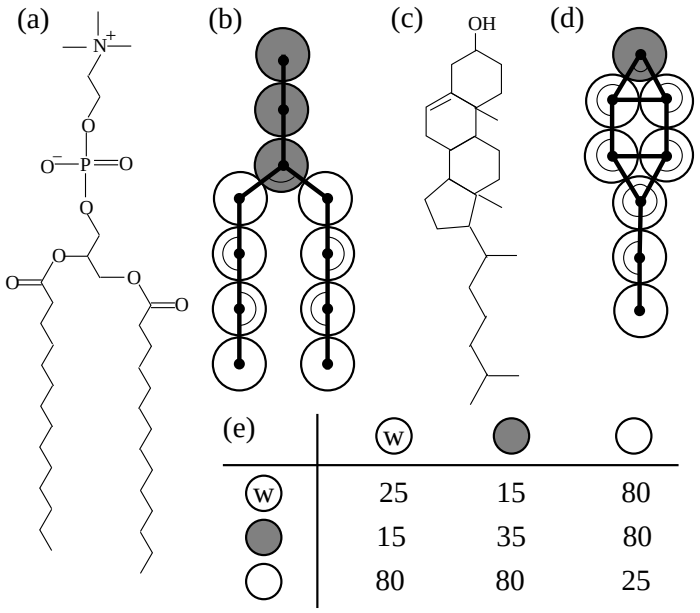

Figure 4.2: Molecular structure and mesoscopic model of DMPC (a, b) and cholesterol (c, d). The hydrophilic and the hydrophobic beads are depicted in black and white, respectively. Angles restricted by a harmonic bending potential are specified. In Table (e) the values of the soft-repulsive parameters a_{ij} are given.

At this point it is important to mention that there is no consensus on the values of these parameters. Molecular simulations (228) and simple molecular models show that the hydrophobic length of a single cholesterol molecule is comparable with the hydrophobic length of a single DMPC molecule and that the length of the cholesterol tetrameric ring is comparable with the length of the cholesterol tail. Experiments by McMullen *et al.* (119) point out that, in a phospholipid bilayer, the total hydrophobic part of cholesterol matches with the length of a phospholipid tail containing 17 carbon atoms, *i.e.* 17.5 Å. DMPC, which contains a tail of 14 carbon atoms, should hence have a hydrophobic part that is 3-4 Å shorter than the hydrophobic part of cholesterol. We chose a cholesterol model in which the hydrophobic length is slightly longer than

the DMPC tail length, and in which the length of the cholesterol ring is equal to the length of the cholesterol tail.

In the phospholipid model, one hydrophobic bead represents three to four carbon atoms. To ensure that the effective volume of a cholesterol molecule is consistent with the lipid models, we assume that the cholesterol tail is represented by two beads and that the stiff tetrameric ring is represented by 5 beads. The five methyl groups are not directly represented in our model. Our model gives a temperature-independent area per cholesterol value of 40.3 Å^2, which is in excellent agreement with the most recent experimental value of 41 Å^2 for a cholesterol monolayer (236).

At this point it is important to notice that both the cholesterol and DMPC models are very simple, and may thus represent a large variety of sterols and lipids. Experiments and all-atom molecular simulations indicate that the main effects of a sterol on a saturated lipid bilayer are independent of the type of sterol, but that the degree to which a given sterol perturbs a lipid bilayer varies (224, 226, 237, 238). As a result, the models used in this simulation study can mainly extract general effects of cholesterol on the DMPC structures.

The hydrophobic and hydrophilic interactions are modeled with soft-repulsive potentials, the strength of which are shown in Fig. 4.2. The energy parameter a_{ww} has been fitted such that the coarse-grained water has the same compressibility as water at ambient conditions (87). It has been shown that the other energy parameter values can be linked to Flory-Huggins solubility parameters (87). To be fully correct, these parameters should be refit at each temperature. However, we have found it fruitful to hold these parameters constant to explore the phase behavior in the vicinity of the ambient temperature of 24 °C. As a result, the connection between the coarse-grained temperature, T_r, and real temperature, T, is less well defined than for the properties related to density. To relate these temperatures, we use the empirical estimate that $T = 108.75T_r - 8.6$, with T_r the reduced temperature, a relationship that was obtained by fitting to the phase transition temperatures. Harmonic bond and bond-bending potentials control the structure and the flexibility of the molecules (see Chapter 2).

The mesoscopic model was studied with the DPD simulation technique (87, 94, 95). Since unconstrained lipid bilayers are essentially in a tensionless state (98), we reproduced this condition by simulating the system in the $NP_\perp\gamma T$ ensemble, where γ is the surface tension of the lipid bilayer, set to zero. We simulate this ensemble via a hybrid Monte Carlo (MC) and dissipative particle dynamics (DPD) approach. Each cycle of the simulation consists of one of the following possible moves: (1) a DPD trajectory of 1 to 50 steps which applies a thermostat to the dynamics, (2) a constant surface tension MC move, and (3) a constant normal pressure MC move. These moves are chosen with a likelihood of 60%–20%–20%, respectively. For a detailed description of the simulation method and its applications, we refer to Chapter 2 and to relevant articles (71, 80, 100, 210).

To minimize finite-size effects, a sufficiently large bilayer patch should be simulated. We have performed simulations on several bilayers which contained 400, 1000,

and 4000 molecules. Differences between simulation results of the bilayers containing 400, 1000, and 4000 molecules were found to be minimal. Hence we performed our systematic study on bilayers which contain 400 molecules and the results presented in this article should barely be subjected to finite-size effects. Because the phase behavior of a lipid bilayer strongly depends on the level of hydration it is important to assure sufficient hydration. Moreover, phase transitions might occur with a change of the local hydration of the bilayer (102). Therefore, we considered 25 water beads per lipid or cholesterol. The simulation in the $NP_\perp\gamma T$ ensemble allows for local changes in the hydration of the bilayer head groups. The normal component of the stress tensor, $P_\perp$, is equal to the bulk pressure of the water phase. This pressure is usually kept constant in the experiments. The same simulations have also been performed in the $NV\gamma T$ ensemble, giving very similar results as in the $NP_\perp\gamma T$ ensemble.

We performed simulations of bilayers with different cholesterol concentrations ranging from 0 to 50 mol% at dimensionless temperatures ranging from 0.1 to 1.0. The pure bilayer can be obtained from a self-assembly process. For this study we generated an initial bilayer in which cholesterol was incorporated by randomly replacing a lipid molecule by a cholesterol molecule in such a way that the total number of lipid and cholesterol molecules on both sides of the membrane are equal. Bennett *et al.* (230) observed flip-flop of cholesterol between the two bilayer sides. We did not observe this.

All-atom MD simulations on bilayers composed of DMPC and cholesterol were used for quantitative comparison. A membrane of 72 molecules in total (DMPC and cholesterol) was assembled using the CHARMM-GUI input generator (239). The replacement method for membrane building was used. An initial constrained equilibration was preformed according to the scheme provided by CHARMM-GUI (240). An equal number of cholesterol molecules were inserted into both leaflets of a DMPC membrane. Three-dimensional periodic boundary conditions were enforced, and a hydration layer of 30 TIP3P water molecules per lipid was used to reduce the mutual influence of images in the direction normal to the bilayer. An initial area of 60 Å^2 per DMPC molecule was set for lower cholesterol concentrations ($< 20\%$) while at higher cholesterol concentrations this value was reduced to 50 Å^2. Both the initial energy minimization and the longer MD simulations were performed using the CHARMM package (52) with the optimized lipid parameters (241). At this point it is important to mention that our all-atom simulations are relatively small. Such small systems are sufficient to obtain accurate data on the structural properties and allow us to compute these properties for many different cholesterol concentrations. However, larger bilayers are required to obtain mechanical parameters or to study cholesterol clustering.

The MD simulations were performed using the leapfrog Verlet integrator over a time step of 2 fs. A temperature of 30 °C was kept constant throughout the simulation as well as constant normal pressure (1 atm) and surface tension (0 dyne/cm), therefore sampling at the $NP_\perp\gamma T$ ensemble. The non-bonded van der Waals interactions were

smoothed by a switching function between 10-12 Å. The particle mesh Ewald (242) method was used to calculate the long-ranged interactions beyond this cutoff. Bonds involving hydrogen atoms were kept fixed using the SHAKE algorithm with tolerance of 10^{-6}. An initial 500 ps minimization was performed according to the scheme provided in CHARMM-GUI (239). Statistical averages were then obtained from a ns trajectory following 3.5 ns of equilibration.

4.3 Results

4.3.1 Comparison with Mechanical and Structural Properties at 30 °C

First, we test our model by a detailed comparison with the experimental data on the effect of cholesterol on various structural and mechanical properties of the bilayer with our simulation results using both all-atom and mesoscopic simulations. Most of these experiments were performed at 30 °C, right above the main transition temperature of pure DMPC, which is 24 °C. We also compare with the data obtained by all-atom simulations, as a further validation of the coarse-grained model.

Structural Fig. 4.3a shows our simulation results for the average molecular area, A_{M}, as a function of cholesterol composition together with the experimental data, which have been extracted from X-ray scattering experiments (44, 134). The all-atom simulations reproduce the experimental data very well. For pure DMPC our mescopic model gives a slightly smaller area. Fig. 4.3a shows that experimentally a non-linear decrease of the area per molecule as a function of cholesterol concentration is observed. The A_{M} is smaller than the A_{M} calculated from the mixing rule. This non-ideal mixing behavior is called the condensation effect of cholesterol. Both all-atom and molecular simulations correctly predict the non-linear decrease of the area per molecule as a function of cholesterol concentration.

Fig. 4.3b shows the relative increase in bilayer thickness in the presence of cholesterol. Experimentally, X-ray scattering provides the phosphorus to phosphorus distance (PtP) as a measure of this thickness (44, 134). We used the same definition in our all-atom simulations. For our mesoscopic model we used the average distance between the beads containing the phosphorus atoms. For a pure DMPC bilayer we obtained a bilayer thickness of 38.7 Å for the mesoscopic and 36.1 Å for the all-atom simulations. These data compare well with the experimental value of 36 Å (44). Both experiments and simulations show a strong swelling of the bilayer thickness when up to 20-30 mol% cholesterol is added. This increase levels off when more cholesterol is added to the bilayer.

The effect of cholesterol on the ordering of the lipid tails is illustrated in Fig. 4.3c. In the experiments the lipid tail order parameter, S_{NMR}, is obtained from deuterium

NMR experiments and is related to the average angle θ, between a C-D bond and the normal to the bilayer, by $S_{\mathrm{NMR}} = 2|S_{\mathrm{CD}}| = |\langle 3\cos^2\theta - 1\rangle|$. From all-atom simulations one can directly obtain this NMR order parameter. The average angle β between a C-C bond and the normal to the bilayer are geometrically related to the desired angle θ. Hence, $2|S_{\mathrm{CD}}|$ and $2|S_{\mathrm{CC}}| = |\langle 3\cos^2\beta - 1\rangle|$ are expected to follow the same qualitative trend. We tested and validated this with our all-atom simulations (see Fig. 4.3c). Therefore we use $2S_{TT} = |\langle 3\cos^2\alpha - 1\rangle|$ as tail order parameter in our mesoscopic simulation, with α being the angle between two consecutive tail beads and the bilayer normal. Both all-atom molecular simulations and mesoscopic simulations reproduce the experimentally observed increase in lipid tail order when cholesterol is added to the bilayer, although the agreement is quantitatively better for all-atom molecular simulations.

The experimental data allows us to validate our model through various structural properties. It does not, however, allow us to validate the specific molecular organization of the lipids. To this end we use the comparison to all-atom simulations. Fig. 4.4 compares the density profiles of the cholesterol and DMPC head groups in the mesoscopic bilayer with all-atom simulations at various cholesterol concentrations. The comparison shows that our mesoscopic model follows the atomistic density profiles reasonably well, considering the loss of degrees of freedom by coarse-graining. The figure clearly shows the swelling of the bilayer induced by increasing concentration of cholesterol, as the head groups move increasingly away.

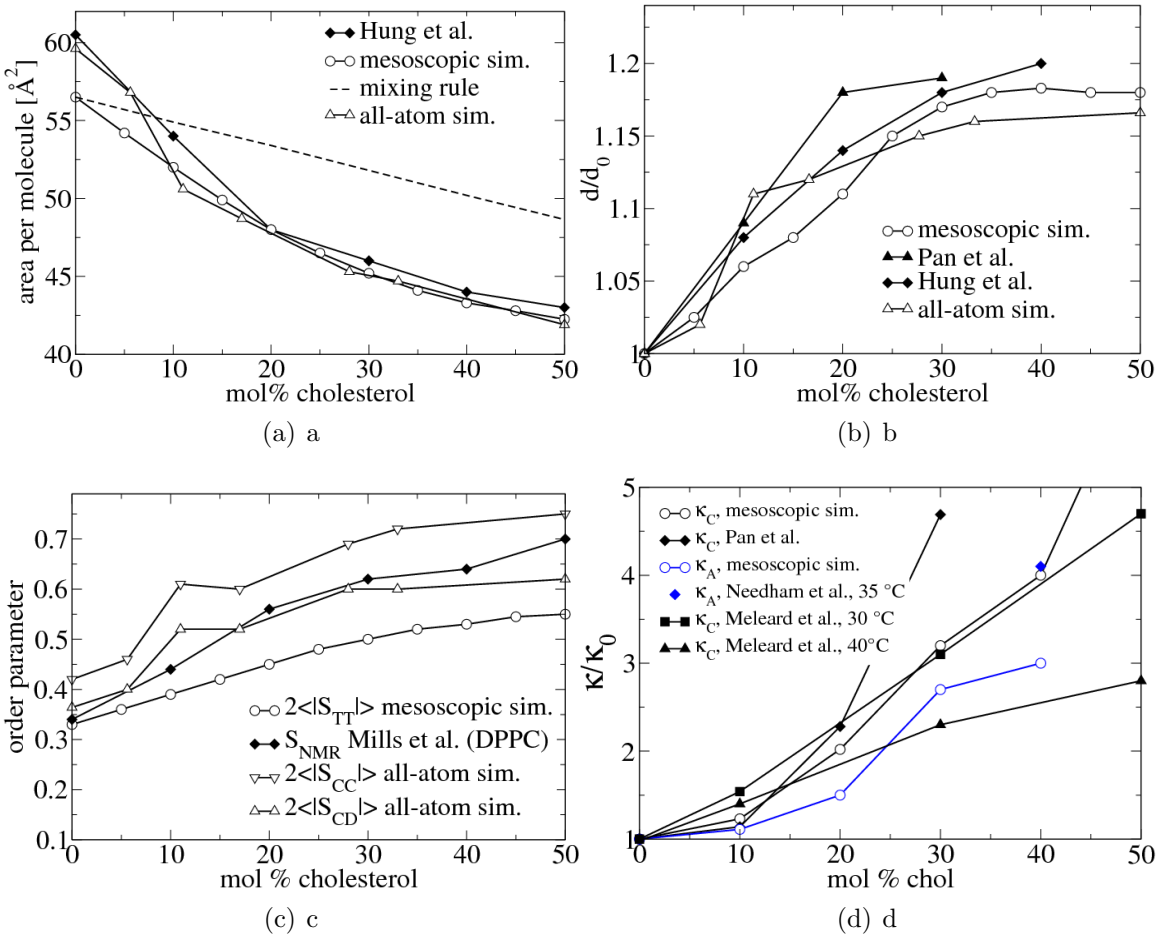

Figure 4.3: Comparison of structural and mechanical parameters as a function of cholesterol concentration obtained from X-ray scattering experiments (unless specified), all-atom and mesoscopic simulations. All data are at 30 °C (unless specified). (a): Area per molecule, A_{m}. Experimental data from Hung *et al.* (44) and Pan *et al.* (133, 134). The dotted line represents the area per molecule calculated with the mixing rule. (b): Relative bilayer thickness, d/d_0. Experimental data from Hung *et al.* (44) and Pan *et al.* (133). d is the phosphorus to phosphorus distance in the electron density profile and d_0 is the thickness of the pure bilayer. (c): Lipid tail order parameter. Experimental data from Mills *et al.* (136). Illustration of the qualitative agreement between S_{CC} and S_{CH} using all-atom simulations and comparison to S_{TT} from mesoscopic simulations. (d): Relative bending modulus, κ_C/κ_{C0}, and relative area compressibility modulus, κ_A/κ_{A0}. Experimental data from Pan *et al.* (133) and from Meléard *et al.* (243), extracted from fluctuations of giant vesicles observed by microscope, and from Needham *et al.* (244), obtained from pipet pressurization. κ_C is the bending modulus and κ_{C0} is the bending modulus of the pure bilayer. κ_A is the area compressibility modulus and κ_{A0} is the area compressibility modulus of the pure bilayer.

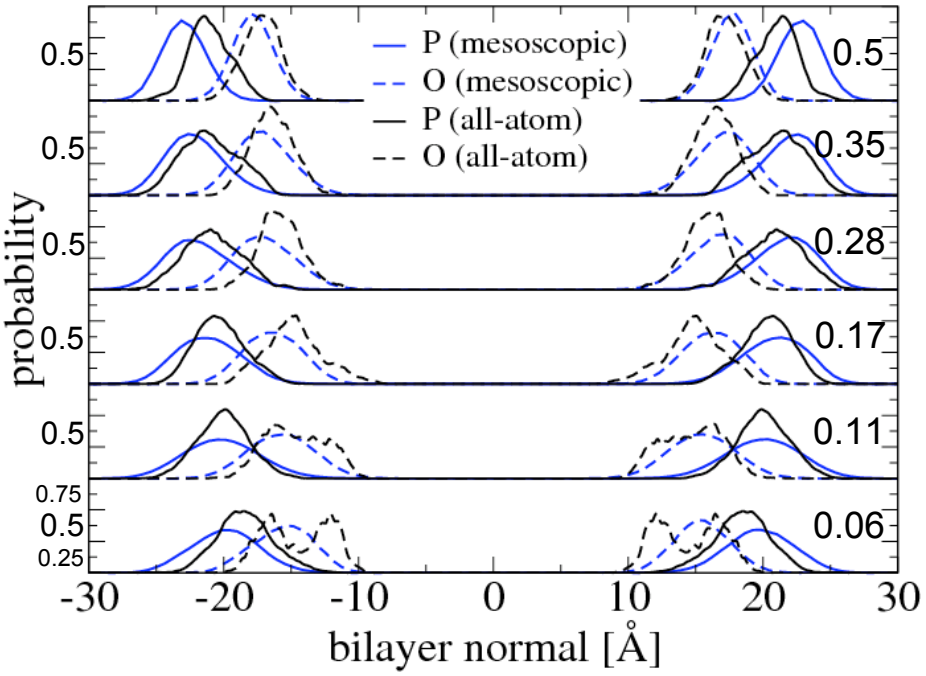

Figure 4.4: Comparison of the probability density distribution functions of the all-atom simulations (black lines) with the distribution functions from the coarse-grained simulations (blue lines) for different cholesterol mole fractions at T=30 °C. The data are shifted three units along the vertical axis for increasing cholesterol concentration. In the comparison we focus on the lipid phosphorous atom (solid lines) and the cholesterol oxygen atom (dashed lines). For the mesocopic simulations we plot the density distribution of the lipid head bead containing the phosphorous atom (middle head bead) and the cholesterol bead containing the oxygen. The cholesterol mole fractions are given by the numbers on the right side of the graph.

Mechanical Fig. 4.3d shows the relative area compressibility κ_A/κ_{A_0} and bending modulus κ_C/κ_{C_0}. The area compressibility was computed using $\kappa_A = k_B T A_t / \langle \delta A_t^2 \rangle$ (245), with A_t the total bilayer area and $\langle \delta A_t^2 \rangle$ the mean square of the fluctuations in the area. Given the large scatter in the experimental values (144 ± 10.5 dyn/cm (244) and 234 ± 23 dyn/cm (127)), our result for pure DMPC, $\kappa_A = 250 \pm 50$ dyn/cm, compares reasonably well. We predict a strong decrease in area fluctuations $\langle \delta A_t^2 \rangle$ when cholesterol is added, and thus a strong increase in area compressibility, in agreement with experimental observations (244). To estimate the effect of cholesterol on the bending modulus, κ_C, we use the polymer brush model which relates κ_A to κ_C: $\kappa_C = (1/24)\kappa_A(PtP - 10\ \text{Å})^2$ (127). For pure DMPC we compute $\kappa_C = 7.5 \pm 2\ 10^{-20}$ J, which is of the same order of magnitude as the experimental value of 5-6 10^{-20} J (127, 133). Our model correctly reproduces the increase in bending modulus due

to the addition of cholesterol.

From this comparison of our mesoscopic model with experimental and all-atom simulation data we can conclude that our very simple model reproduces, almost quantitatively, most structural and mechanical properties of DMPC. At this point it is important to mention that we have also computed the diffusion coefficients for this model. As can be expected, due to the soft-repulsive interaction these diffusion coefficients are 2-3 orders of magnitude larger compared to experimental values.

4.3.2 Temperature Dependence of the Structural and Mechanical properties

The bilayer structural and mechanical properties strongly depend on the temperature and the composition. In addition, we can distinguish different bilayer structures at different temperatures and compositions. Fig. 4.5 summarizes the phase behavior of our mesoscopic system. In this text we also call the different bilayer structures phases. Here we briefly describe the different bilayer structures to facilitate the interpretation of the temperature dependence of the mechanical and structural properties of the membrane. In a later section, we outline in detail how this phase diagram is obtained.

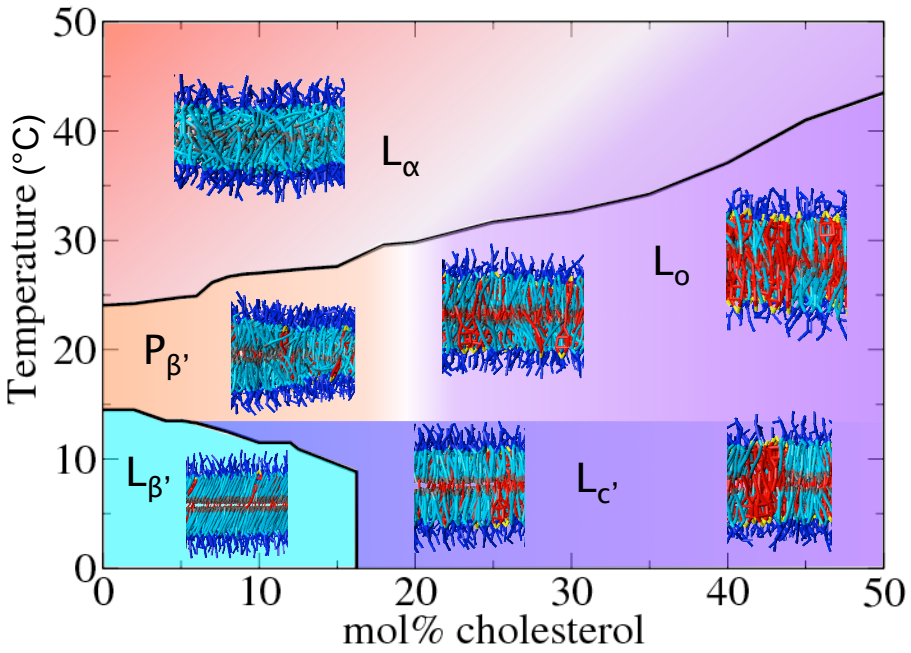

Figure 4.5: Temperature-composition structure diagram of DMPC-cholesterol bilayer. The full lines were determined using inflection points of order parameters of the phase transition. All other regions are characterized via visual inspection of the snapshots, some of which are shown in the figure. Lipid head and tail beads are depicted in dark and light blue, respectively. The lipid tail end bead is depicted in grey. The cholesterol hydrophilic and hydrophobic beads are depicted in yellow and red, respectively. The snapshots were taken at the following conditions: T=35 °C, pure DMPC (L_α phase), T=20 °C, 10 mol% cholesterol ($P_{\beta'}$ phase), T=10 °C, 5 mol% cholesterol ($L_{\beta'}$ phase), T=30 °C, 30 mol% cholesterol (L_o phase, left), T=30 °C, 50 mol% cholesterol (L_o phase, right, with random cholesterol clusters), T=10 °C, 15 mol% cholesterol ($L_{c'}$ phase, left), T=10 °C, 50 mol% cholesterol ($L_{c'}$ phase, right, with pure cholesterol patterns). The background colors depict the different phases and the broadness of the transition between different colors represents the broadness of the transitions.

For a pure DMPC bilayer we observed a disordered structure at high temperatures (L_α, or liquid phase), a rippled structure at intermediate temperatures ($P_{\beta'}$), and a tilted and ordered structure at lower temperatures ($L_{\beta'}$, or gel phase).

At high temperatures, we observed that the disordered bilayer structure gradually becomes more ordered when cholesterol is added to the bilayer. This ordered structure is called the L_o phase. As temperature increases, the cholesterol concentration at which the L_o phase is formed increases as well. At intermediate temperatures, we observe a transition from the $P_{\beta'}$ to the L_o phase. At low temperatures the addition of cholesterol results in a non tilted highly ordered structure, called the $L_{c'}$ phase. Larger snapshots of different bilayer structures are shown in Fig. 4.6.

Structural Similar to the validation at 30 °C, we computed the area per molecule, the bilayer thickness and the lipid tail order and tilt as a function of temperature and bilayer composition.

Area per molecule A_{M} as a function of the bilayer composition and temperature is shown in Fig. 4.7a. In this figure isolines connect points with the same value of A_{M}. At high temperatures the bilayer is in the liquid L_α phase, where the tails are disordered and have the highest value of A_{M}. A_{M} decreases significantly if the temperature is decreased. As cholesterol occupies a smaller area ($A_{\mathrm{Chol,0}}$=40.3 Å^2) the addition of cholesterol decreases A_{M}. Addition of cholesterol decreases the temperature dependence of A_{M}. At low temperatures, in the gel phase, the effect of cholesterol on the area is much weaker.

Needham *et al.* (244) used micropipet aspiration of giant unilamellar vesicles to determine changes in area as a function of temperature (see Fig. 4.7b). Needham *et al.* report a typical S-shape with a sudden decrease in bilayer area around the main transition temperature T_M. This S-shape is also reproduced by our simulations, although less steep. When 25 mol% cholesterol is added to the bilayer, the S-shape in the experimental curve disappears, the transition area is much smaller and below T_M the temperature hardly affects the area anymore. As the cholesterol concentration is further increased to 50 mol%, the experimental curve shows no S-shape anymore and becomes almost flat. Our simulations nicely reproduce this experimental trend.

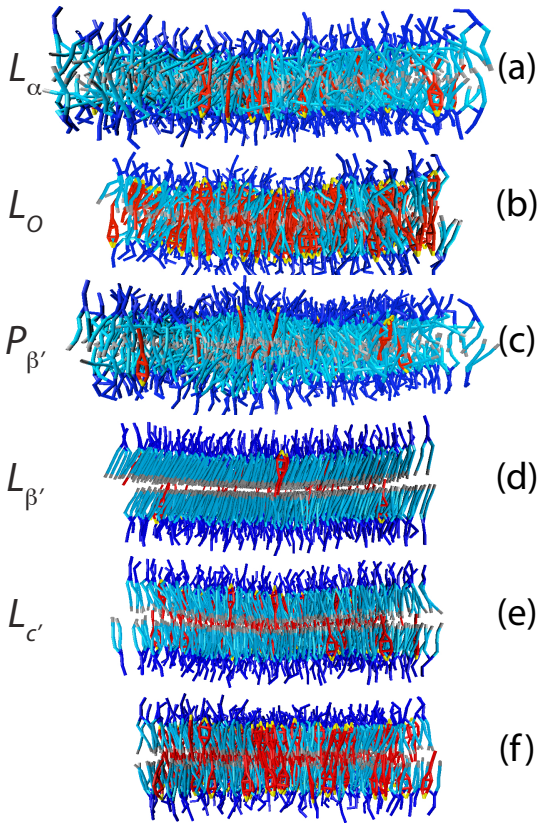

Figure 4.6: Snapshots of a side view of the bilayer. (a) L_α phase for 10% cholesterol at T = 37°C. (b) L_o phase for 40% cholesterol at 37°C. (c) Ripple ($P_{\beta'}$) phase for 5% cholesterol at T = 20°C. (d) $L_{\beta'}$ phase for 5% cholesterol at T = 5°C. (e) $L_{c'}$ phase for 15% cholesterol at T = 5°C. (f) $L_{c'}$ phase for 40% cholesterol at T = 5°C. The hydrophilic and the hydrophobic beads of the phospholipids are depicted in dark blue and in light blue, respectively. The end beads of the lipid tails are depicted in gray. The cholesterol headgroup is depicted in yellow, the cholesterol tetrameric ring and tail beads are depicted in red. For clarity, water beads are not shown. The difference in the width of the bilayers illustrates the condensation effect nicely.

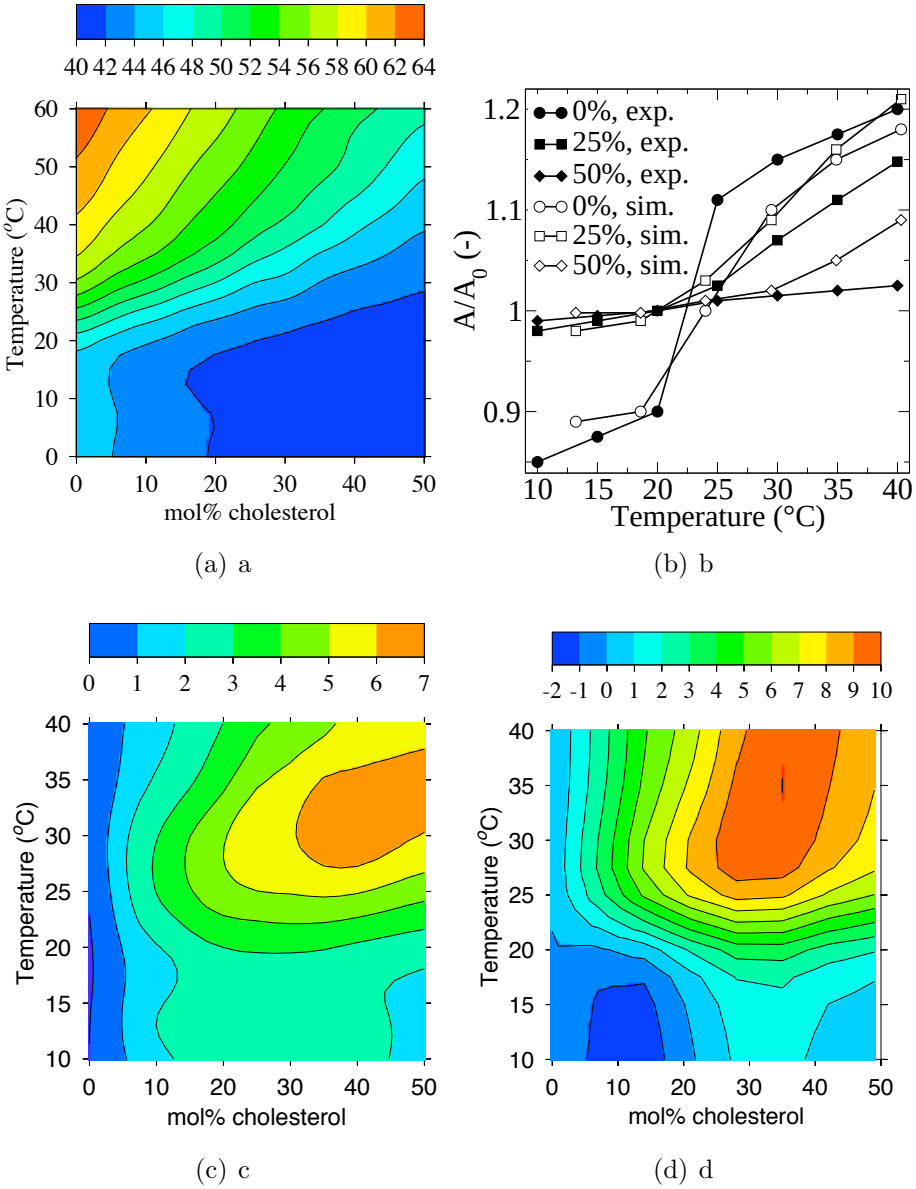

(a) a (b) b

(c) c (d) d

Figure 4.7: (a): Area per molecule, in Å^2, simulated with the mesoscopic model as a function of temperature and cholesterol concentration. (b): Comparison of the relative areas of bilayers containing 0, 25 and 50 mol% cholesterol, as a function of temperature, obtained from heating/cooling micropipet experiments by Needham *et al.* (244) and from our mesoscopic simulations. For the pure DMPC bilayer, A_0 is the area at the main transition temperature. For bilayers containing 25 and 50 mol% cholesterol, A_0 is the area at 20 °C. (c): Simulated condensation effect, in Å^2, defined as the difference between A_M simulated with the mesoscopic model and A_{M}^{IM} calculated according to the ideal mixing rule, as function of temperature and cholesterol concentration. (d): Experimental condensation effect estimated from the relative areas reported by Needham *et al.* (244) and absolute areas reported by Hung *et al.* (44).

Condensation effect An interesting property of cholesterol is its condensation effect (44, 232, 246). Cholesterol causes the area per molecule to decrease much more than one would expect on the basis of ideal mixing: $A_{\mathrm{M}}^{IM} = (1-x)A_{\mathrm{pc},0} + xA_{\mathrm{Chol},0}$, where $A_{\mathrm{pc},0}$ and $A_{\mathrm{Chol},0}$ are the area per pure lipid and cholesterol, respectively.

Fig. 4.7c shows the influence of the temperature on the condensation effect. At low cholesterol concentrations the condensation effect is small and does not depend on temperature. We find a strongly condensed region above the main transition of pure DMPC for cholesterol concentrations above 20 mol%. This condensation gap has not been measured directly. Interestingly, one can find indirect proof of this gap by combining the relative area measurements of Needham *et al.* (244) with the absolute values of A_m obtained by Hung *et al.* (44). Fig. 4.7d shows a clear condensation gap for these combined data at similar conditions as our mesoscopic model. Quantitatively, the experimental maximum condensation effect is about 4 Å^2 higher than simulated and located at lower cholesterol concentrations, indicating that our model slightly underestimates the strength of the condensation effect. Apart from this, the agreement is surprisingly good. In Sec. 4.4 we present a discussion on the molecular mechanism of the cholesterol condensation effect.

Bilayer Thickness In Fig. 4.8a the relative bilayer thickness, defined as the phosphorous to phosphorous (PtP) distance divided by the PtP distance of pure DMPC at 30 $^\circ C$, is shown as a function of temperature and cholesterol content for the DMPC-cholesterol bilayer. The behavior is similar to the area per molecule. For pure DMPC we observe a strong temperature dependence around T_M. The addition of cholesterol smoothens out the temperature dependence of the bilayer thickness. At high temperatures, cholesterol increases the bilayer thickness, while at low temperatures, cholesterol does not affect the bilayer thickness much. Thus, the bilayer thickness depends on the relative importance of two different effects: the swelling of the bilayer when the temperature is decreased and the swelling of the bilayer when cholesterol is added.

Little experimental data is available for the bilayer thickness and the effect of cholesterol on the bilayer thickness is still subject to debate. The main transition of a pure DMPC bilayer is accompanied by a sudden increase in bilayer thickness, and small amounts of cholesterol do not seem to influence this bilayer swelling significantly (247). This is confirmed by our simulation results. Also, it was observed for a DPPC-cholesterol bilayer that, above 25 mol% cholesterol, the bilayer is thicker in the fluid phase and thinner in the gel phase than the pure DPPC bilayer (171). This is exactly what we compute. Several studies such as the neutron diffraction study of Léonard *et al* (248) mention an increase of the hydrophobic thickness by 3-4 Å when cholesterol is added to the DMPC bilayer, independent of the temperature. We clearly simulate a cholesterol dependence of the hydrophobic thickness that does also depend on the temperature. It was also recently reported that the cholesterol-induced bilayer swelling is not observed *in vivo* (19).

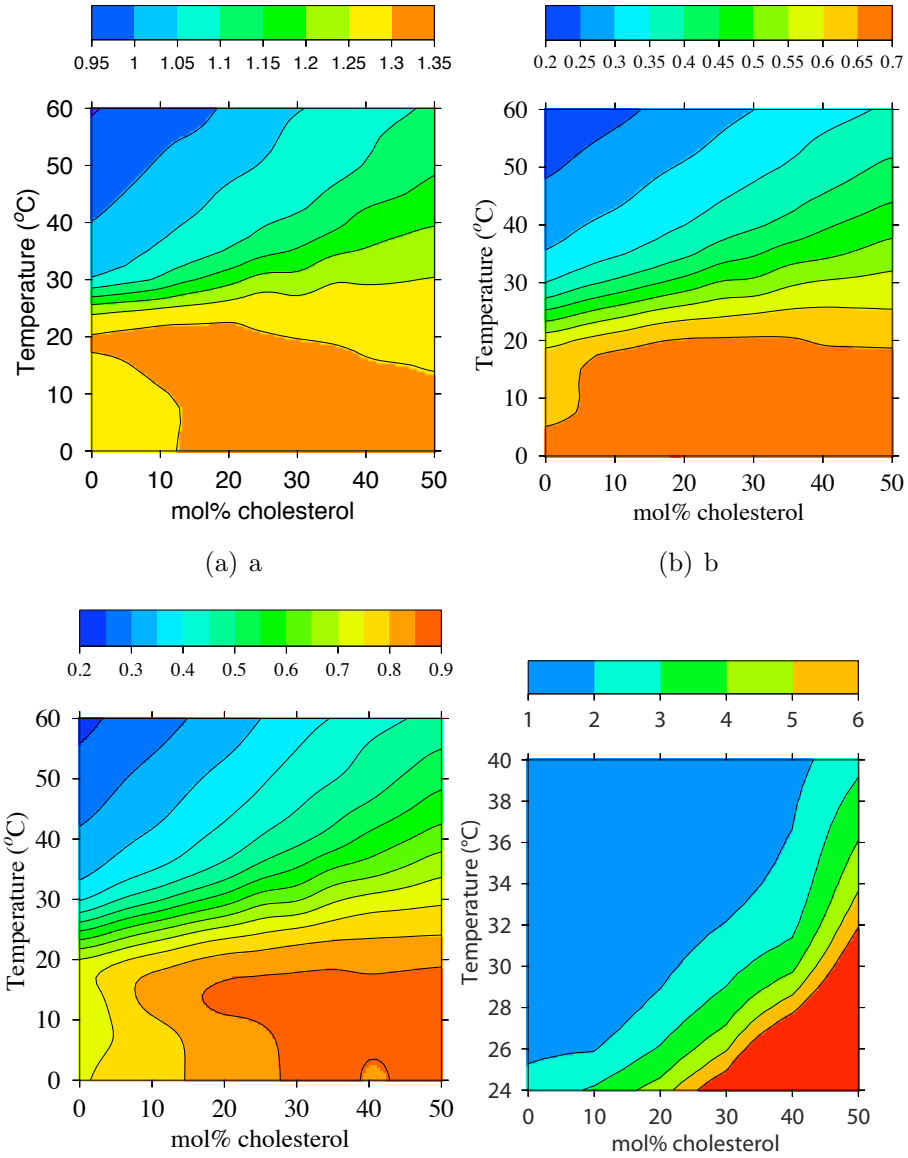

(a) a (b) b

(c) c (d) d

Figure 4.8: (a): Bilayer thickness, relative with respect to the cholesterol-free bilayer thickness at 30 °C, as function of cholesterol concentration and temperature, in °C. (b): Average lipid tail order (S_{TT}). (c): Lipid tail tilt (S_{T1T4}). (d): Membrane bending modulus, relative with respect to the cholesterol-free membrane modulus at 30 °C.

Lipid Tail Order and Tilt The average tail order parameter is shown in Fig. 4.8b as a function of the bilayer composition and the temperature for the DMPC-cholesterol mixture. At high temperatures, the average order of the lipid tails increases steadily when cholesterol is added to the bilayer. At low temperatures, cholesterol does not really seem to affect the order parameter much. At intermediate temperatures the lipid tail order increases up to a given cholesterol concentration after which it remains rather constant.

The temperature and composition dependence of the average tail tilt is quite similar. This is shown in Fig. 4.8c. The only qualitative difference is that at low temperatures cholesterol concentrations ranging from 0 to 30 mol% also increase the tilt parameter, which corresponds to a decrease in lipid tail tilt. The tilt parameter is defined as $2S_{T1T4} = |\langle 3\cos^2\alpha - 1\rangle|$, with α being the angle between the first and the last tail beads and the bilayer normal.

Systematic qualitative experiments have been performed by Wilson-Ashworth *et al* (249) for the DPPC-cholesterol mixture. Their results can be summarized as follow: above the main phase transition temperature cholesterol induces an ordering, which is comparable to the order of pure DPPC between the main and the pre-transition temperature. Between the main and the pre-transition temperature cholesterol induces ordering comparable to the order of the pure DPPC below the pre-transition temperature. Below the pre-transition temperature cholesterol does not seem to affect the order. Qualitatively this is exactly what we simulate.

The ordering effect of cholesterol above T_M is agreed upon in the literature. This is not the case for the ordering effect of cholesterol below T_M. Shimshick *et al* (250) report a slight increase of the average tail order parameter with increasing cholesterol concentration, at temperatures below T_M. The lower the temperature, the smaller the cholesterol range over which the biggest increase of S_{NMR} occurs. This is not in agreement with the results of Ipsen *et al* (143), who report a decreasing order parameter with increasing cholesterol concentration.

In a DMPC-cholesterol and in a DPPC-cholesterol mixture, a phase was observed below the pre-transition temperature T_P where the lipid chains are less tilted than in the $L_{\beta'}$ phase (139, 177). Karmakar *et al* (139) called this phase the P_β phase. However, experimentally, no agreement has been reached over the exact cholesterol content interval over which this phase occurs. Karmakar *et al* (139) mention a pure $L_{\beta'}$ phase up to 2 mol% cholesterol, a coexistence of $L_{\beta'}$ and P_β between 2 and 13 mol% cholesterol, and a pure P_β phase between 13 to 21 mol% cholesterol. Knoll *et al* (177) observe a strong decrease of the lipid tail tilt between 8 and 24 mol% cholesterol. In our simulations, for a pure DMPC bilayer, the value of the tilt parameter in the $L_{\beta'}$ is around 0.71, corresponding with a tilt of approximately 26°, which compares well with the most recent experimental estimate of 32.3° (128). Between 0 and 25 mol% cholesterol the value of the tilt parameter increases up to 0.9, corresponding with a tilt angle of of approximately 15°. Thus, our model correctly predicts the decrease in tilt in the gel phase due to the addition of cholesterol.

Mechanical Fig. 4.8d shows the membrane bending modulus, relative to the cholesterol-free membrane modulus at 30 °C, as function of the composition, and over the temperature range 24-40 °C, i.e., above the main transition temperature of DMPC, which is 24 °C. In this temperature range, the bending modulus of DMPC is hardly temperature-dependent. At a constant temperature of, for example, 26 °C, addition of cholesterol results in an increase of the bilayer bending modulus. For example, 30 mol% cholesterol multiplies the bending modulus by a factor of 5. With increasing temperature, however, this effect of cholesterol strongly decreases, and at 40 °C the addition of 40 mol% cholesterol multiplies the bending modulus only by a factor of 2. This is in good agreement with the factor 2.5, measured experimentally by Meléard *et al.* (243). This is shown in Fig. 4.3d.

4.3.3 Temperature Dependence of the Lateral Organization of Cholesterol

In Figures 4.9-4.11, the bilayer hydrophobic thickness variations and the local cholesterol concentrations are shown at various cholesterol concentrations for different temperatures. The lateral organization of cholesterol is difficult to measure experimentally, but is important for the interpretation of some experiments and for the modeling of cholesterol-lipid interactions (219).

At T=30 °C (Fig. 4.9), when pure DMPC is well in the liquid phase, there are only small and local variations in bilayer thickness. This remains so when cholesterol is added to the bilayer. There are very small regions with and without cholesterol. Dips in the fluorescence intensity as function of cholesterol concentration have often been presented as evidence for a regular distribution of cholesterol on a fixed hexagonal superlattice in DMPC bilayers. This regular distribution implies that every cholesterol molecule has a preferential location in the plane of the membrane with respect to the other cholesterol molecules. A dip is observed at, for example, 20 mol% cholesterol (167–169). However, we could not observe any form of regular cholesterol distribution in our simulations. At higher cholesterol concentrations, i.e., when the bilayer is in the liquid-ordered phase, small dynamical cholesterol clusters are present.

Experimentally, it would be very difficult to detect such small cholesterol clusters. From the analysis of fluorescence resonance energy transfer data, Troup *et al.* (181, 182) concluded that cholesterol clusters exist in the DMPC bilayer with 40 mol% cholesterol, above the main phase transition temperature of pure DMPC. Using all-atom simulations, Dai *et al.* (219) did not observe clustering of cholesterol, but their cholesterol content was never higher than 20 mol% cholesterol. It might well be that part of the cholesterol clustering we observe is related to the slight underestimation of the cholesterol condensation effect.

At T=21 °C (Fig. 4.10) the hydrophobic thickness variations (20 Å for the thin and 29 Å for the thick part) illustrate the ripple phase at 0% cholesterol. Due to the

addition of cholesterol the ripples gradually disappear. In the rippled phase, there seems to be a slight preference of cholesterol for the thicker bilayer domains. In the liquid-ordered phase small dynamical cholesterol clusters appear. The disappearance of the ripple phase around 20 mol% cholesterol and the preference of cholesterol for the thicker bilayer domains is in agreement with the experimental observations of Mortensen *et al.* (217).

At T=10 °C (Fig. 4.11) the pure DMPC bilayer is well in the gel phase. At high cholesterol concentrations cholesterol forms larger clusters. It is also more likely to find a cholesterol molecule in both layers at the same position.

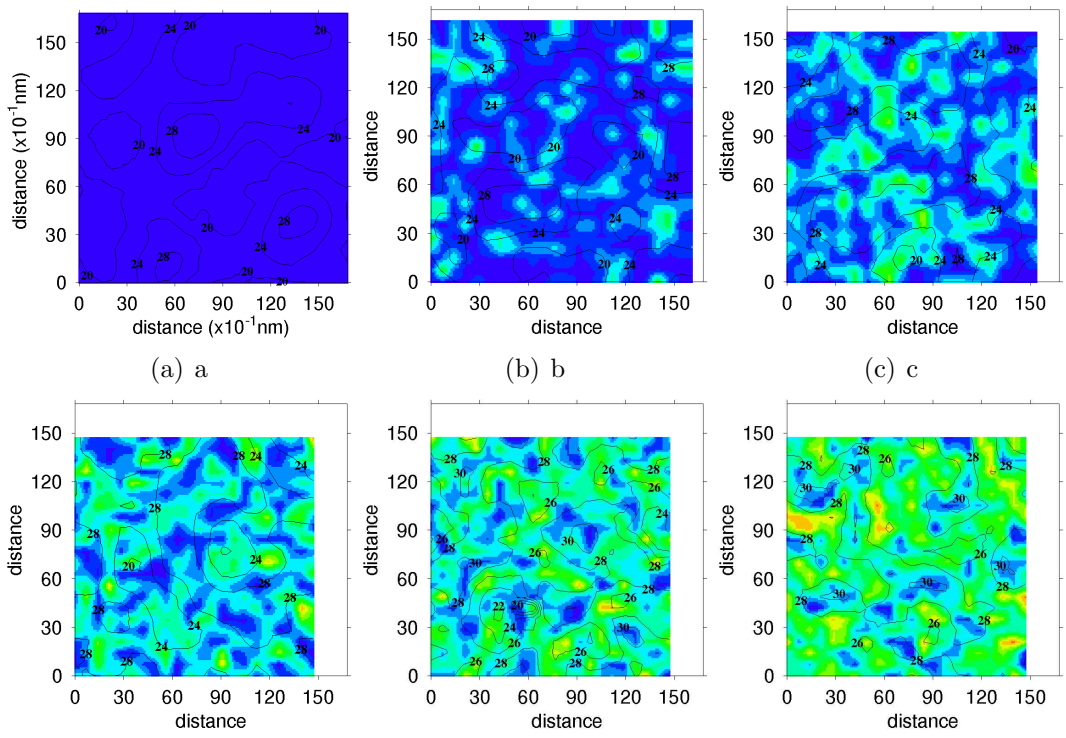

(a) a (b) b (c) c

(d) d (e) e (f) f

Figure 4.9: Hydrophobic thickness variation, in Å, and local mole fractions, for T= 30 °C, at various cholesterol concentrations (0 (a), 10 (b), 20 (c), 30 (d), 40 (e), 50 (f)). The figure shows a top view of the bilayer in which the lines and numbers give the thickness and the colors the local cholesterol concentration. Blue indicates that both layers contain only lipids and red indicates that both layers contain a cholesterol. The axis are in Å.

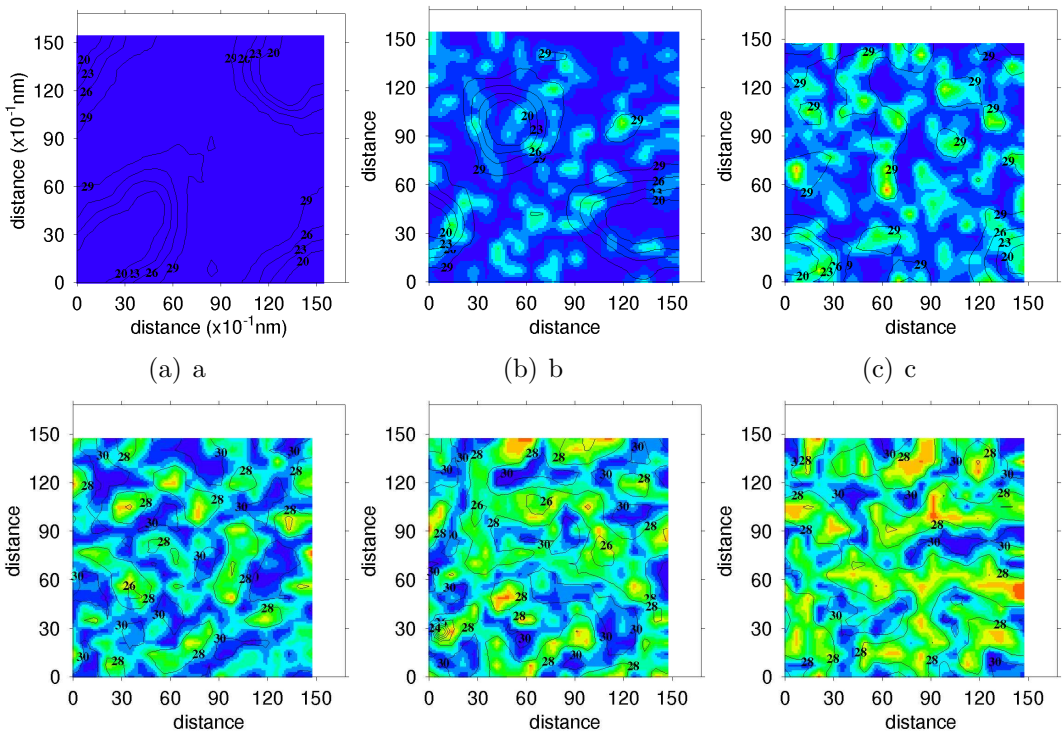

(a) a (b) b (c) c

(d) d (e) e (f) f

Figure 4.10: Hydrophobic thickness variation, in Å, and local cholesterol mole fractions, for T= 21 °C, at various cholesterol concentrations (0 (a), 10 (b), 20 (c), 30 (d), 40 (e), 50 (f)).

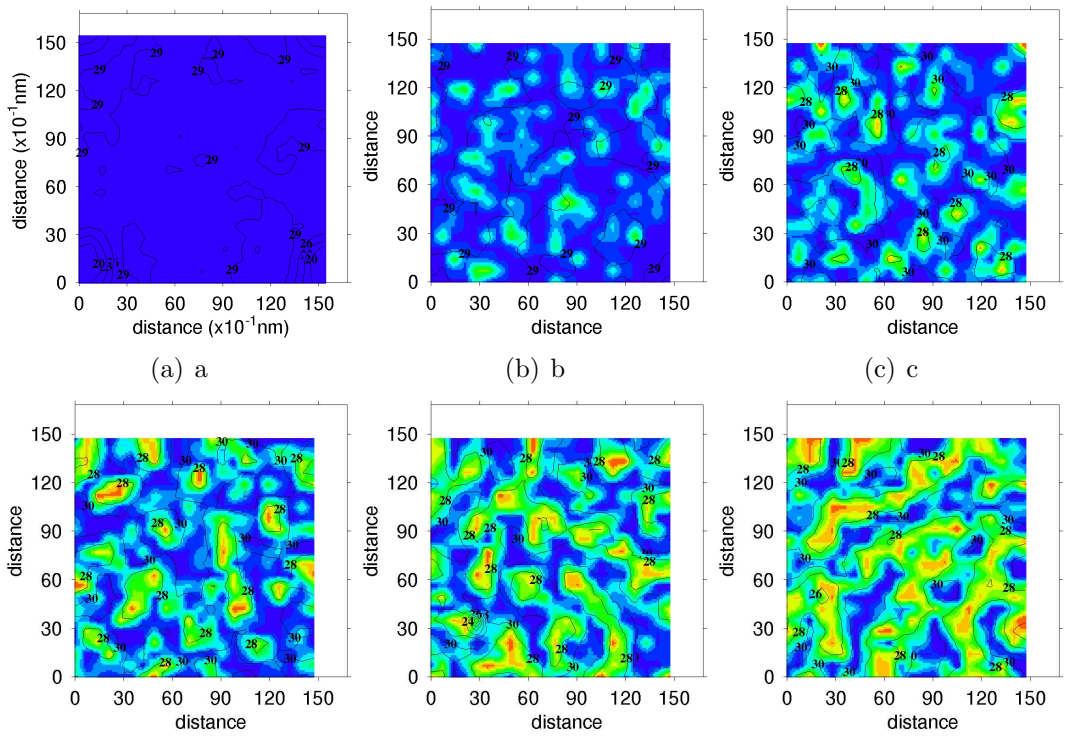

(a) a (b) b (c) c

(d) d (e) e (f) f

Figure 4.11: Hydrophobic thickness variation, in Å, and local cholesterol mole fractions, for T= 10 °C, at various cholesterol concentrations (0 (a), 10 (b), 20 (c), 30 (d), 40 (e), 50 (f)).

4.3.4 Temperature-Composition Structure Diagram

Ideally, one would use a change in the enthalpy as a signature for a phase transition. However, for our system, molecular simulations of the heat capacity signature of DSC experiments are very difficult due to the large bulk water contribution. As an alternative we used order parameters of the phase transition, which are parameters of which the value significantly changes during a phase transition. For this system, the area per molecule, the bilayer thickness, and the tail order and tilt parameters were considered as order parameters of a phase transition. We defined the inflection points of the curves of the temperature dependence of the order parameters as the boundaries between the phases. For pure DMPC, heating and cooling simulations were performed to check the reversibility of the phase transitions. The rate of heating and cooling was 1 °C per simulation. For the main transition no hysteresis was observed, while for the pre-transition a slight hysteresis ($\Delta T = \pm 1$ °C) was present. For the DMPC-cholesterol bilayers only cooling simulations were performed. For the transitions $L_\alpha \rightarrow P_{\beta'}$, $L_\alpha \rightarrow L_o$, $P_{\beta'} \rightarrow L_{\beta'}$, and $L_{c'} \rightarrow L_{\beta'}$ we could observe a

clear inflection point. All other regions were identified by visual inspection of the snapshots.

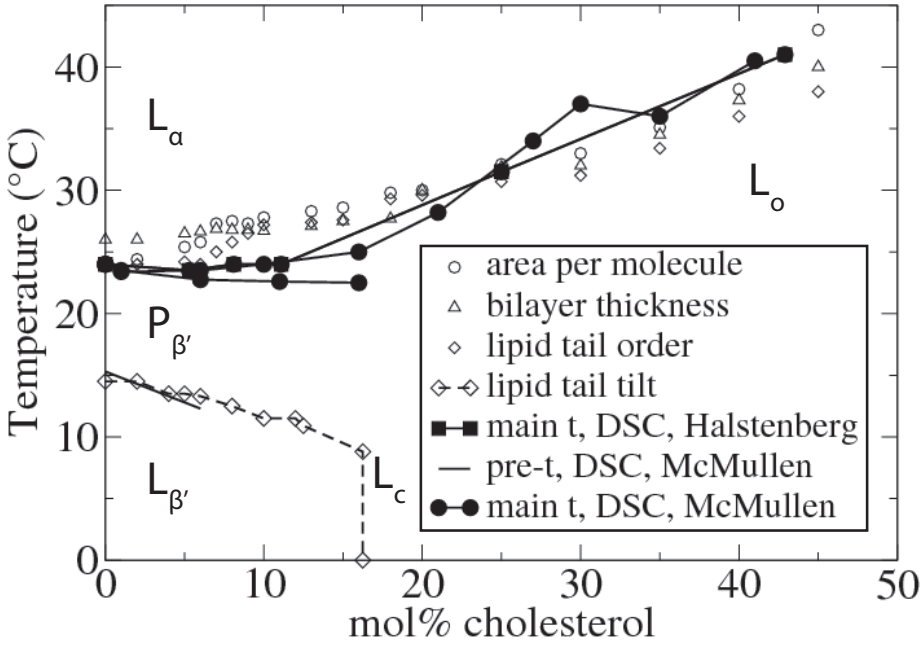

Figure 4.12: Effect of cholesterol on the main and the pre-transition temperature of a DMPC bilayer. The experimental data were obtained from differential scanning calorimetry by Halstenberg *et al.* (111) and from deconvolution of the main transition temperature DSC peak by McMullen *et al.* (119). The open symbols are the results of the simulations using the temperature-composition position of the inflection points of the curves representing the values of the area per molecule, lipid tail order, lipid tail tilt, and bilayer thickness as a function of temperature, at a given cholesterol concentration.

Fig. 4.12 collects the inflection points of these different order parameters as a function of cholesterol composition. Within the accuracy at which these inflections points can be determined, all order parameters give similar results. At low cholesterol concentrations, we observed a relatively sharp inflection. For concentrations above 20% cholesterol this transition became much more gradual. For the $L_\alpha \rightarrow P_{\beta'}$ and $L_\alpha \rightarrow L_o$ transitions, our data nicely follow the DSC experiments by Halstenberg *et al.* (111) and McMullen *et al.* (119). The temperature at which the heat capacity peak is maximal remains approximately constant until 10-15 mol% cholesterol is added, after which the temperature increases. At 15 mol% cholesterol, the DSC peak broadens and a gradual transition or a crossover to the L_o phase takes place and the main transition enthalpy approaches zero between 40 and 45 mol% cholesterol. Also for the pretransition our results are in very good agreement with the DSC experiments of McMullen *et al.* (119).

It is instructive to compare our phase diagram (Fig. 4.5) with the experimental ones shown in Fig. 4.1. The effect of cholesterol on T_M in the structure diagram of Recktenwald *et al.* (218) (see Fig. 4.1b), obtained with fluidity measurements, is very similar to the effect observed by the DSC experiments and our simulations. In contrast, the structure diagram of Mortensen *et al.* (217) (Fig. 4.1a) shows a slight decrease of the temperature of the transition from the L_α to the $P_{\beta'}$ structure, up to 20 mol% cholesterol.

The DPPC-cholesterol phase diagrams (145, 171, 251–253) show some qualitative agreements with the DMPC-cholesterol diagrams (119). In fact, for our mesoscopic model the difference in tail length between DMPC and DPPC is too small to be described by the addition or removal of an extra tail bead. Vist *et al.* (171) (Fig. 4.1c) observed a decrease of the main phase transition up to 8 mol% cholesterol, followed by a liquid-liquid immiscible region. We do not observe such a liquid-liquid immiscibility gap. However, the gradual transition of the L_α to the L_o phase might explain the broadening of the NMR signal (171). Recent X-ray scattering experiments also concluded that liquid-liquid immiscibility is not present in the DPPC-cholesterol system (179).

Below the main-transition temperature, the addition of cholesterol induces a gradual transition from a $P_{\beta'}$ to a L_o phase. Our mesoscopic simulations indicate that the ripple phase exists up to 20 mol% cholesterol, in agreement with the experiments of Mortensen *et al.* (217) (see Fig. 4.1a). Vist *et al.* (171) (Fig. 4.1c) observe the coexistence of gel and L_o phase; however, recent X-ray scattering experiments concluded that gel-L_o immiscibility is not present in the DPPC-cholesterol system (179). We do not find evidence from our simulations for this coexistence. It might be that the change in NMR signal, which lead Vist *et al.* (171) conclude that immiscibility of two phases might be present, is due to the presence of small ripples, as observed in our simulations. The term liquid-ordered phase was introduced (254) because it was experimentally observed that, although the lipid tails in the L_o phase were highly ordered, the diffusion coefficient was, although lower, still of the same order of magnitude as in the L_α phase (149), and surface shear rigidity was absent (244). The DSC experiments and our simulations show that cholesterol increases the $L_\alpha \rightarrow L_o$ transition temperature, which is a natural continuation of the main phase transition line, with the L_o phase at the gel-side of the crossover.

As mentioned previously, DSC experiments indicate that the pre-transition temperature decreases when up to 6 mol% cholesterol is added and thereafter disappears. The pre-transition, as obtained from DSC experiments, is interpreted as the transition from the $P_{\beta'}$ to the $L_{\beta'}$ phase (252). Above 6 mol% cholesterol no significant change in enthalpy was observed. If we compare this with our phase diagram, at approximately these conditions we observe a transition from the $P_{\beta'}$ to the $L_{\beta'}$ and a transition from the $L_{\beta'}$ to the $L_{c'}$ phase. In the $L_{\beta'}$ phase we observe that the tilt order decreases as a function of temperature, while in the $L_{c'}$ phase the tilt order increases. This behavior gives a very interesting temperature dependence at 10 mol%, in which we

observed three inflection points. The simulated $L_{c'}$ phase, in which the lipid chains are less tilted than in the $L_{\beta'}$ phase, was also experimentally observed (177, 179).

4.4 The Cholesterol Condensation Effect

Let us now address a seemingly simple thermodynamic question: how does the area per molecule of a phospholipid membrane change if we add cholesterol? This question was first posed by Leathes (246) in 1925 and is still being discussed today. The significance of this question relates directly to the importance of cholesterol for the functioning of membranes of higher eukaryotes. For example, cholesterol regulates the fluidity of the membrane and modulates the function of membrane proteins. Understanding these mechanisms has motivated many researchers to investigate the lipidcholesterol interactions in detail. Because a membrane can be seen as a two-dimensional liquid, a first estimate of how the area per molecule would change upon the addition of cholesterol would be to assume ideal mixing, where the area per molecule is simply a weighted average of the pure-components areas. In 1925 Leathes showed that, instead of ideal mixing, one observes a striking nonideal behavior (246). This nonideal behavior is called the condensing effect because the area per molecule is much lower compared with ideal mixing. Because a membrane behaves as an incompressible fluid, a decrease of the area per molecule will result in a corresponding significant increase of the total thickness of the bilayer. Such an increase of the thickness signals a reorganization of the structure of the membrane. Because changes in the structure of the membrane may have important consequences for the functioning of proteins, it is important to have a better molecular understanding of the cholesterol-induced changes.

Different conceptual models have been proposed to explain the nonideal cholesterol-lipid interactions. Examples include the condensed-complexes model (255, 256), the superlattice model (169), and the umbrella model (234). The condensed-complexes model explains the condensation effect by assuming that cholesterol induces the reversible formation of a stoichiometric cholesterol-lipid complex. In such a complex the membrane is condensed as the lipid acyl chains are more ordered. At a given cholesterol concentration, an equilibrium composition exists between these condensed cholesterol-lipid complexes and ordinary lipids. The superlattice model assumes that at critical concentrations the cholesterol molecules exhibit a specific long-ranged order. The umbrella model takes the point of view that the hydrophilic part of cholesterol is too small and therefore the lipids need to contribute to the screening of the cholesterol molecules from hydrophobic interactions with water. The phospholipids can only create this umbrella if these molecules straighten to make space for cholesterol. In these models the underlying mechanisms leading to condensing are very different. Interestingly, a recent experimental study concluded that their data supported the condensed-complexes model (257), whereas another set of experiments

did not find any indication of the condensed complexes and supported the umbrella model (235). These differences in insights motivated us to use our molecular simulations to shed some light on the lateral organization of cholesterol in lipid membranes and the underlying lipid-cholesterol interactions that induce the condensation effect.

Fig. 4.7c shows that the condensation effect is maximal at a temperature just above the main transition. The reason is that at these conditions the pure bilayer is in a liquid-disordered state, whereas the addition of cholesterol to the bilayer transforms it into a liquid-ordered phase, which has an area per lipid that is much smaller compared to the liquid-disordered state. This large difference causes a large condensation effect. At higher temperatures, the liquid phase remains stable for all cholesterol concentrations, giving a much smaller condensation effect. At lower temperatures, the pure lipid bilayer has an area per lipid that is much closer to the area per lipid of the liquid-ordered phase, and as a result the condensation effect is far less.

The above results indicate that the condensation effect is a direct consequence of particular changes in the phase behavior that cholesterol is inducing. In the literature there are various speculations about those aspects of the cholesterol structure that are specifically responsible for its condensing effect. For example, the umbrella model is based on the notion that compared with phospholipids, the hydrophilic part of cholesterol is much smaller and needs the phospholipid, as an umbrella, for additional screening from interactions with water. This suggests that an additional hydrophilic group would change the properties completely. Another important factor is the bulky ring structure; if we replace the ring by a tail we obtain a molecule that resembles more an alcohol molecule. However, shortening the hydrophobic tail would have little effect. Fig. 4.13a shows the modified cholesterol molecules that mimic these changes: one in which we decrease the hydrophobic tail length (see Fig. 4.13(i)), one in which we add an additional hydrophobic group (see Fig. 4.13(ii)), and one in which we replace the ring by a simple chain (see Fig. 4.13(iii)).

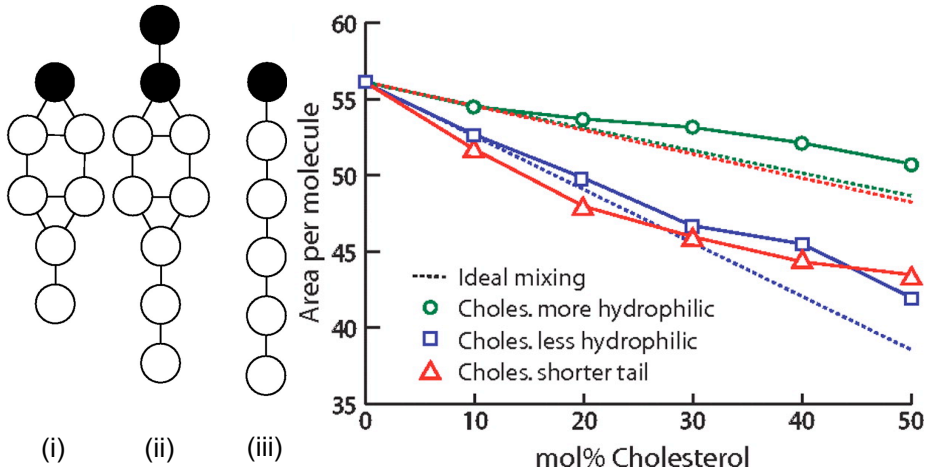

Figure 4.13: (a) To study the effect of change in the chemical structure of cholesterol we introduce three new molecules in which we change the hydrophobic-hydrophilic balance of cholesterol. (i) Cholesterol with a shorter tail length. (ii) Cholesterol that is more hydrophilic. (iii) Cholesterol that is less hydrophobic. The model contains hydrophobic (white) and hydrophilic (black) beads that are connected with springs and bond-bending potentials. (b) Area per molecule as a function of the cholesterol concentration for the molecules shown in (a). We compare our simulation results with the ideal mixing estimates. This estimate is given by $A_{\mathrm{M}}^{IM} = (1-x)A_{\mathrm{pc},0} + xA_{\mathrm{Chol},0}$, where $A_{\mathrm{pc},0}$ and $A_{\mathrm{Chol},0}$ are the area per pure lipid and (modified) cholesterol, respectively. The simulations were at T = 30 °C. Effect of changes of the cholesterol hydrophobic-hydrophilic balance; the circles are for cholesterol in which the hydrophilic part is increased (ii), the squares are for cholesterol with a decreased hydrophobic part (iii), and the triangles are for cholesterol with a shorter tail length (i).

Indeed, the results in Fig. 4.13b show that shortening the tail of cholesterol shows the same condensation effect. However, Fig. 4.13b shows that for both other modifications of the cholesterol molecule, adding an additional hydrophilic group and replacing the ring by a linear chain, no condensing effect is observed. We observe the opposite effect: adding these molecules causes the bilayer to become more expanded compared with ideal mixing. The effect of (smaller) alcohols on the area per molecule has been measured experimentally, and the experimental data also show an increase (258). Closely connected to this, we observed that for both cases in the phase diagram the liquid phase was stable over the entire concentration range. In fact, we observe that adding these molecules decreases the main transition temperature, and hence there is no region in the phase diagram where there is a large condensation effect.

Simulations with these structural variations of cholesterol indicate how surpris-

ingly subtle the mechanism is. The main transition in a pure bilayer is very sensitive to the hydrophobic interactions. The headgroups of the lipids screen the hydrophobic tails from the water. At high temperatures, the area per lipid is high, and this screening is far from optimal; but at these conditions the chain entropy dominates. Decreasing the temperature makes it increasingly important to screen the hydrophobic interactions and at the main transition eventually induces an ordering of the chains. A key aspect is to understand how cholesterol destabilizes the liquid phase. Cholesterol has a smaller hydrophilic head and is therefore less efficient in shielding the hydrophobic interactions. At high temperatures, the lipid bilayer can accommodate this, but at lower temperatures the lipids can only contribute to the screening of the cholesterol by decreasing its area per lipid. This causes the observed ordering and explains why the main transition increases. The two changes we introduced to the cholesterol structure influence its hydrophobic screening; in both variants the intrinsic undershielding of cholesterol disappears. If these molecules are added to the bilayer, there is no need for additional screening of the hydrophobic interactions, and these molecules prevent the formation of an ordered phase.

Let us compare our observations with the previous models that have been introduced to explain the condensation effect. First, our model does not give any indication of long-range ordering as is assumed in the superlattice model. Implicit in both the umbrella model and the condensed complexes is the assumption of some kind of local organization. For example, in the umbrella model it is assumed that one lipid molecule could screen one or two neighboring cholesterol molecules (see e.g., (259)). Our simulations show a much more disordered structure in which we cannot identify these ordered structures. At this point it is important to recall that our model contains many assumptions, and this raises the question of whether the conclusions we draw from our simulations are relevant for the experimental systems.

Chapter 5

Molecular Simulation of the Effect of Cholesterol on Lipid-Mediated Protein-Protein Interactions

Experiments and molecular simulations have shown that the hydrophobic mismatch between proteins and membranes contributes significantly to lipid-mediated protein-protein interactions. In the present chapter, we discuss the effect of cholesterol on lipid-mediated protein-protein interactions as function of hydrophobic mismatch, protein diameter and protein cluster size, lipid tail length, and temperature. To do so, we study a mesoscopic model of a hydrated bilayer containing lipids and cholesterol in which proteins are embedded, with a hybrid dissipative particle dynamics - Monte Carlo method. We propose a mechanism by which cholesterol affects protein interactions: protein-induced, cholesterol-enriched or cholesterol-depleted lipid shells surrounding the proteins affect the lipid-mediated protein-protein interactions. Our calculations of the potential of mean force between proteins and protein clusters show that the addition of cholesterol dramatically reduces repulsive lipid-mediated interactions between proteins (protein clusters) with positive mismatch, but does not affect attractive interactions between proteins with negative mismatch. Cholesterol has only a modest effect on the repulsive interactions between proteins with different mismatch.

5.1 Introduction

The detection of an increasing number of transmembrane proteins in submicrometer-sized clusters (31, 32, 40, 42, 45) with organization that strongly depends on the membrane composition (e.g. lipid tail length (31, 32, 42), or cholesterol content (31, 33, 46–50)) has seriously challenged the idea that individual proteins freely diffuse in a passive biological membrane (260) and only interact via direct protein-protein interactions.

Understanding the role of the membrane in the interactions between membrane proteins has become an active area of research (11, 261).

In these studies, hydrophobic mismatch, i.e., the difference, d, between the length of the hydrophobic region of the protein and the bilayer hydrophobic thickness, has been frequently invoked as an important physical property that regulates lipid-protein and lipid-mediated protein-protein interactions. For example, several studies have shown that modulations of the bilayer thickness, protein tilting, protein functioning, and protein aggregation strongly depend on the protein hydrophobic mismatch, on the protein diameter, and on the lipid properties (11, 19, 38, 39, 80, 81, 201–204, 209, 210, 262–270). The concept of hydrophobic mismatch has therefore significantly contributed to the insight that lipids and proteins show a collective behavior.

Theoretical studies on protein-lipid and indirect protein-protein interactions investigate mostly single-component bilayers. Several models also exist of membrane-mediated organization in lipid membranes containing two types of lipids or two phases (271–273). Examples are the lipid-annulus model (271) and the wetting and capillary condensation model (272). These models show that a preferential interaction between the proteins and a specific lipid or phase might lead to a clustering of the proteins.

In this chapter, we present a molecular simulation study of the effect of cholesterol on protein-lipid and lipid-mediated protein-protein interactions. Cholesterol has a significant effect on protein aggregation (31, 33, 45–50) and on a wide range of other membrane processes involving proteins (274–276). These effects are intimately related to various diseases (51).

Different mechanisms have been identified to explain why cholesterol affects the proteins. For many proteins the exact mechanism remains unclear. In general, these mechanisms have been strongly related to the partitioning of proteins in cholesterol-rich or in cholesterol-poor regions (155, 277). Three fundamentally different but not mutually exclusive mechanisms have been proposed (51, 155, 277):

- Many proteins have been observed to have a specific sterol-sensing domain (278). As a result, proteins and cholesterol interact preferentially and directly with each other, leading to a partitioning of proteins in cholesterol-rich regions.

- Indirect attractive protein-cholesterol interactions could originate from a preferential interaction between a smooth protein surface and the rigid cholesterol tetrameric ring. Proteins might be expelled from sterol rich domains when the opposite is true (279).

- The presence of cholesterol induces changes in the bilayer material and biophysical properties, which could influence the protein-lipid and protein-protein interactions (31, 33, 49).

The third mechanism is the most frequently invoked. For example, in model membranes, cholesterol-rich regions might have an increased area compressibility modulus,

which could lead to a partitioning of the membrane components (170, 275, 277). The chain ordering and bilayer thickening effect of cholesterol could lead to hydrophobic mismatch between the hydrophobic part of the protein and the bilayer or change the hydrophobic mismatch conditions such that lipid-mediated protein aggregation takes place (31, 33, 49). This mechanism is illustrated in Fig. 1.5.

Experiments indicate that the effect of cholesterol on the bilayer properties strongly depends on lipid type and temperature (134). For example, at physiologically relevant temperatures, the effects of cholesterol are smaller on unsaturated lipids compared to saturated lipids (134). Moreover, in real biological membranes, the addition of cholesterol does not seem to modify the membrane thickness (19). Interestingly, the increased protein aggregation in the presence of cholesterol has been observed in saturated bilayers (49), in unsaturated lipid bilayers (31, 33, 47), and in real membranes (46, 48, 50). The fact that cholesterol promotes protein clustering in different types of bilayers, but that its effect on structural and mechanical properties is not universal indicates that there might be another mechanism. Moreover, protein clusters have been observed to be enriched in cholesterol (46), which is not accounted for by mechanisms implying a change in bilayer properties, although there might be a combination with the indirect or direct cholesterol-protein interaction mechanisms.

The mechanism implying a change of the bilayer properties focuses solely on the effect of lipids on the organization of proteins, while in reality there should also be a strong effect of proteins on the distribution of the lipids and on the properties of the bilayer, as proteins make up to 50 mass% of the membrane. In this context the hypothetical concept of a lipid shell, a lipid domain surrounding a protein and induced by the latter, was introduced (155, 280). Lipid shells might extend up to 10 nm from the protein surface, might be enriched or depleted in cholesterol, do not need to form a separate phase and exist as mobile entities in the plane of the membrane. Lipid shells should not be confounded with the first-shell lipids (281) or the lipid annulus (271, 280), which is the first layer of lipids surrounding the proteins due to direct or indirect chemical and physical interactions. Multiple ways have been proposed in which shells might form, for example, due to hydrophobic mismatch between protein and lipids (155).

Recent experiments indicate that model proteins with positive mismatch, when embedded in a bilayer containing DMPC and cholesterol, are surrounded by a cholesterol-enriched region, while less cholesterol is observed around proteins with a smaller hydrophobic length (20). This experiment supports the shell hypothesis. Similarly, Epand *et al* has reported several experimental studies indicating a protein-induced formation of cholesterol-rich domains (282–284). It thus seems that there might exist another mechanism by which cholesterol affects protein-protein interactions: the lipid shell mechanism. When cholesterol is added to a bilayer, certain proteins might induce a cholesterol-enriched or cholesterol-depleted lipid shell and those lipid shells might subsequently affect the interactions between the proteins.

Experimentally it would be a difficult task to distinguish between the different

mechanisms. Atomistic simulation studies identified specific cholesterol-sensing domains of certain proteins (278). However, for a systematic study of the collective behavior of lipids and proteins within a reasonable simulation time, a mesoscopic approach is required.

In this chapter we build on the developed coarse-grained model of a hydrated bilayer containing a phospholipid and cholesterol and in which peptides are embedded (71, 80, 232, 285). We systematically study the effect of cholesterol on the interactions between proteins. In particular, we use the flexibility of our model to study the effect of cholesterol at conditions where cholesterol hardly changes the properties of the bilayer and at conditions where cholesterol has a larger influence on the bilayer properties. We compute the potential of mean force between two proteins with positive mismatch in a bilayer with and without 40 mol% cholesterol at different temperatures and provide evidence for the lipid shell mechanism.

5.2 Model and Simulation Methods

Previously, Kranenburg *et al.* and Venturoli *et al.* developed a mesoscopic model of a hydrated lipid bilayer and transmembrane proteins, respectively (61, 71, 80). The phase behavior of the saturated lipid model and the adaptation of the bilayer and the protein to hydrophobic mismatch agree very well with the experimental observations (61). In Chapter 3, we used this mesoscopic model to study the free energy of lipid-mediated interactions between two proteins as a function of hydrophobic mismatch and protein diameter (210) and in Chapter 4 we extended this model of a hydrated lipid bilayer to include cholesterol (232). This model correctly describes the effects of cholesterol on the mechanical and structural properties of a saturated phosphatidylcholine bilayer and reproduces the main features of the experimental cholesterol-saturated lipid phase diagram. In this chapter, we combine the mesoscopic models of water, lipid, cholesterol, and protein. The model is summarized in Fig. 5.1.

The mesoscopic model was studied using a hybrid DPD-MC method. Simulations were performed in the $NP_{\perp}\gamma T$ ensemble, with $\gamma = 0$. For a detailed description of the simulation method and its applications, we refer to Chapter 2 and to relevant articles (71, 80, 100, 210). All simulations were performed in bilayers containing approximately 3,000 lipid or cholesterol molecules. For every cholesterol or lipid molecule, we have 25 water beads.

For the simulations we use a reduced temperature. The relation with the physical temperature can for example be estimated from comparison with experimental main and pre-transition temperatures. For $h_3(t_4)_2$ one obtains T=108.75T_r-8.6, with T_r the reduced temperature and T the Celsius temperature (285). For $h_3(t_5)_2$ one obtains T=133T_r-33 (80). For phospholipid-cholesterol systems it is useful to present the results as function of ΔT=T-T_m, with T_m the reduced temperature at which the

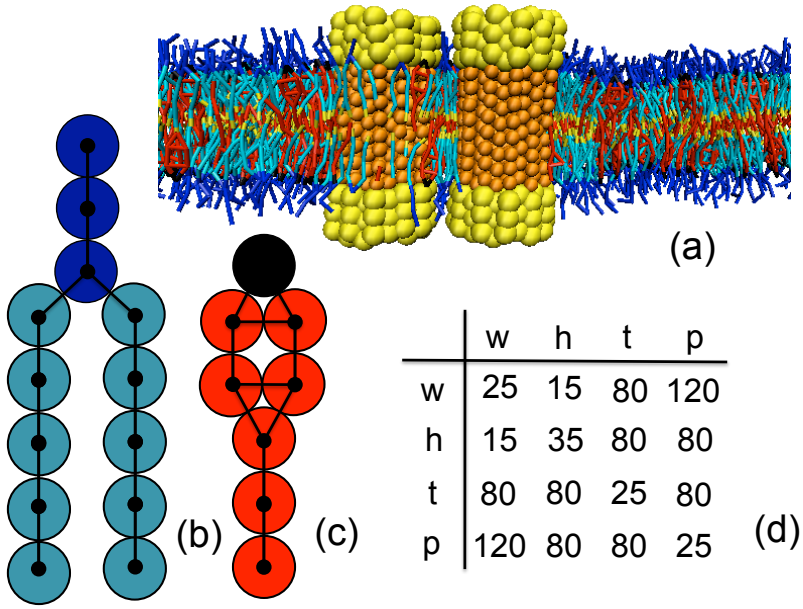

	w	h	t	p
w	25	15	80	120
h	15	35	80	80
t	80	80	25	80
p	120	80	80	25

Figure 5.1: Coarse-grained model and soft-repulsive interaction parameters. (a) Snapshot of a model bilayer containing phospholipids and cholesterol and in which two proteins are embedded. Water (type w) is not shown for clarity. The protein hydrophilic (type h) and hydrophobic (type p) beads are depicted in yellow and orange, respectively. (b) Coarse-grained model of a $h_3(t_5)_2$ phospholipid. Hydrophilic head beads (type h) are depicted in dark blue, while the hydrophobic tail beads (type t) are depicted in light blue. (c) Coarse-grained model of cholesterol. The hydrophilic (type h) and hydrophobic (type t) beads are depicted in black and red, respectively. (d) Table with the soft-repulsive interaction parameters a_{ij} between the four types of beads: water (w), hydrophilic (h), hydrophobic (t) and hydrophobic protein bead (p).

main phase transition of the bilayer takes place. $T_{m,h_3(t_4)_2}$=0.32 and $T_{m,h_3(t_5)_2}$=0.42.

5.3 Results

5.3.1 Effect of Cholesterol on Lipid Bilayer

It is useful to briefly review some aspects of the temperature-dependence of the effects of cholesterol on a phospholipid bilayer. In Fig. 5.2 a, the partial phase diagram is shown for a $h_3(t_4)_2$-cholesterol system (285) (see Chapter 4). At high temperatures, the $h_3(t_4)_2$ bilayer is in a liquid-disordered phase, while below the main phase transition temperature (T_m) the bilayer is in a rippled gel phase. Addition of cholesterol above T_m results in a gradual transition (crossover) of the liquid-disordered phase to

a so-called liquid-ordered phase. At sufficiently high temperatures the bilayer remains in the liquid-disordered phase.

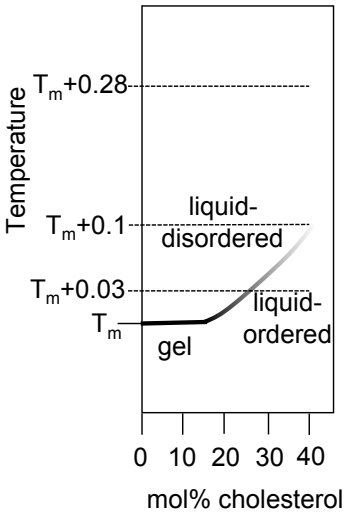

(a)

	hydrophobic thickness (Å)		average tail order		bending modulus (10^{-20} J)		
Δt / %c	0	40	0	40	0	40	
0.03	21.5$^+$	27.8$^+$	0.34	0.54	7.5	45.3	
0.1	20.4$^+$	25.8$^+$	0.25	0.4	6.9	23.0	$h_3(t_4)_2$
0.38	18.6$^+$	22. 0$^+$	0.18	0.28	6.2	10.3	
0.28	24.0$^+$	25.2$^+$	0.19	0.26	8.0	12.2	$h_3(t_5)_2$
6 °C	25.6	31.8*	4.6$^\sharp$	9.0$^{\sharp *}$	6.0	27.0*	DMPC
24 °C	-	-	3.5$^\sharp$	7.0$^{\sharp *}$	6.0	14.0*	
47 °C	26.8	30.2	0.28	0.6	7.5	7.0	DOPC
-	25.0	25.5	-	-	-	-	BPM

(b)

Figure 5.2: (a) Simulated partial phase diagram of $h_3(t_4)_2$-cholesterol (232, 285), with T_m the main phase transition temperature. b) Effect of cholesterol on the properties of a phospholipid bilayer at different temperatures $\Delta T=T-T_m$. Data are reported for 0 and 40 mol% cholesterol. The data for $h_3(t_4)_2$ and $h_3(t_5)_2$ are obtained from simulations, the data for DMPC, DOPC and BPM are experimental (19, 134, 286). DMPC and DOPC bilayers are examples of model saturated and unsaturated membranes, respectively, while BPM (basolateral plasma membrane) is an example of a real membrane. $T_{m,DMPC}=24^oC$, $T_{m,DOPC}=-17^oC$. notes: (*) data for 30 mol% cholesterol, (+) distance between the hydrophobic beads linked to the hydrophilic ones, (♯) first moment (10^{-4} Hz) of NMR spectrum, which is proportional to the tail order parameter, (-) no data available.

The effect of cholesterol on the bilayer hydrophobic thickness, average lipid tail order, and bilayer bending modulus is shown in Fig. 5.2 b for three different temperatures above T_m. For $\Delta T=T-T_m=0.03$, cholesterol significantly increases all three parameters due to the transition to the liquid-ordered phase. For $\Delta T=0.1$, the effect of cholesterol on the bending modulus is strongly reduced, and for $\Delta T=0.38$ the effect on all three parameters is much weaker. As shown in Fig. 5.2 b, similar trends have been observed experimentally, for example, for the DMPC-cholesterol system (285).

These different temperatures allow us to separate the different effects of cholesterol on the interactions of proteins. At high temperatures, cholesterol has very little effect on the properties of the bilayer. Experimentally this would correspond to a high-temperature DMPC bilayer. Or, if we use a different mapping of our mesoscopic

parameters, to those types of bilayer for which the addition of cholesterol has little effect (for example, strongly unsaturated lipid bilayers and real membranes (19)).

5.3.2 Protein Clustering

To explore the effect of cholesterol on the interactions between small transmembrane proteins, we simulated a system consisting of 49 small (diameter: 13.5 Å) proteins inserted in a large $h_3(t_5)_2$ bilayer of 100 nm^2 at ΔT=0.28. The proteins have a positive mismatch of 3.5 Å. Initially, the proteins were located at a maximal distance from each other on a square lattice. Figs. 5.3 a and b show snapshots after 10^6 DPD-MC cycles, which corresponds to approximately 0.1 to 0.4 ms (69). Without cholesterol relatively small protein clusters form (Fig. 5.3 a), while with 40 mol% cholesterol, we observed the formation of much larger protein clusters (Fig. 5.3 b).

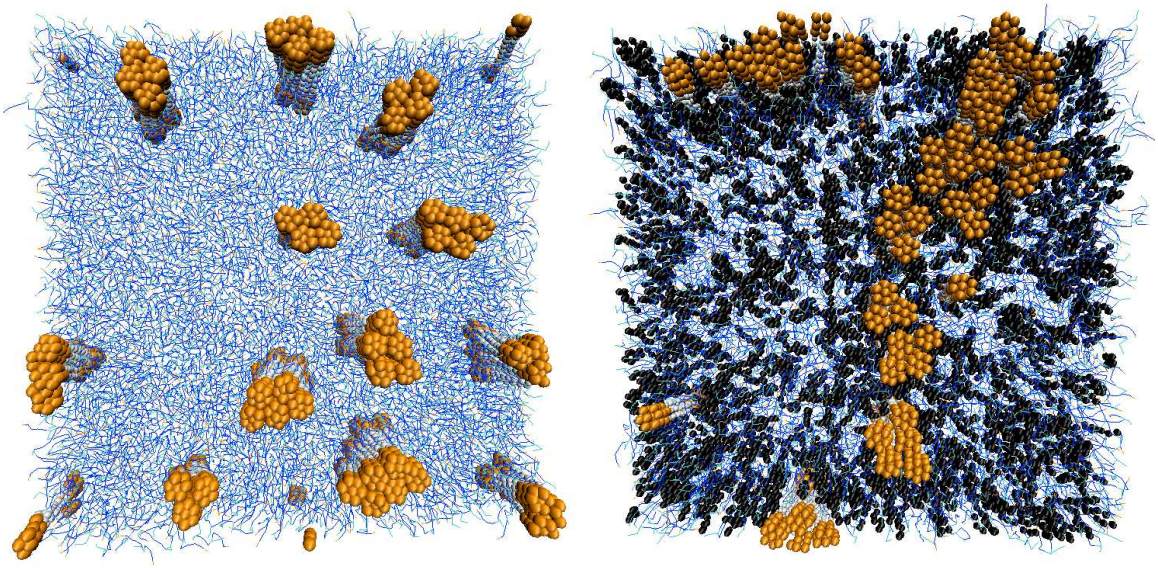

(a) (b)

Figure 5.3: Snapshot of a top view of a lipid bilayer after 10^6 MC-DPD cycles. The lipids are depicted in blue, cholesterol in black. The proteins, in orange, have a small diameter of 13.5 Å and a positive mismatch of 3.5 Å in (a) and 2.3 Å in (b). Water beads are not shown for clarity. Periodic boundary conditions apply. Initially the proteins were embedded as far as possible from each other. In (b), the $h_3(t_5)_2$ bilayer contains 40 mol% cholesterol. ΔT=0.28.

These simulations indicate that the lipid-mediated interactions between the proteins depend on the presence of cholesterol. Ideally, one would like to use these simulations to quantitatively compare with, for example, the FRET efficiency measured during relevant protein clustering experiments (31, 32). However, detailed analysis

shows that these simulations are not sufficiently long and that our system size is not sufficiently big to determine reliable equilibrium cluster-size distributions from these snapshots. The simulations, however, do suggest a marked effect of cholesterol on the interactions between membrane proteins, i.e., cholesterol enhances the formation of clusters, which is also observed experimentally (31, 33, 45–50). To quantify these effects of cholesterol on the interactions between proteins, we computed the potential of mean force.

The potential of mean force (PMF) as a function of the distance ξ between the centers of mass of two proteins (or cluster of proteins) was computed using a similar method as described in detail in Chapter 3 and in (210). A first estimation of the PMF was obtained using umbrella sampling with a harmonic heavyside biased potential. To unbias we used the weighted histogram analysis method (WHAM) (211, 212). We performed a forward and a backward PMF calculation. In a second step the biased potential is the sum of a heavyside potential and the inverse average PMF obtained from the previous step. This step was repeated, updating the PMF, until all the individual histograms of the windows showed a uniform distribution. Generally, 3 to 10 iterations were required to satisfy this condition.

5.3.3 Interactions between Two Proteins

Effect of Cholesterol We computed the PMF between two large proteins (N_P=43) with diameter 32 Å at the three temperatures ΔT=0.03, 0.1, and 0.38 in a $h_3(t_4)_2$-cholesterol bilayer. In Fig. 5.4 a, the PMFs are shown for ΔT=0.03 and 0.1. In a pure $h_3(t_4)_2$ bilayer the PMFs are mainly repulsive, except for the short-range direct protein-protein contact. The cut-off diameter of the soft-repulsive interactions is 6.46 Å, and thus the repulsive interaction between the proteins is entirely lipid-mediated. In Fig. 5.4 a, we also show an experimental PMF (36), for a comparable system: alamethicin pores (diameter 36 Å) in DMPC at 30^{o}C ($T_{m,DMPC}$= 24^{o}C). It is believed that alamethicin has a slight positive mismatch in DMPC because of its tilt (36). The amplitude and the range of the simulated and experimental repulsive interaction agree very well. The experimental PMF was obtained by fitting a quadratic potential to X-ray diffraction data. Therefore this PMF does not show the short-range oscillations.

At these low temperatures cholesterol significantly increases the hydrophobic thickness of the membrane. Due to the addition of 40 mol% cholesterol the bilayer hydrophobic thickness becomes approximately the same as the protein hydrophobic length. The hydrophobic mismatch becomes d=1.0 and d=-1.0 Å, for ΔT=0.03 and 0.1, respectively. As a result we expect that the lipid-mediated interactions disappear. Indeed, this is exactly what we observe, as shown in Fig. 5.4 a. It is interesting to compare these results with a situation where the hydrophobic mismatch remains constant. We changed the length of the protein such that the hydrophobic mismatch is the same in a bilayer with and without cholesterol. This was achieved by increasing

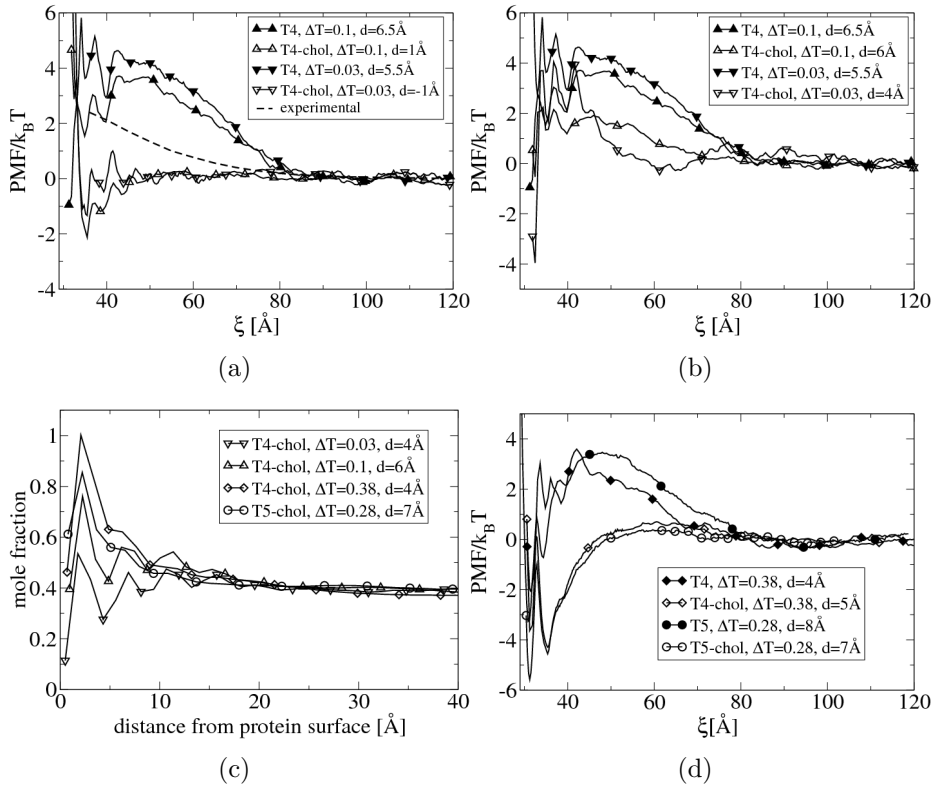

Figure 5.4: (a), (b) Potential of mean force as a function of the distance ξ between two proteins with diameter 32 Å, in a $h_3(t_4)_2$ bilayer with and without 40 mol% cholesterol at different temperatures ΔT=T-T$_m$. d is the positive hydrophobic mismatch between bilayer and protein. The dotted line represents the experimental PMF. In (a), d changes because of the bilayer thickening effect of cholesterol. In (b) we keep d constant by modifying the hydrophobic length of the protein. (c) mole fraction of cholesterol as function of the distance from the protein surface. The $h_3(t_4)_2$ and $h_3(t_5)_2$ bilayer contains 40 mol% cholesterol. (d) idem as (b), but at higher values of ΔT.

the protein hydrophobic length by one bead. The use of a coarse-grained model does not allow to have exactly the same hydrophobic mismatch in every case. The results are shown in Fig. 5.4 b. The repulsive interactions are again strongly reduced, particularly between 45 and 80 Å. This indicates that a change in hydrophobic mismatch is not the only mechanism by which cholesterol affects the protein-protein interactions.

In Fig. 5.4 c, the mole fraction of cholesterol is shown around a single protein for ΔT=0.03 and 0.1. The protein surface is enriched in cholesterol, most likely due to the preferential interaction between the rigid cholesterol ring and the smooth protein surface. However, the cholesterol-enrichment clearly extends up to a distance of 3 nm from the protein surface. This corresponds to 5 to 6 layers of lipids. The clear

presence of maxima and minima in the curves suggests a liquid-ordered phase. In fact, the fraction of cholesterol in this domain is strongly dependent on the hydrophobic mismatch. A cholesterol-depleted region is observed around proteins with negative mismatch (see Fig. 5.5).

Anderson *et al* (155) defined lipid shells as protein-induced domains which might extend up to 10 nm from the protein surface, might be enriched or depleted in cholesterol, do not need to form a separate phase and exist as mobile entities in the plane of the membrane. This description indicates that the protein-induced domains we observe are lipid shells.

It is, however, unclear whether cholesterol reduces the repulsive protein interactions due to the presence of the cholesterol-enriched shells. Indeed, as shown in Fig. 5.2 b, the addition of cholesterol also significantly increases the average lipid-tail order and the bending modulus. The change in these parameters could also affect the protein interactions.

Therefore, we performed a similar simulation at a higher temperature: ΔT=0.38. At this temperature the effect of cholesterol on the tail order and bending modulus is considerably less (see Fig. 5.2 b). The results are shown in Fig. 5.4 d. The hydrophobic mismatch is again kept constant. In a pure $h_3(t_4)_2$ bilayer, the PMF is similar to the PMF obtained at lower temperatures. When 40 mol% cholesterol is added to the bilayer the repulsive interaction between 45 and 80 Å is again strongly reduced. Moreover, the short distance between proteins is dramatically stabilized. In Fig. 5.4 c is shown that also for this case there exists a cholesterol-enriched shell around the proteins. Thus, it is very likely that the protein-induced, cholesterol-enriched domains also affect the lipid-mediated protein-protein interactions.

To check whether our results depend on the lipid tail length, we performed similar simulations in a $h_3(t_5)_2$ bilayer. The results for ΔT=0.28 are shown in Fig. 5.4 c and Fig. 5.4 d and are very similar to the $h_3(t_4)_2$ system. Because at higher temperature the lipid shell mechanism is less superadded by effects of cholesterol on the structural and mechanical bilayer properties, we use the $h_3(t_5)_2$-cholesterol system at ΔT=0.28 to further investigate the lipid shell mechanism.

The Lipid Shell Mechanism The region surrounding one protein with positive mismatch is slightly enriched in cholesterol. We simulated the local membrane composition around two interacting proteins. For example, from Fig. 5.6 a, b (red line), one can see an increasing cholesterol concentration between two proteins interacting at 58 and 45 Å. At a distance of 58 Å, the fraction of cholesterol between both proteins is 0.5, while at 45 Å it becomes 0.8. In Fig. 5.7, the average cholesterol mole fraction around both proteins is shown for the entire membrane. According to the lipid shell mechanism, the effect of cholesterol on the PMF between two proteins with positive mismatch is related to the local composition around the two interacting proteins.

To understand how the high cholesterol fraction between the two approaching proteins affects the PMF, the concept of hydrophilic shielding is useful. We introduced

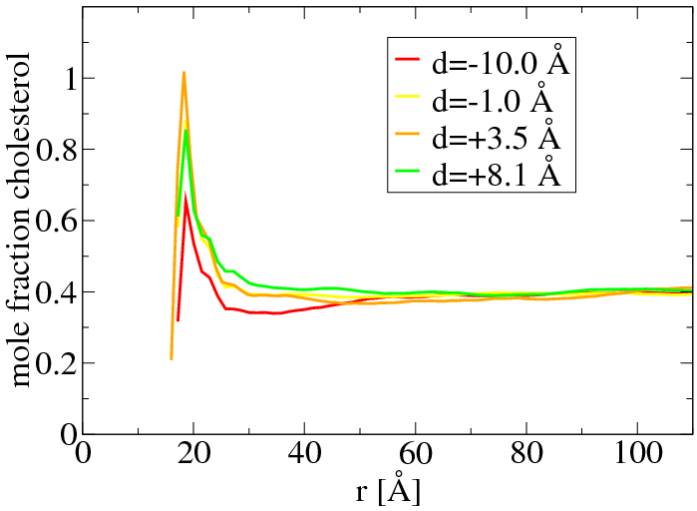

Figure 5.5: Mole fraction of cholesterol, as function of the distance r from the center of mass of a large protein with diameter 32 Å with different mismatches, in a $h_3(t_5)_2$ bilayer with and without 40 mol% cholesterol. ΔT=0.28

the hydrophilic shielding parameter in Chapter 3 as a measure for the relative number of hydrophilic beads shielding the hydrophobic beads from the water, at a given position in the membrane plane (210). Within this concept, the protein interactions are interpreted as resulting from the dynamic reorganization of the entire system to maintain an optimal hydrophilic shielding of the protein and lipid hydrophobic parts, constrained by the flexibility of the components. For this we define the lipid head fraction as the number of lipid head beads at a given position in the plane of the lipid bilayer in which the protein is embedded divided by the average number of lipid head beads of a pure bilayer without embedded proteins. The lipid tail fraction is defined in an analogous way. The hydrophilic shielding parameter, defined at every position in the plane of a lipid bilayer, is the ratio of the lipid head fraction and the lipid tail fraction, and is a measure for the relative number of hydrophilic beads shielding the hydrophobic tail beads from the water at a given position. This parameter is one at sufficient distances from a protein. When the hydrophilic shielding parameter is bigger than one, the density of the lipid heads shielding the lipid tails present is higher than in the pure lipid bilayer.

Fig. 5.6 a, b shows the hydrophilic shielding parameter for the two proteins. In a bilayer without cholesterol (green lines), at a distance sufficiently far from the proteins, the bilayer is not perturbed due to the presence of the proteins and the value of the hydrophilic shielding parameter fluctuates per definition around one. In the regions close to, and in particular in between, the proteins there is a large deviation from the optimal hydrophilic shielding. When both proteins come closer, from 58 to 45 Å, the hydrophilic shielding in between both proteins further decreases.

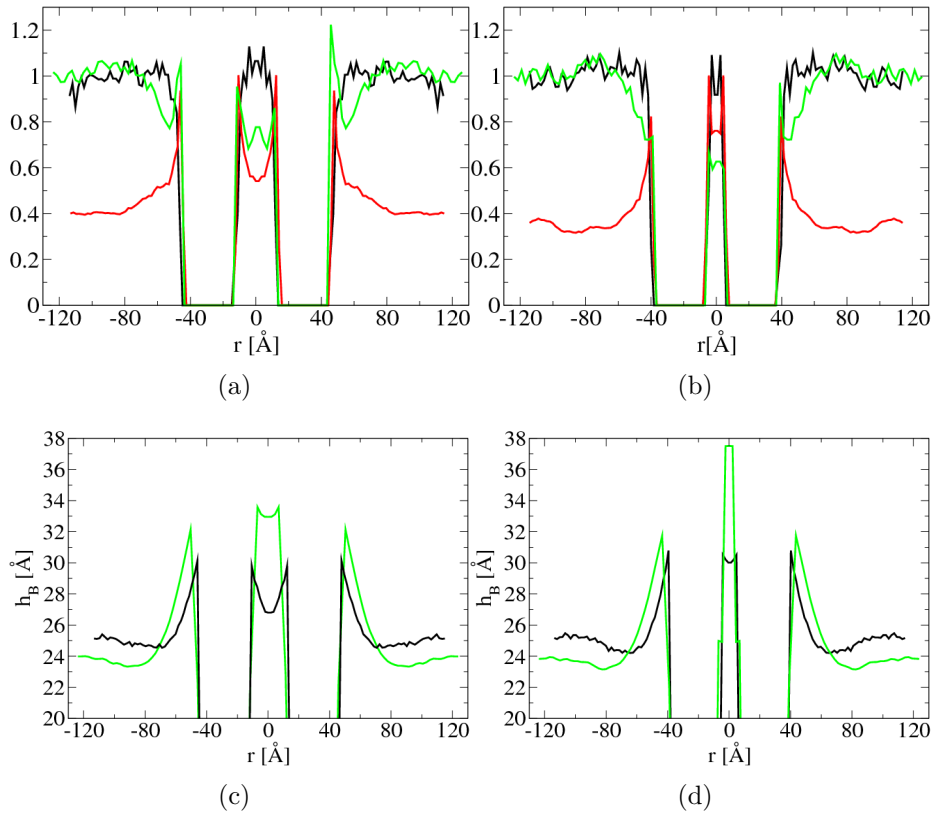

Figure 5.6: (a), (b): Average cholesterol mole fraction (red) and hydrophilic shielding parameters (black, green) around two large proteins. Simulations were performed in a bilayer without (green lines) and with (black lines) 40 mol% cholesterol. (c), (d): Hydrophobic thickness of the bilayer surrounding two large proteins. The proteins are at a distance of 58 Å (a,c) and 45 Å (b,d). Proteins have a diameter of 32 Å and a positive mismatch of +8.1 Å.

Thus, the lipids in between the proteins can only reorganize in a way that further decreases the hydrophilic shielding in between the proteins. This is reflected in the PMFs by the free energy increase between 58 and 45 Å (see Fig. 5.4 d).

The addition of cholesterol causes a completely new organization of the remaining lipids and cholesterol, with an improved shielding as result (black lines). This effect is particularly strong in between both proteins, where the shielding is now around one. Because the hydrophilic shielding parameter is a measure of the membrane perturbation due to the presence of the proteins, this result indicates that cholesterol naturally alleviates the unfavorable lipid perturbations due to positive hydrophobic mismatch. When both proteins come closer, from 58 to 45 Å, the average hydrophilic shielding in between both proteins does not change. This is reflected in the PMFs by the constant free energy between 58 and 45 Å (see Fig. 5.4 d). In the SI we discuss

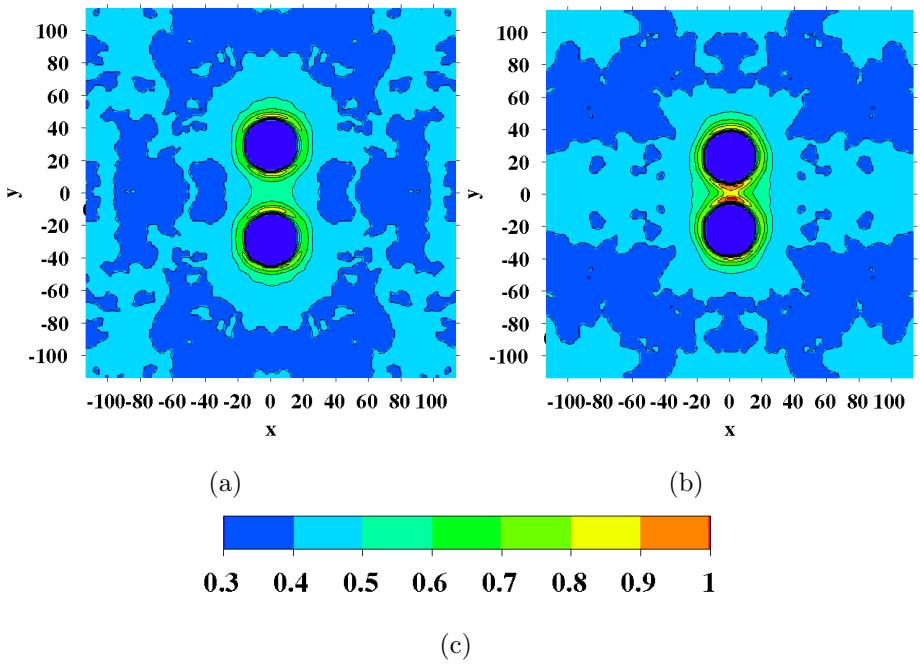

Figure 5.7: Average cholesterol mole fraction around two large proteins with diameter 32 Å with a positive mismatch of 7 Å. The proteins (dark blue circles) are at a distance of 58 Å (a) and 45 Å (b). The $h_3(t_5)_2$ bilayer contains 40 mol% cholesterol. The values were averaged over both bilayer leaflets. Distances are in Å. ΔT=0.28.

the effect of cholesterol on the hydrophobic thickness profile around both proteins.

In Fig. 5.6 c, d, the hydrophobic thickness of the bilayer around the two large proteins with positive mismatch is shown. One can see that the hydrophobic thickness of the bilayer increases by only 1.2 Å due to the addition of cholesterol. The different hydrophobic thickness profiles in between both proteins reflect the different ways bilayers with and without cholesterol adapt to the approach of both molecules. It seems that in a lipid bilayer without cholesterol it is difficult to maintain the negative curvature in between both proteins when they come close. When cholesterol, which has an intrinsic negative curvature, is added to the bilayer, the region between the two approaching proteins has a nice negative curvature until both proteins touch.

When the bilayer contains 40 mol% cholesterol, the effective hydrophobic mismatch decreases by 1.2 Å. Considering only the effect of hydrophobic mismatch, one would thus expect that due to the addition of cholesterol the free energy of the protein dimer configuration would increase. As shown in Fig. 5.4 d, we observe the opposite. This indicates that the composition of the membrane surrounding the proteins also plays a very important role.

5.3.4 PMFs for Protein Clustering

To obtain some quantitative insights into the clustering behavior, we computed the PMFs between two small (diameter 13.5 Å) proteins, between a cluster of 7 proteins and a single protein and between two clusters of 7 proteins (see Fig. 5.8). Using geometric arguments one can see that a cluster of 7 proteins is relatively stable under mismatch conditions.

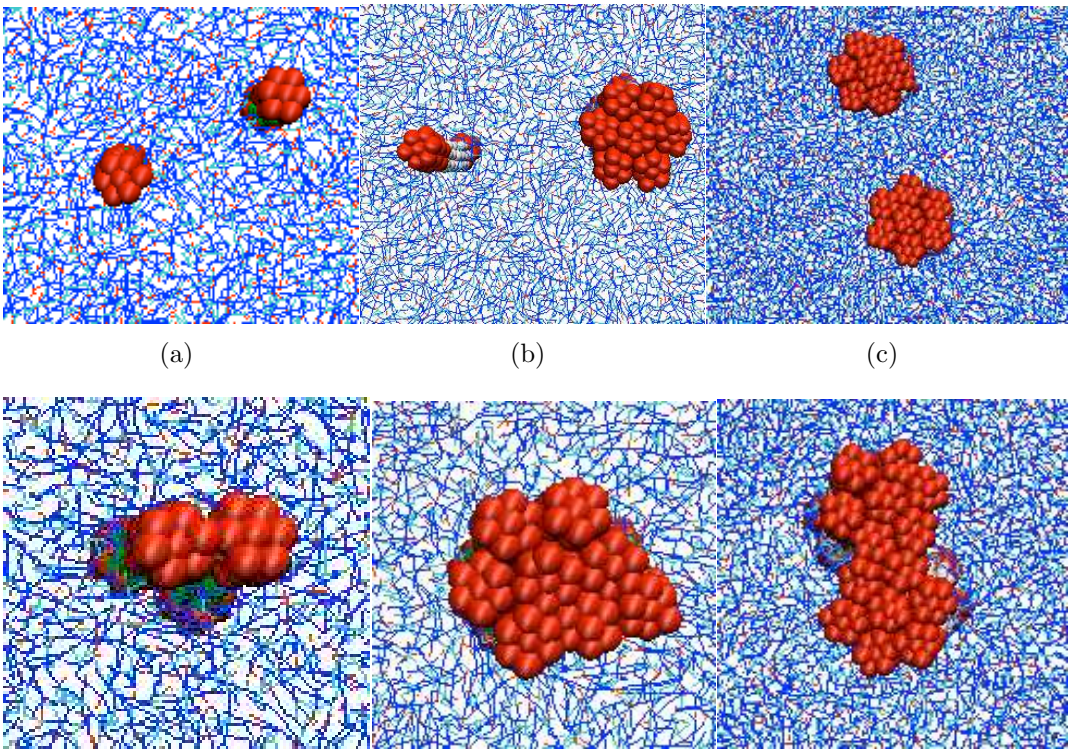

Figure 5.8: Protein and protein cluster configurations related to the PMF calculations. Snapshot of a a top view of a lipid bilayer. The lipids are depicted in blue, the proteins in red. (a), (b) and (c) correspond to the dissociated configuration for the 1-1, 7-1 and 7-7 PMF calculations, respectively. (d), (e) and (f) illustrate the associated configurations for the 1-1, 7-1 and 7-7 PMF calculations, respectively. In the associated configuration both clusters are in close contact, as shown in the pictures. The further merging of clusters is not described.

Fig. 5.9 a shows the PMFs for the interaction between two single proteins, between a single protein and a cluster of seven, and between two clusters of 7 proteins with slight positive mismatch. In a bilayer without cholesterol, we observe two trends. First, the depth of the free energy minimum, corresponding to the associated configuration, increases in the order: 1-1 $<$ 7-1 $<$ 7-7. Secondly, the height of the repulsive

barrier at intermediate distance increases in the order: 1-1 (1.5 k_BT) < 7-1 (3 k_BT) <7-7 (10.5 k_BT). The presence of this repulsive barrier explains why our simulations show small clusters that were stable during the length of the simulations.

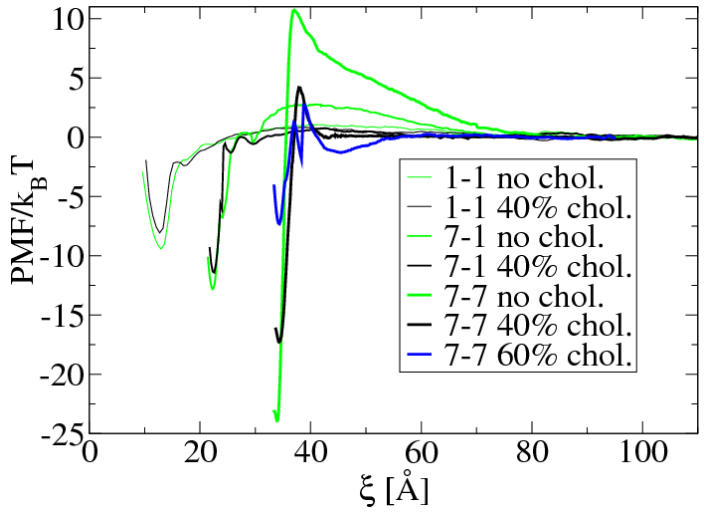

(a)

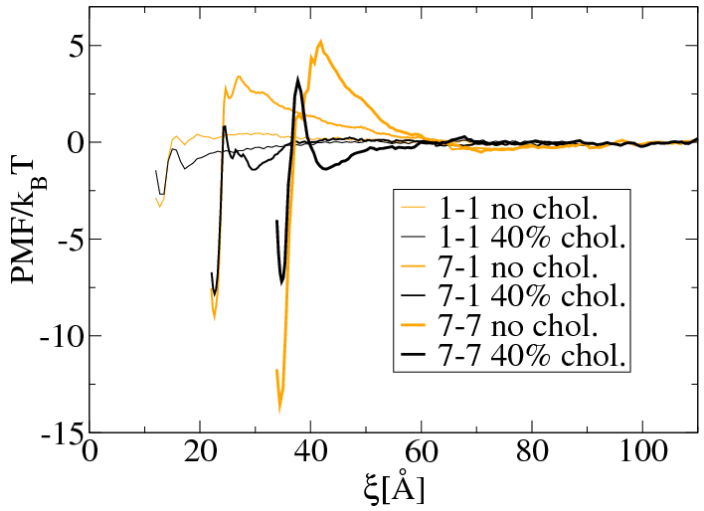

(b)

Figure 5.9: Potential of mean force as a function of the distance ξ between two proteins (1-1), between a single protein and a cluster of seven proteins (1-7) and between two clusters of 7 proteins (7-7) in a $h_3(t_5)_2$ bilayer without (orange, green), with 40 mol% (black) and with 60 mol% (blue) cholesterol. The proteins in (a) have a positive mismatch of +8.1 Å, while the proteins in (b) have a positive mismatch of +3.5 Å. ΔT=0.28.

The addition of cholesterol slightly weakens the free energy minima. More im-

portantly, cholesterol has a dramatic effect on the aggregation barriers. At 40 mol% cholesterol, the barrier is reduced from a wide barrier of 10.5 k_BT to a small short-range barrier of 4 k_BT. A second free energy minimum of -1.5 k_BT, corresponding to the presence of cholesterol between the proteins (protein clusters) appears at a distance of 45 Å in a bilayer with 60 mol% cholesterol.

We repeated the same simulations for proteins with slight positive mismatch (4 Å). The results are shown in Fig. 5.9 b and are similar to the results for mismatch 8.1 Å. The hight of the wide repulsive barrier between both clusters is now smaller (5.5 k_BT), and the addition of cholesterol again reduces the barrier to a short-range barrier of 3.5 k_BT. Less cholesteroll is required for the second free energy minimum to appear.

Because the aggregation barrier directly originates from the reorganization of lipids, one expects it to rise with increasing protein or protein cluster diameter. Indeed, the larger the protein or the cluster, the larger the perturbed area in between the two approaching entities. A larger membrane area with a lower hydrophilic shielding corresponds to a higher increase in the free energy. On the other hand, the effect of cholesterol should not only depend on the size of the proteins or clusters but also on the cholesterol concentration in the bulk. Indeed, the bigger the size of the protein clusters, the more cholesterol will be required in between both clusters to alleviate the membrane perturbations.

Similarly, we performed simulations for proteins with negative mismatch. The results are shown in Fig. 5.10. For negative mismatch the small aggregation barrier does not grow with increasing cluster size. Cholesterol does not affect the lipid-mediated attractive PMF between proteins with negative mismatch.

5.3.5 Effect on the Selectivity

We considered a system similar to the one shown in Fig. 5.3, but with small proteins with three different types of mismatch: negative (-10 Å), negligible (-1 Å) and positive (8.1 Å). We observed that proteins selectively aggregate with proteins with the same mismatch (a snapshot of the system is shown in Fig. 5.11). In Fig. 5.12 a, the PMFs are shown between two proteins with positive and negligible, two with negative and positive and two with negligible and positive mismatch. The lipid-mediated interactions are purely repulsive in all three cases. The PMFs between proteins with the same mismatch are attractive. These PMFs explain the selective aggregation between the proteins. We performed the same simulations again, but now in a bilayer containing 40 mol% cholesterol. The PMFs between proteins with different mismatch are shown in Fig. 5.12 b. Although cholesterol slightly reduces the repulsion, its effect on this type of repulsive interactions is very small. An exception is the interaction between a protein with negative and negligible mismatch, which becomes attractive due to the addition of cholesterol.

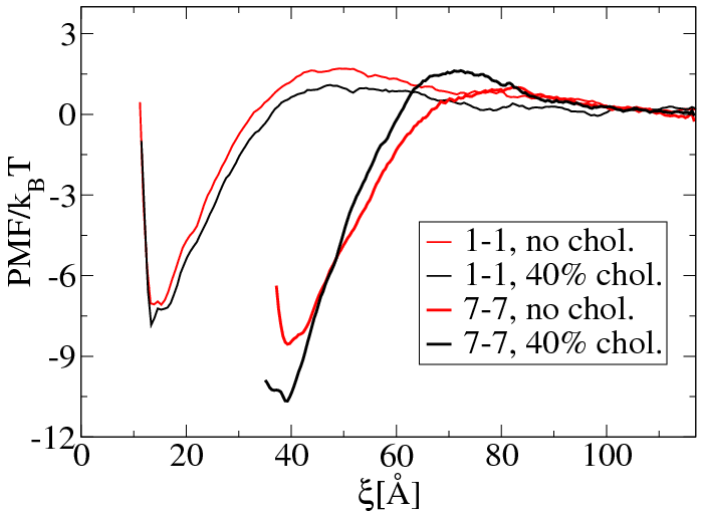

Figure 5.10: Potential of mean force as a function of the distance ξ between two proteins (1-1) and between two clusters of 7 protein (7-7) in a $h_3(t_5)_2$ bilayer without (red) and with (black) 40 mol% cholesterol. The proteins have a negative mismatch of -10 Å. ΔT=0.28.

5.4 Discussion

The simulated PMFs between proteins (protein clusters) with positive mismatch indicate that there is an aggregation barrier, the size of which increases with growing cluster size. For proteins with negative mismatch no growing aggregation barrier is observed. Thus, the cluster formation for positive mismatch will be very different from negative mismatch. For negative mismatch one expects a phase separation between proteins and lipids, while for positive mismatch the aggregation barriers or the purely repulsive interactions might significantly slow down or inhibit the clustering process. This is indeed observed experimentally (32). Unfortunately, many protein clusters observed in real membranes contain a number of proteins much larger than accessible with our mesoscopic model and simulation method within a reasonable time (45, 46, 48).

Several independent experiments indicate that the addition of cholesterol further enhances the aggregation of membrane proteins (31, 33, 45–50). In this chapter we provide simulation evidence for a lipid-shell mechanism by which cholesterol modifies lipid-mediated protein-protein interactions. We show that proteins with hydrophobic mismatch induce cholesterol-enriched or cholesterol-depleted shells surrounding the proteins in agreement with the shell hypothesis proposed by Anderson *et al* (155). The protein-induced shells then modify the lipid-mediated interactions between the proteins. Interestingly, Nyholm *et al* (20) recently found experimental indication for a cholesterol-enriched region around a model protein with positive mismatch in a

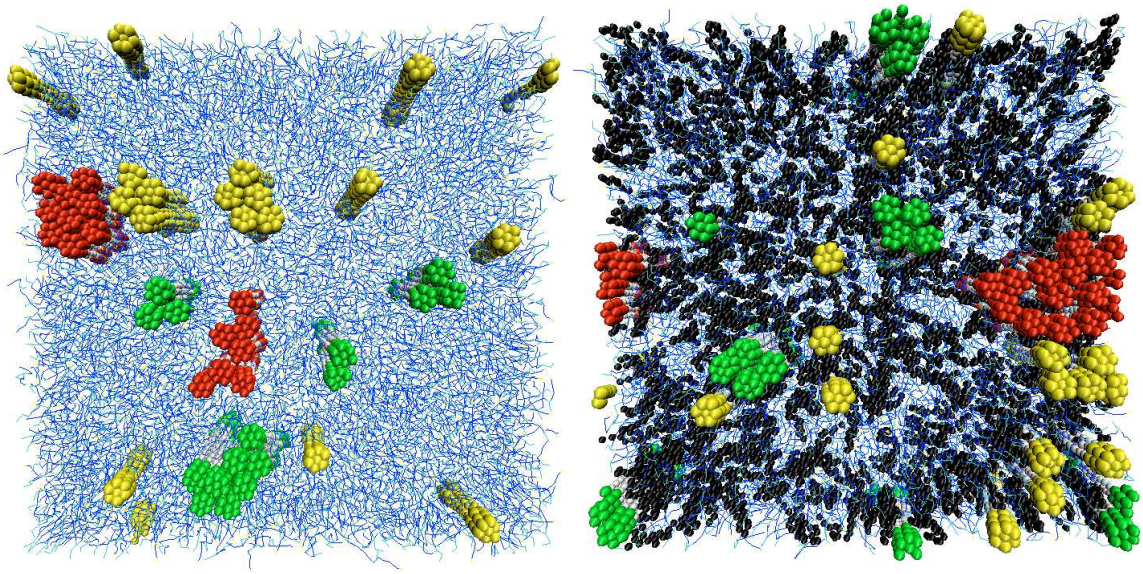

(a) (b)

Figure 5.11: Snapshot of a top view of a lipid bilayer after 10^6 MC-DPD cycles. The bilayer in (a) and (b) contains 3 different types of proteins. The $h_3(t_5)_2$ lipids are depicted in blue, cholesterol in black. Proteins with a negative mismatch of -10 Å are red, with negligible mismatch of -1 Å are yellow and with a positive mismatch of +8.1 Å are green. Water beads are not shown for clarity. Periodic boundary conditions apply. Initially the proteins were mixed and embedded as far as possible from each other. In (b), the bilayer contains 40 mol% cholesterol. The addition of cholesterol changes the mismatch by -1.2 Å. ΔT=0.28.

DMPC bilayer containing a small amount of cholesterol. In agreement with our simulation results they observed that the cholesterol-enrichment is less around proteins with no or negative mismatch. It would be very interesting to see whether all-atom simulations find evidence for the shell hypothesis.

Our results thus suggest that proteins with positive mismatch would prefer cholesterol-rich regions because cholesterol naturally replaces the perturbed lipids, and thus alleviates the perturbation. Several authors made similar observations, but explained them using solely structural and mechanical arguments, and suggested that this sorting might play a role in the secretory pathway (186, 275, 287, 288).

The interaction between two proteins with positive mismatch surrounded by cholesterol-enriched shells is significantly less repulsive. In some cases the interaction even becomes attractive. Thus, our results suggest the formation of much larger, cholesterol-enriched, protein clusters in the presence of cholesterol. This is for example observed for syntaxin proteins in different real membranes (46). However, the direct comparison with experimental results is difficult, because our protein model is very general,

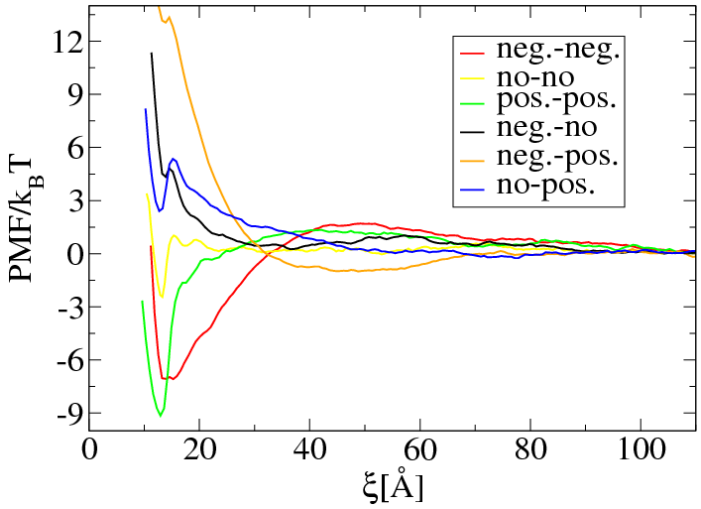

(a)

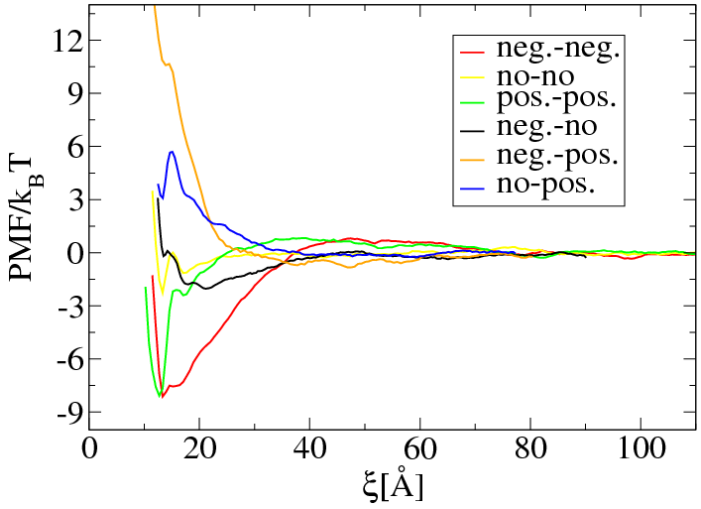

(b)

Figure 5.12: Potential of mean force as a function of the distance ξ between two proteins (1-1) in a $h_3(t_5)_2$ bilayer without (a) and with (b) 40 mol% cholesterol. The six PMFs describe the six possible single protein - single protein interactions that might occur in the system shown above. Negative mismatch is -10 Å, negligible mismatch is -1 Å and positive mismatch is +8.1 Å. The addition of cholesterol changes the mismatch by -1.2 Å. ΔT=0.28.

while in reality specific protein-protein interactions exist which also determine the protein-protein interactions.

It is interesting to compare the shell mechanism to the wetting and capillary condensation mechanism proposed by Gil *et al* (272) for a membrane consisting of

two coexisting phases and proteins. In the shell mechanism the two-phase coexistence is not a preexisting condition and the proteins are not surrounded by one particular phase but by a domain induced by the proteins, and with a different composition (not necessarily a different phase) than the bulk membrane. In the absence of the proteins, the two phases are present in the wetting model, while in the shell model, a single-phase homogeneous membrane exists.

We show that the origin of lipid-mediated selectivity is a lipid-mediated repulsive interaction between the different proteins. Cholesterol has only a modest effect. Experiments directly mimicking this simulation are not available in the literature. If we interpret the degree of hydrophobic mismatch as a parameter quantifying the unfavorable hydrophobic exposure of a misfolded protein, our results show how lipid-mediated interactions might play a role in the experimentally observed selective aggregation of misfolded proteins with misfolded proteins with a similar hydrophobicity (289).

In this chapter we presented a lipid shell mechanism by which cholesterol might affect lipid-mediated protein-protein interactions. In line with the shell hypotheses we show that proteins induce cholesterol-enriched and cholesterol-depleted shells, which modify the interactions between the proteins. The simulation results are in line with, and might explain, several experimental observations related to an increased protein aggregation in the presence of cholesterol.

Chapter 6

Conclusions

In this thesis we presented a simulation study of a mesoscopic model of a hydrated phospholipid bilayer with embedded protein pairs of different diameters and at different hydrophobic mismatch conditions. The only direct interactions considered in our model are the short-range soft repulsive interactions between the different bead-types, representing hydrophobic and hydrophilic forces, and the internal rigidity of the proteins and the lipids. Because of its simplicity, our model provides a framework to gain insight into the mechanism by which hydrophobic and hydrophilic interactions induce a reorganization of all the components of the system (water, lipids, and proteins) after the insertion in the bilayer of one or more proteins. Specific long-range attractive and repulsive protein-protein interactions were found to spontaneously emerge during the dynamic reorganization of the components of the system to improve the hydrophilic shielding of the hydrophobic parts of the proteins and the lipids. The nature of the protein-protein interactions was quantitatively described by calculating the potential of mean force as a function of the distance between two proteins and it was found to depend on the degree of hydrophobic mismatch and on the size of the proteins.

To study the effect of cholesterol we have introduced a very simple model of a hydrated saturated phospholipid (DMPC) and cholesterol. In this model, cholesterol is characterized by a bulky hydrophobic core, a small hydrophilic head, and a small hydrophobic tail. These ingredients give our model of cholesterol many unique properties. Our model agrees well with experimental data on structural and mechanical properties of the bilayer, as well as with all-atom simulations. This agreement coupled with the reproduction of many experimentally observed DMPC-cholesterol structural and mechanical properties indicates that our model captures the essence of DMPC-cholesterol mixing. The temperature-composition dependence of the lateral organization of cholesterol might give important information to better interpret experimental data.

For most thermodynamic systems the addition of a second component induces disorder into the system. The addition of cholesterol, however, causes the lipid molecules to order. Our simulations show that this effect strongly depends on temperature.

At very high temperature the membrane can accommodate a significant amount of cholesterol without structural changes. At low temperatures cholesterol induces different phases in which the lipid tails are more ordered. Such a more ordered structure allows the lipids to support cholesterol by reducing the water hydrophobic contacts. In this context one can understand the role of the bulky hydrophobic core and the relatively small hydrophilic head.

A main result is the phase diagram shown in Fig. 4.5. We have argued that one can find experimental evidence for most of these phases. However, more importantly our model calculations may provide a rationale for why the "true" experimental phase diagram is not known. The simulations show that cholesterol induces many subtle structural changes, which may or may not be observable for different experimental techniques. Reflecting the simplicity of the model, we obtain general insights which may shed some light on the experimental phase diagrams.

We found that cholesterol significantly reduces the repulsive interactions between large proteins with a positive mismatch. We showed that cholesterol affects the protein interactions via a lipid-shell mechanism: in line with the shell hypotheses proteins induce cholesterol-enriched and cholesterol-depleted shells, which modify the interactions between the proteins.

The simulated PMFs between clusters of proteins with positive mismatch indicate that there is an aggregation barrier, the size of which increases with growing cluster size. In the presence of cholesterol this aggregation barrier is absent. A second minimum occurs corresponding with the cholesterol-enriched configuration: cholesterol in between the two protein clusters. For proteins with negative mismatch no growing aggregation barrier is observed. Thus, the cluster formation for positive mismatch is very different from negative mismatch. For negative mismatch one expects a phase separation between proteins and lipids, while for positive mismatch the aggregation barriers or the purely repulsive interactions might significantly slow down or inhibit the clustering process. We also showed that the origin of lipid-mediated selectivity is a lipid-mediated repulsive interaction between proteins with a different mismatch. Cholesterol has only a modest effect on this selectivity. It is surprising to see how our simple model leads to such a rich and complex behavior.

Many two-dimensional models exist to study protein clustering with Monte Carlo methods. These models are often applied to interpret experimental measurements of protein clustering (for example FRET or X-ray diffraction experiments). Only proteins are represented, interacting via a potential which is fitted to the experimental data. Only two-body interactions are considered. However, our simulations clearly show that many-body interactions cannot be neglected. For example, modeling the clustering of proteins with negative mismatch based on only the two-body potential (the PMF between two single proteins) would lead to an increasing aggregation barrier with cluster size. Due to many-body interactions this is not observed in our mesoscopic simulations.

The two- and many-body interactions between proteins and protein clusters ob-

tained from our mesoscopic simulations might be used to develop more precise two-dimensional models of protein clustering. It would not only allow to better interpret experimental results, but also to study systems which are statistically significant and thus comparable with, for example, FRET experiments. Such a two-dimensional model would also allow to combine lipid-mediated interactions with direct protein-protein interactions.

In this work we showed that a single extra component like cholesterol might significantly change the nature of the interaction between proteins. Real biological systems contain a wide variety of lipids. The question thus arises wether diverse membrane compositions lead to a wide range of indirect protein-protein interactions or wether sterols like cholesterol are unique in affecting protein interactions. Hence, a next logical step to gain insight into this collective behavior is to add an extra lipid to the membrane, for example an unsaturated lipid, and to study its effect on the protein interactions.

Real biological membranes not only contain a much wider variety of lipids, they also contain a significant amount of proteins. In most experimental model membranes and in our mesoscopic model the membrane is a lipid bilayer in which a relatively low concentration of proteins is embedded. It would be interesting to investigate the effect of cholesterol on the properties of a lipid bilayer and on lipid-mediated protein interactions at a high protein concentration.

Bibliography

[1] Alberts, B., A. Johnson, J. Lewis, M. Raff, K. Roberts, and P. Walter, 2002. Molecular Biology of the cell. Garland Science, New York.

[2] Kovacs, F., J. Quine, and T. A. Cross, 1999. Validation of the single-stranded channel conformation of gramicidin A by solid-state NMR. *Proc. Natl. Acad. Sci. USA* 96:7910–7915.

[3] Tanford, C., 1978. The hydrophobic effect and the organization of living matter. *Science* 200:1012–1018.

[4] Tanford, C., 1980. Hydrophobic Effect: Formation of Micelles and Biological Membranes. Wiley, New York.

[5] Chandler, D., 2005. Interfaces and the driving force of hydrophobic assembly. *Nature* 437.

[6] Meyer, E. E., K. J. Rosenberg, and J. Israelachvili, 2006. Recent progress in understanding hydrophobic interactions. *Proc. Natl. Acad. Sci. USA* 103:15739–15746.

[7] Edidin, M., 2003. Lipids on the frontier: a century of cell-membrane bilayers. *Nat. Rev. Mol. Cell Bio.* 4:414–418.

[8] Bangham, A. D., and R. W. Horne, 1964. Negative staining of phospholipids and their structural modification by surface-active agents as observed in the electron microscope. *J. Mol. Biol.* 8:660–668.

[9] Bowie, J. U., 2005. Solving the membrane protein folding problem. *Nature* 438:581–589.

[10] Zhang, W., A. Campbell, S. C. King, and W. Dowhan, 2005. Phospholipids as determinants of membrane protein topology. *J. Biol. Chem.* 280:26032–26038.

[11] Killian, J. A., 1998. Hydrophobic mismatch between proteins and lipids in membranes. *Biochim. Biophys. Acta* 1376:401–416.

[12] Bouvier, M., 2001. Oligomerization of G-protein-coupled transmitter receptors. *Nature Reviews Neuroscience* 2:274–286.

[13] George, S. R., B. F. O'Dowd, and S. P. Lee, 2002. G-protein-coupled receptor oligomerization and its potential for drug discovery. *Nature Drugs Disovery* 1:808–820.

[14] Killian, J. A., 2003. Synthetic peptides as models for intrinsic membrane proteins. *FEBS Lett.* 555:134–138.

[15] Lee, A. G., 2003. Lipid-protein interactions in biological membranes: a structural perspective. *Biochim. Biophys. Acta* 1612:1–40.

[16] Lee, A. G., 2004. How lipids affect the activities of integral membrane proteins. *Biochim. Biophys. Acta* 1666:62–87.

[17] Killian, J. A., and T. K. M. Nyholm, 2006. Peptides in lipid bilayers: the power of simple models. *Curr. Opin. Struct. Biology* 16:473–479.

[18] Nyholm, T. K. M., S. Özdirekcan, and J. A. Killian, 2007. How protein transmembrane segments sense the lipid environment. *Biochemistry* 46:1457–1465.

[19] Mitra, K., I. Ubarretxena-Belandia, T. Taguchi, G. Warren, and D. M. Engelman, 2004. Modulation of the bilayer thickness of exocytic pathway membranes by membrane proteins rather than cholesterol. *Proc. Natl. Acad. Sci. USA* 101:4083–4088.

[20] Nyström, J. H., M. Lönnfors, and T. K. M. Nyholm, 2010. Transmembrane peptides influence the affinity of sterols for phospholipid bilayers. *Biophys. J.* 99:526–533.

[21] de Planque, M. M. R., D. V. Greathouse, R. E. Koeppe II, H. Schäfer, D. Marsh, and J. A. Killian, 1998. Influence of lipid/peptide hydrophobic mismatch on the thickness of diacylphosphatidylcholine bilayers. A ^2HNMR adn ESR study using designed transmembrane α-helical peptides and gramicidin A. *Biochemistry* 37:9333–9345.

[22] Ridder, A. N. J. A., W. Van De Hoef, J. Stam, A. Kuhn, B. De Kruijff, and J. A. Killian, 2002. Importance of hydrophobic matching for spontaneous insertion of a single-spanning membrane protein. *Biochemistry* 41:4946–4952.

[23] Strandberg, E., S. Özdirekcan, D. T. S. Rijkers, P. C. A. van der Wel, R. E. Koeppe II, R. M. J. Liskamp, and J. A. Killian, 2004. Tilt angles of transmembrane model peptides in oriented and non-oriented lipid bilayers as determined by ^{2}H solid state NMR. *Biophys. J.* 86:3709–3721.

[24] M., W. T., P. C. A. van der Wel, J. A. Killian, R. E. Koeppe II, and H. W. Huang, 2003. Hydrophobic mismatch between helices and lipid bilayers. *Biophys. J* 84:379–385.

[25] Özdirekcan, S., D. T. S. Rijkers, R. M. J. Liskamp, and J. A. Killian, 2005. Influence of flanking residues on tilt and rotation angles of transmembrane peptides in lipid bilayers. A solid-state ^{2}H NMR study. *Biochemistry* 44:1004–1012.

[26] de Planque, M. R. R., and J. A. Killian, 2003. Protein-lipid interactions studied with designed transmembrane peptides: role of hydrophobic matching and interfacial anchoring. *Mol. Membr. Biol.* 20:271–284.

[27] Lehtonen, J. Y. A., and P. K. J. Kinnunen, 1997. Evidence for phospholipid microdomain formation in liquid crystalline liposomes reconstituted with Escherichia coli lactose permease. *Biophys. J* 72:1247–1257.

[28] Dumas, F., M. M. Sperotto, M. C. Lebrum, J.-F. Tocanne, and O. G. Mouritsen, 1997. Molecular sorting of lipids by bacteriorhodopsin in dilauroylphosphatidylcholine/distearoylphosphatidylcholine lipid bilayers. *Biophys. J.* 73:1940–1953.

[29] Ridder, A. N. J. A., E. R. J. Spelbrink, J. A. A. Demmers, D. T. S. Rijkers, R. M. J. Liskamp, J. Brunner, A. J. R. Heck, B. De Kruijff, and J. A. Killian, 2004. Photo-crosslinking analysis of preferential interactions between a transmembrane peptide and matching lipids. *Biochemistry* 43:4482–4489.

[30] Holt, A., L. Rougier, V. Reat, F. Jolibois, O. Saurel, J. Czaplicki, J. A. Killian, and A. Milon, 2010. Order parameters of a transmembrane helix in a fluid bilayer: case study of a WALP peptide. *Biophys. J.* 98:1864–1872.

[31] Sparr, E., W. L. Ash, P. V. Nazarov, D. T. S. Rijkers, M. A. Hemminga, D. P. Tieleman, and J. A. Killian, 2005. Self-association of transmembrane α-helices in model membranes. Importance of helix orientation and role of hydrophobic mismatch. *J. Biol. Chem.* 280:39324–39330.

[32] Botelho, A. V., T. Huber, T. P. Sakmar, and M. F. Brown, 2006. Curvature and hydrophobic forces drive oligomerization and modulate activity of rhodopsin in membranes. *Biophys. J.* 91:4464–4477.

[33] de Almeida, R. F. M., L. M. S. Loura, M. Prieto, A. Watts, A. Fedorov, and F. J. Barrantes, 2004. Cholesterol modulates the organization of the γ M4 transmembrane domain of the muscle nicotinic acetylcholine receptor. *Biophys. J.* 86:2261–2272.

[34] Polozova, A., and B. J. Litman, 2000. Cholesterol dependent recruitment of di22:6-PC by a G protein-coupled receptor into lateral domains. *Biophys. J.* 79:2632–2643.

[35] Yoshiaki, Y., and K. Matsuzaki, 2006. Measurement of thermodynamic parameters for hydrophobic mismatch 1: self-association of a transmembrane helix. *Biochemistry* 45:3370–3378.

[36] Constantin, D., G. Brotons, A. Jarre, C. Li, and T. Salditt, 2007. Interaction of alamethicin pores in DMPC bilayers. *Biophys. J.* 92:3978–3987.

[37] Pan, J., P. Tieleman, J. F. Nagle, N. Kucerka, and S. Tristram-Nagle, 2009. Alamecithin in lipid bilayers: Combined use of X-ray scattering and MD simulations. *Biochim. Biophys. Acta* 1788:1387–1397.

[38] Constantin, D., 2009. Membrane-mediated repulsion between gramicidin pores. *Biochim. Biophys. Acta* 1788:1782–1789.

[39] Harroun, T. A., W. T. Heller, T. M. Weiss, L. Yang, and H. W. Huang, 1999. Experimental Evidence for Hydrophobic Matching and Membrane-Mediated Interactions in Lipid Bilayers Containing Gramicidin. *Biophys. J.* 76:937–945.

[40] Ivanova, V. P., I. M. Makarov, T. E. Schäffer, and T. Heimburg, 2003. Analyzing heat capacity profiles of peptide-containing membranes: cluster formation of gramicidin A. *Biophys. J.* 84:2427–2439.

[41] Casuso, I., P. Sens, F. Rico, and S. Scheurig, 2010. Experimental evidence for membrane-mediated protein-protein interaction. *Biophys. J.* 99:L47–L49.

[42] Lewis, B. A., and D. M. Engelman, 1983. Bacteriorhodopsin remains dispersed in fluid phospholipid bilayers over a wide range of bilayer thickness. *J. Mol. Biol.* 166:203–210.

[43] Anderson, O. S., and R. E. Koeppe II, 2007. Bilayer thickness and membrane protein function: an energetic perspective. *Annu. Rev. Biophys. Biomol. Struct.* 36:107–130.

[44] Hung, W.-C., M.-T. Lee, F.-Y. Chen, and H. W. Huang, 2007. The condensing effect of cholesterol in lipid bilayers. *Biophys. J.* 92:3960–3967.

[45] Sieber, J. J., K. I. Willig, C. Kutznwe, C. gerding Reimers, B. Harke, G. Donnert, B. Rammner, C. Eggeling, S. W. Hell, H. Grübmuller, and T. Lang, 2007. Anatomy and Dynamics of a supramolecular membrane protein cluster. *Science* 317:1072–1076.

[46] Lang, T., D. Bruns, D. Wenzel, D. Riedel, P. Holroyd, C. Thiele, and R. Jahn, 2001. SNAREs are concentrated in cholesterol-dependant clusters that define docking and fusion sites for exocytosis. *EMBO Journal* 20:2202–2213.

[47] Murtola, T., M. Karttunen, and I. Vattulainen, 2009. Systematic coarse graining from structure using internal states: application to phospholipid/cholesterol bilayer. *J. Chem. Phys.* 131:055101–055115.

[48] Vereb, G., J. Matkó, G. Vámosi, S. Ibrahim, E. Magyar, S. Varga, J. Szöllösi, A. Jenei, R. Gáspár Jr, T. Waldmann, and S. Damjanovich, 2000. Cholesterol-dependent clustering of IL-2Rα and its colocalization with HLA and CD48 on T lymphoma cells suggest their functional association with lipid rafts. *Proc. Natl. Acad. Sci. USA* 97:6013–6018.

[49] Cristian, L., J. D. Lear, and W. F. DeGrado, 2003. Use of the thiol-disulfide equilibria to measure the energetics of assembly of transmembrane helices in phospholipid bilayers. *Proc. Natl. Acad. Sci. USA* 100:14772–14777.

[50] Schneider, H., M. Höchli, and C. R. Hackenbrock, 1982. Relationship between the density distribution of intramembrane particles and electron transfer in the mitochondrial inner membrane as revealed by cholesterol incorporation. *J. Cell Biol.* 94:387–393.

[51] Maxfield, F. R., and I. Tabas, 2005. Role of cholesterol and lipid organization in disease. *Nature* 438:612–621.

[52] Brooks, B. R., R. E. Bruccoleri, B. D. Olafson, D. J. States, and S. Swaminathan, 1983. CHARMM: A program for macromolecular energy, minimization, and dynamics calculations. *J. Comput. Chem.* 4:187–217.

[53] Klauda, J. B., R. M. Venable, A. D. MacKerell Jr., and R. W. Pastor, 2008. Considerations for lipid force field development. *Current Topics in Membranes* 60:1–48.

[54] Tu, K., D. J. Tobias, J. K. Blasie, and M. L. Klein, 1996. Molecular dynamics investigation of the structure of a fully hydrated gel-phase dipalmitoylphosphatidylcholine bilayer. *Biophys. J.* 70:595–608.

[55] Essmann, U., L. Perera, and M. L. Berkowitz, 1995. The origin of the hydration interaction of lipid bilayers from MD simulation of dipalmitoylphosphatidylcholine membranes in gel and liquid crystalline phases. *Langmuir* 11:4519–4531.

[56] Venable, R. M., R. B. Brooks, and R. W. Pastor, 2000. Molecular dynamics simulations of gel ($L_{\beta I}$) phase lipid bilayers in constant pressure and constant surface area ensemble. *J. Chem. Phys.* 112:4822–4832.

[57] de Vries, A. H., S. Yefimov, A. E. Mark, and S. J. Marrink, 2005. Molecular structure of the lecithin ripple phase. *Proc. Natl. Acad. Sci. USA* 102:5392–5396.

[58] Hénin, J., A. Pohorille, and C. Chipot, 2005. Insights into the recognition and association of transmembrane alpha helices. The free energy of alpha-helix dimerization in glycophorin A. *J. Am. Chem. Soc.* 127:8478–8484.

[59] Klauda, J. B., N. Kucerka, B. R. Brooks, R. W. Pastor, and J. F. Nagle, 2006. Simulation-based methods for interpreting X-ray data from lipid bilayers. *Biophys. J.* 90:2796–2807.

[60] Petrache, H. I., K. C. Tu, and J. F. Nagle, 1999. Analysis of simulated NMR order parameters for lipid bilayer structure determination. *Biophys. J.* 76:2479–2487.

[61] Venturoli, M., M. M. Sperotto, M. Kranenburg, and B. Smit, 2006. Mesoscopic models of biological membranes. *Phys. Rep.* 437:1–57.

[62] Shelley, J. C., M. Y. Shelley, R. C. Reeder, S. Bandyopadhyay, and M. L. Klein, 2001. A coarse grain model for phospholipid simulations. *J. Phys. Chem. B* 105:4464–4470.

[63] Izvekov, S., M. Parrinello, C. J. Burnham, and G. A. Voth, 2004. Effective force field for condensed phase systems from *ab initio* molecular dynamics simulations: A new method for force-matching. *J. Chem. Phys.* 120:10896–10913.

[64] Izvekov, S., and G. A. Voth, 2005. A multiscale coarse-graining method for biomolecular systems. *J. Phys. Chem. B* 109:2469–2473.

[65] Izvekov, S., and G. A. Voth, 2006. Multiscale Coarse-Graining of Mixed Phospholipid/Cholesterol Bilayers. *J. Chem. Theory. Comput.* 2:637–648.

[66] Shinoda, W., R. DeVane, and M. L. Klein, 2010. Zwitterionic lipid assemblies: Molecular dynamics studies of monolayers, bilayers, and vescicles using a new coarse grain force field. *jpcb* 114:6836–6849.

[67] Goetz, R., and R. Lipowsky, 1998. Computer simulations of bilayer membranes: Self-assembly and interfacial tension. *J. Chem. Phys.* 108:7397–7409.

[68] Marrink, S. J., H. J. Risselada, S. Yefimov, D. P. Tieleman, and A. H. de Vries, 2007. The MARTINI force field: Coarse grained model for biomolecular simulations. *J. Phys. Chem. B* 111:7812–7824.

[69] Venturoli, M., 2004. Mesoscopic models of lipid bilayers and bilayers with embedded proteins. PhD Thesis, University of Amsterdam.

[70] Marrink, S. J., A. H. de Vries, and A. E. Mark, 2004. Coarse grained model for semiquantitative lipid simulations. *J. Phys. Chem. B* 108:750–760.

[71] Kranenburg, M., and B. Smit, 2005. Phase behavior of model lipid bilayers. *J. Phys. Chem. B* 109:6553–6563.

[72] Marrink, S. J., J. Risselada, and A. E. Mark, 2005. Simulation of gel phase formation and melting in lipid bilayers using a coarse grained model. *Chem. Phys. Lipids* 135:223–244.

[73] Lenz, O., and F. Schmid, 2007. Structure of Symmetric and Asymmetric Ripple Phases in Lipid Bilayers. *Phys. Rev. Lett.* 98:058104–058108.

[74] Faller, R., and S. J. Marrink, 2004. Simulation of domain formation in DLPC-DSPC mixed bilayers. *Langmuir* 20:7686–7693.

[75] Kranenburg, M., M. Venturoli, and B. Smit, 2003. Phase behavior and induced interdigitation in bilayers studied with dissipative particle dynamics. *J. Phys. Chem. B* 107:11491–11501.

[76] Wang, Z. J., and D. Frenkel, 2005. Modeling flexible amphiphilic bilayers: A solvent-free off-lattice Monte Carlo study. *J. Chem. Phys.* 122:Art. N. 234711.

[77] Noguchi, H., and M. Takasu, 2001. Fusion pathways of vesicles: A Brownian dynamics simulation. *J. Chem. Phys.* 115:9547–9551.

[78] Marrink, S. J., and A. E. Mark, 2003. The mechanism of vesicle fusion as revealed by molecular dynamics simulations. *J. Am. Chem. Soc.* 125:11144–11145.

[79] Yamamoto, S., and S. Hyodo, 2003. Budding and fission dynamics of two-component vesicles. *J. Chem. Phys.* 118:7937–7943.

[80] Venturoli, M., B. Smit, and M. M. Sperotto, 2005. Simulation studies of protein-induced bilayer deformations, and lipid-induced protein tilting, on a mesoscopic model for lipid bilayers with embedded proteins. *Biophys. J.* 88:1778–1798.

[81] Nielsen, S. O., C. F. Lopez, G. Srinivas, and M. L. Klein, 2004. Coarse grain models and the computer simulation of soft materials. *J. Phys.-Condes. Matter* 16:R481–R512.

[82] Lopez, C. F., S. O. Nielsen, P. B. Moore, and M. L. Klein, 2004. Understanding nature's design for a nanosyringe. *Proc. Natl. Acad. Sci. U. S. A.* 101:4431–4434.

[83] Bond, P. J., and M. S. Sansom, 2006. Insertion and assembly of membrane proteins via simulation. *J. Am. Chem. Soc.* 128:2697–2704.

[84] Kranenburg, M., J.-P. Nicolas, and B. Smit, 2004. Comparison of mesoscopic phospholipid-water models. *Phys. Chem. Chem. Phys.* 6:4142 – 4151.

[85] Forrest, B. M., and U. W. Suter, 1995. Accelerated equilibrium of polymer melts by time-coarse-graining. *jcp* 102:7256–7266.

[86] Groot, R. D., and K. L. Rabone, 2001. Mesoscopic simulation of cell membrane damage, morphology change and rupture by nonionic surfactants. *Biophys. J.* 81:725–736.

[87] Groot, R. D., and P. B. Warren, 1997. Dissipative particle dynamics: Bridging the gap between atomistic and mesoscopic simulation. *J. Chem. Phys.* 107:4423–4435.

[88] Groot, R. D., 2000. Mesoscopic simulation of polymer-surfactant aggregation. *Langmuir* 16:7493–7502.

[89] Wijmans, C. M., B. Smit, and R. D. Groot, 2001. Phase behavior of monomeric mixtures and polymer solutions with soft interaction potentials. *J. Chem. Phys.* 114:7644–7654.

[90] Maiti, A., and S. McGrother, 2004. Bead-bead interactions parameters in dissipative particle dynamics: relation to bead-size, solubility parameter, and surface tension. *J. Chem. Phys.* 120:1594–1601.

[91] Venturoli, M., and B. Smit, 1999. Simulating the self-assembly of model membranes. *Phys.Chem.Comm.* 2:art.no. 10.

[92] Kranenburg, M., M. Venturoli, and B. Smit, 2003. Molecular simulations of mesoscopic bilayer phases. *Phys. Rev. E* 67:art. no. 060901.

[93] Kranenburg, M., C. Laforge, and B. Smit, 2004. Mesoscopic simulations of phase transitions in lipid bilayers. *Phys. Chem. Chem. Phys.* 6:4531–4534.

[94] Hoogerbrugge, P. J., and J. M. V. A. Koelman, 1992. Simulating microscopic hydrodynamics phenomena with dissipative particle dynamics. *Europhys. Lett.* 19:155–160.

[95] Español, P., and P. B. Warren, 1995. Statistical mechanics of dissipative particle dynamics. *Europhys. Lett.* 30:191–196.

[96] Allen, M. P., and D. J. Tildesley, 1987. Computer Simulation of Liquids. Clarendon Press, Oxford.

[97] Serrano, M., G. De Fabritiis, P. Espagnol, and P. V. Coveney, 2006. A stochastic Trotter integration scheme for dissipative particle dynamics. *Mathematics and Computers in Simulation* 72:190–194.

[98] Marrink, S. J., E. Lindahl, O. Edholm, and A. E. Mark, 2001. Simulation of the spontaneous aggregation of phospholipids into bilayers. *J. Am. Chem. Soc.* 123:8638–8639.

[99] Frenkel, D., and B. Smit, 2002. Understanding Molecular Simulations: from Algorithms to Applications. Academic Press, San Diego, 2nd edition.

[100] Rodgers, J. M., M. Webb, and B. Smit, 2010. Alcohol solubility in a lipid bilayer: Efficient grand-canonical simulation of an interfacially active molecule. *J. Chem. Phys.* 132:3437–3441.

[101] Jähnig, F., 1996. What is the surface tension of a lipid membrane? *Biophys. J.* 71:1348–1349.

[102] M'Baya, G., Y. Mely, G. Duportail, and A. S. Klymchenko, 2008. Liquid ordered and gel phases of lipid bilayers: fluorescent probes reveal close fluidity but different hydration. *Biophys. J.* 95:1217–1225.

[103] Mathai, J. C., S. Tristram-Nagle, J. F. Nagle, and M. L. Zeidel, 2007. Structural determinants of water permeability through the lipid membrane. *J. Gen. Physiol.* 131:69–76.

[104] Greenwood, A. I., S. Tristram-Nagle, and J. F. Nagle, 2006. Partial molecular volumes of lipids and cholesterol. *Chem. Phys. Lip.* 143:1–10.

[105] Pan, J., S. Tristram-Nagle, N. Kucerka, and J. F. Nagle, 2008. Temperature dependence of structure, bending rigidity, and bilayer interactions of dioleoylphosphatidylcholine bilayers. *Biophys. J.* 94:117–124.

[106] Oldfield, E., and D. Chapman, 1972. Dynamics of lipids in membranes: heterogeneity and the role of cholesterol. *FEBS Letters* 23:285–297.

[107] L., P. P., and N. N. Khechinashvili, 1974. A thermodynamic approach to the problem of stabilization of globular protein structure. *J. Mol. Biol.* 86:665–684.

[108] Blume, A., 1983. Apparent molar heat capacities of phospholipids in aqueous dispersion. Effect of chain length and head group structure. *Biochemistry* 22:5436–5442.

[109] Heimburg, T., 2007. Thermal biophysics of membranes. Wiley-VCH, Weinheim, 1st edition.

[110] Ulrich, A. S., M. Sami, and A. Watts, 1994. Hydration of DOPC bilayers by differential scanning calorimetry. *Biochim. Biophys. Acta* 1191:225–230.

[111] Halstenberg, S., T. Heimburg, T. Hianik, U. Kaatze, and R. Krivanek, 1998. Cholesterol-Induced Variations in the Volume and Enthalpy Fluctuations of Lipid Bilayers. *Biophys. J.* 75:264–271.

[112] Hinz, H.-J., and J. M. Sturtevant, 1972. Calorimetric investigation of the influence of cholesterol on the transition properties of bilayers formed from synthetic L-α-Lecithins in aqueous suspension. *J. Biol. Chem.* 247:3697–3700.

[113] Mabrey, S., and J. M. Sturtevant, 1976. Investigation of phase transitions of lipids and lipid mixtures by high sensitivity differential scanning calorimetry. *Proc. Natl. Acad. Sci. USA* 11:3862–3866.

[114] Mabrey, S., P. I. Mateo, and J. M. Sturtevant, 1978. High-sensitivity scanning calorimetric study of mixtures of cholesterol with dimyristoyl- and dipalmitoylphosphatidylcholines. *Biochemistry* 17:2466–2468.

[115] Curatolo, W., R. Radhakrishnan, C. M. Gupta, and H. G. Khorana, 1981. Photoactivatable carbene-generating phospholipids: physical properties and use in detection of phase separations in lipid mixtures. *Biochemistry* 20:1374–1378.

[116] Davis, P. J., and K. M. W. Keough, 1983. Differential scanning calorimetric studies of aqueous dispersions of mixtures of cholesterol with some mixed-acid and single-acid phosphatidylcholines. *Biochem.* 22:6334–6340.

[117] Curatolo, W., B. Sears, and L. J. Neuringer, 1985. A calorimetry and deuterium NMR study of mixed model membranes of 1-palmitoyl-2-oleylphosphatidylcholine and saturated phosphatidylcholines. *Biochim. Biophys. Acta* 817:261–270.

[118] Singer, M. A., and L. Finegold, 1990. Cholesterol interacts with all of the lipid in bilayer membranes. *Biophys. J.* 57:153–156.

[119] McMullen, T. P. W., R. N. A. H. Lewis, and R. N. McElhaney, 1993. Differential scanning calorimetric study of the effect of cholesterol on the thermotropic phase behavior of a homologous series of linear saturated phosphatidylcholines. *Biochemistry* 32:516–522.

[120] McMullen, T. P. W., and R. N. McElhaney, 1995. New aspects of the interaction of cholesterol with dipalmitoylphosphatidylcholine bilayers as revealed by high-sensitivity differential scanning calorimetry. *Biochim. Biophys. Acta* 1234:90–98.

[121] Steim, J. M., M. E. Tourtelotte, J. C. Reinet, R. N. McElhaney, and R. L. Rader, 1999. Calorimetric evidence for the liquid-crystalline state of lipids in a biomembrane. *Proc. Natl. Acad. Sci. USA* 63:104–109.

[122] Nagle, J. F., and S. Tristram-Nagle, 2000. Structure of lipid bilayers. *Biochim. Biophys. Acta-Rev. Biomembr.* 1469:159–195.

[123] Katsaras, J., N. Kucerka, and M. P. Nieh, 2008. Structure from substrate supported lipid bilayers. *Biointerphases* 3:55–63.

[124] Lyatskaya, Y., Y. Liu, S. Tristram-Nagle, J. Katsaras, and J. F. Nagle, 2000. Method for obtaining structure and interactions from oriented lipid bilayers. *Phys. Rev. E* 63:011907 1–9.

[125] Liu, Y., and J. F. Nagle, 2004. Diffuse scattering provides material parameters and electron density profiles of biomembranes. *Phys. Rev. E* 69:040901 1–4.

[126] Evans, E., and D. Needham, 1986. Giant vesicle bilayers composed of mixtures of lipids, cholesterol and polypeptides. *Faraday Discuss. Chem. Soc.* 81:267–280.

[127] Rawicz, W., K. C. Olbrich, T. J. McIntosh, D. Needham, and E. Evans, 2000. Effect of chain length and unsaturation on elasticity of lipid bilayers. *Biophys. J.* 79:328–339.

[128] Tristram-Nagle, S., Y. Liu, J. Legleiter, and J. F. Nagle, 2002. Structure of gel phase DMPC determined by X-ray diffraction. *Biophys. J.* 83:3324–3335.

[129] Armen, R. S., O. D. Uitto, and S. E. Feller, 1998. Phospholipid component volumes: determination and application to bilayer structure calculations. *Biophys. J.* 75:734–744.

[130] Kucerka, N., Y. Liu, N. Chu, H. I. Petrache, S. Tristram-Nagle, and J. F. Nagle, 2005. Structure of fully hydrated fluid phase DMPC and DLPC lipid bilayers using X-ray scattering from oriented multilamellar arrays and from unilamellar vesicles. *Biophys. J.* 88:2626–2637.

[131] Edholm, O., and J. F. Nagle, 2005. Areas of molecules in membranes consisting of mixtures. *Biophys. J.* 89:1827–1832.

[132] Kucerka, N., J. Nagle, J. Sachs, S. Feller, J. Pencer, A. Jackson, and J. Katsaras, 2008. Lipid bilayer structure determined by the simultaneous analysis of neutron and x-ray scattering data. *Biophys. J.* 95:2356–2367.

[133] Pan, J., T. T. Mills, S. Tristram-Nagle, and J. F. Nagle, 2008. Cholesterol perturbs lipid bilayers nonuniversally. *Phys. Rev. Lett.* 100:198103 1–4.

[134] Pan, J., S. Tristram-Nagle, and J. F. Nagle, 2009. Effect of cholesterol on structural and mechanical properties of membranes depends on lipid chain saturation. *Phys. Rev. E* 80:021931–021943.

[135] Kucerka, N., J. D. Perlmutter, J. Pan, S. Tristram-Nagle, J. Katsaras, and J. N. Sachs, 2008. The effect of cholesterol on short- and long-chain monounsaturated lipid bilayers as determined by molecular dynamics simulations and x-ray scattering. *Biophys. J.* 95:2792–2805.

[136] Mills, T. T., G. E. S. Toombes, S. Tristram-Nagle, D. M. Smilgies, G. W. Feigenson, and J. Nagle, 2008. Order parameter and areas in fluid-phase oriented lipid membranes using wide angle X-ray scattering. *Biophys. J.* 21:669–681.

[137] Sun, W. J., S. Tristram-Nagle, R. M. Suter, and J. F. Nagle, 1996. Structure of the ripple phase in lecithin bilayers. *Proc. Natl. Acad. Sci. U. S. A.* 93:7008–7012.

[138] Wolfe, D. H., L. J. Lis, O. Kucuk, M. P. Westerman, B. A. Cunningham, S. B. Qadri, W. Bras, and P. J. Quinn, 1992. Phase transitions between ripple structures in hydrated phosphatidylcholine-cholesterol multilamellar assemblies. *Phys. Rev. Lett.* 68:1085–1088.

[139] Karmakar, S., and V. A. Raghunathan, 2003. Cholesterol-induced modulated phase in phospholipid membranes. *Phys. Rev. Lett.* 91:098102–1–098102–4.

[140] Copeland, B. R., and H. M. McConnell, 1980. The rippled structure in bilayer membranes of phosphatidylcholine and binary mixtures of phosphatidylcholine and cholesterol. *Biochim. Biophys. Acta* 599:95–109.

[141] Abragam, A., 1961. Principles of Nuclear Magnetism. Oxford University Press, London.

[142] Seelig, J., and W. Niederberger, 1974. Deuterium-labeled lipids as structural probes in liquid crystalline bilayers. A deuterium magnetic resonance study. *J. Am. Chem. Soc.* 96:2069–2072.

[143] Ipsen, J. H., O. G. Mouritsen, and M. Bloom, 1990. Relationships between lipid membrane area, hydrophobic thickness, and acyl-chain oriented order. *Biophys. J.* 57:405–412.

[144] Davis, P. J., 1979. Deuterium magnetic resonance study of the gel and liquid crystalline phases of dipalmitoyl phosphatidylcholine. *Biophys. J.* 27:339–358.

[145] Huang, T.-H., C. W. B. Lee, S. K. Das Gupta, A. Blume, and R. G. Griffin, 1993. A ^{13}C and ^{2}H nuclear magnetic resonance study of phosphatidylcholine/cholesterol interactions: Characterization of liquid-gel phase. *Biochemistry* 32:13277–13287.

[146] Marsan, M. P., I. Muller, C. Ramos, F. Rodriguez, E. J. Dufourc, J. Czaplicki, and A. Milon, 1999. Cholesterol orientation and dynamics in dimyristoylphosphatidylcholine bilayers: A solid state deuterium NMR analysis. *Biophys. J.* 76:351–359.

[147] Lindblom, G., and G. Orädd, 1994. NMR studies of translational diffusion in lyotropic liquid crystals and lipid membranes. *Progress in NMR Spectroscopy* 26:483–515.

[148] Orädd, G., and G. Lindblom, 2008. Lateral diffusion coefficients of raft lipids from pulsed field gradient NMR. *Methodology in Molecular Biology* 398:127–142.

[149] Rubenstein, J. L. R., B. A. Smith, and H. M. McConnell, 1979. Lateral diffusion in binary mixtures of cholesterol and phosphatidylcholines. *Proc. Natl. Acad. Sci. USA* 76:15–18.

[150] Vaz, W. L. C., R. M. Clegg, and D. Hallmann, 1985. Translational diffusion of lipids in liquid-crystalline phase phosphatidylcholine multibilayers: a comparison of experiment with theory. *Biochemistry* 24:781–786.

[151] Almeida, P. F. F., W. L. C. Vaz, and T. E. Thompson, 1992. Lateral diffusion in the liquid phases of dimyristoylphosphatidylcholine cholesterol lipid bilayers: A free volume analysis. *Biochemistry* 31:6739–6747.

[152] Filippov, A., G. Orädd, and L. Göran, 2003. The effect of cholesterol on the lateral diffusion of phospholipids in oriented bilayers. *Biophys. J.* 84:3079–3086.

[153] Filippov, A., G. Orädd, and L. Göran, 2004. Lipid lateral diffusion in ordered and disordered phases in raft mixtures. *Biophys. J.* 86:891–896.

[154] K., S., and E. Ikonen, 1997. Functional rafts in cell membranes. *Nature* 387:569–572.

[155] Anderson, R. G. W., and K. Jacobson, 2002. A Role for Lipid Shells in Targeting Proteins to Caveolae, Rafts, and Other Lipid Domains. *Science* 296:1821–1825.

[156] McMullen, T. P. W., R. N. A. H. Lewis, and R. N. McElhaney, 2004. Cholesterol-phospholipid interactions, the liquid-ordered phase and lipid rafts in model and biological membranes. *Current Opinion in Colloid and Interface Science* 8:459–468.

[157] Hancock, J. F., 2006. Lipid rafts: contentious only from simplistic standpoints. *Nature* 7:456–462.

[158] Jacobson, K., O. G. Mouritsen, and R. G. W. Anderson, 2007. Lipid rafts: at a crossroad between cell biology and physics. *Nat. Cell Biol.* 9:7–14.

[159] Lingwood, D., and K. Simons, 2010. Lipid rafts as a membrane organizing principle. *Nature Review* 327:46–50.

[160] Veatch, S. L., and S. L. Keller, 2005. Seeing spots: Complex phase behavior in simple membranes. *Biochim. Biophys. Acta* 1746:172–185.

[161] Sankaram, M. B., and T. E. Thompson, 1991. Cholesterol-induced fluid-phase immiscibility in membranes. *Proc. Natl. Acad. Sci. USA* 88:8686–8690.

[162] Lentz, B. R., Y. Barenholz, and T. E. Thompson, 1976. Fluorescence depolarization studies of phase transitions and fluidity in phospholipid bilayers. 2. Two-component phosphatidylcholine liposomes. *Biochemistry* 15:4529–4537.

[163] Veatch, S. L., and S. L. Keller, 2002. Organization in lipid membranes containing cholesterol. *Phys. Rev. Lett.* 89:268101 1–4.

[164] Veatch, S. L., and S. L. Keller, 2003. Separation of liquid phases in giant vesicles of ternary mixtures of phospholipids and cholesterol. *Biophys. J.* 85:3074–3083.

[165] Veatch, S. L., I. V. Polozov, K. gawrisch, and S. L. Keller, 2004. Liquid domains in vesicles investigated by NMR and fluorescence microscopy. *Biophys. J.* 86:2910–2922.

[166] Baumgart, T., S. T. Hess, and W. W. Webb, 2003. Imaging coexisting fluid domains in biomembrane models coupling curvature and line tension. *Nature* 425:821–824.

[167] Tang, D., W. Van Der Meer, and S.-Y. S. Chen, 1995. Evidence for a regular distribution of cholesterol in phospholipid bilayers from diphenylhexatriene fluorescence. *Biophys. J.* 68:1944–1951.

[168] Virtanen, J. A., M. Ruonala, M. Vauhkonen, and P. Somerharju, 1995. Lateral organization of liquid-crystalline cholesterol-dimyristoylphosphatidylcholine bilayers. Evidence for domains with hexagonal and centered cholesterol superlattices. *Biochemistry* 34:11568–11581.

[169] Chong, P. L.-G., 1994. Evidence for regular distribution of sterols in liquid crystalline phosphatidylcholine bilayers. *Proc. Natl. Acad. Sci. USA* 91:10069–10073.

[170] Vidal, A., and T. J. McIntosh, 2005. Transbilayer peptide sorting between raft and nonraft bilayers: comparisons of detergent extraction and confocal microscopy. *Biophys. J.* 89:1102–1108.

[171] Vist, M. R., and J. H. Davis, 1990. Phase equilibria of cholesterol dipalmitoylphosphatidylcoline mixtures: ^{2}H nuclear magnetic resonance and differential scanning calorimetry. *Biochemistry* 29:451–464.

[172] Schmidt, M. L., L. Ziani, M. Boudreau, and J. Davis, 2009. Phase equilibria in DOPC/DPPC: conversion from gel to subgel in two component mixtures. *J. Chem. Phys.* 131:175103 1–11.

[173] Davis, J. H., J. J. Clair, and J. Juhasz, 2009. Phase equilibria in DOPC/DPPC-d_{62}/Cholesterol mixtures. *Biophys. J.* 96:521–539.

[174] Veatch, S. L., K. Gawrisch, and S. L. Keller, 2005. Closed-loop miscibility gap and quantitative tie-lines in ternary membranes containing diphytanoyl PC. *Biochim. Biophys. Acta* 1746:172–185.

[175] Veatch, S. L., O. Soubias, S. L. Keller, and K. Gawrisch, 2007. Critical fluctuations in domain-forming lipid mixtures. *Proc. Natl. Acad. Sci. USA* 104:17650–17655.

[176] de Lange, M. J. L., M. Bonn, and M. Müller, 2007. Direct measurement of phase coexistence in DPPC/cholesterol vesicles using Raman spectroscopy. *Chem. Phys. Lip.* 146:76–84.

[177] Knoll, W., G. Schmidt, K. Ibel, and E. Sackmann, 1985. Small-angle neutron scattering study of lateral phase separation in dimyristoylphosphatidylcholine-cholesterol mixed membranes. *Biochemistry* 24:5240–5346.

[178] Mills, T. T., S. Tristram-Nagle, F. A. Heberle, N. F. Morales, J. Zhao, J. Wu, G. E. S. Toombes, J. F. Nagle, and G. W. Feigenson, 2008. Liquid-liquid domains in bilayers detected by wide angles x-ray scattering. *Biophys. J.* 21:669–681.

[179] Mills, T., J. Huang, G. W. Feigenson, and J. Nagle, 2009. Effects of cholesterol and unsaturated DOPC lipid on chain packing of saturated gel-phase DPPC bilayers. *Gen. Physiol. Biophys.* 28:126–139.

[180] Mason, P. R., T. N. Tulenko, and R. F. Jacob, 2003. Direct evidence for cholesterol crystalline domains in biological membranes: role in human pathobiology. *Biochim. Biophys. Acta* 1610:198–207.

[181] Troup, G. M., T. N. Tulenko, S. P. Lee, and S. Wrenn, 2003. Detection and characterization of laterally phase separated cholesterol domains in model lipid membranes. *Colloids and surfaces B: biointerfaces* 29:217–231.

[182] Troup, G. M., T. N. Tulenko, S. P. Lee, and S. Wrenn, 2004. Estimating the size of laterally phase separated cholesterol domains in model membranes with Förster resonance energy transfer: A simulation study. *Colloids and surfaces B: biointerfaces* 33:57–65.

[183] Nazarov, P. V., R. B. M. Koehorst, W. L. Vos, V. V. Apanasovich, and M. A. Hemminga, 2006. FRET study of membrane proteins: simulation-based fitting for analysis of membrane protein embedment and association. *Biophys. J.* 91:454–466.

[184] Chandler, D., 1987. Introduction to modern statistical mechanics. Oxford University Press, Oxford.

[185] Sprong, H., P. van der Sluijs, and G. van Meer, 2001. How proteins move lipids ans lipids move proteins. *Nature Reviews Molecular Cell Biology* 2:504–513.

[186] Bretscher, M. S., and S. Munro, 1993. Cholesterol and the Golgi apparatus. *Science* 261:1280–1281.

[187] Munro, S., 1998. Localization of proteins to the Golgi apparatus. *Trends Cell Biol.* 8:11–15.

[188] Webb, R. J., J. M. East, R. P. Sharma, and A. G. Lee, 1998. Hydrophobic mismatch and the incorporation of peptides into lipid bilayers: a possible mechanism for retention in the Golgi. *Biochemistry* 37:673–679.

[189] Cornelius, F., 2001. Modulation of Na, K-ATPase and Na-ATPase activity by phospholipids and cholesterol. I. Steady-state kinetics. *Biochemistry* 40:8842–8851.

[190] Cornelius, F., N. Turner, and H. R. Z. Christensen, 2003. Modulation of Na, K-ATPase by phospholipids and cholesterol. II. Steady-state and presteady-state kinetics. *Biochemistry* 42:8541–8549.

[191] Hinderliter, A., R. L. Biltonen, and P. F. F. Almeida, 2004. Lipid modulation of protein-induced membrane domains as a mechanism for controlling signal transduction. *Biochemistry* 43:7102–7110.

[192] Luecke, H., B. Schobert, H.-T. Richter, J.-P. Cartailler, and J. K. Lanyi, 1999. Structure of bacteriorhodopsin at 1.55 $\dot{A}$ resolution. *J. Mol. Biol.* 291:899–911.

[193] Brown, M. F., 1994. Modulation of rhodopsin function by properties of the membrane bilayer. *Chem. Phys. Lipids* 73:159–180.

[194] Kota, P., P. J. Reeves, U. L. Raj Bahandary, and H. G. Khorana, 2006. Opsin is present as dimers in COS1 cells: Identification of amino acids at the dimeric interface. *Proc. Natl. Acad. Sci. USA* 103:3054–3059.

[195] Mansoor, S. E., K. Palczewski, and D. L. Farrens, 2006. Rhodopsin self-associates in asolectin liposomes. *Proc. Natl. Acad. Sci. USA* 103:3060–3065.

[196] Fisher, L. E., D. M. Engelman, and J. N. Sturgis, 2003. Effects of detergents on the association of the glycophorin A transmembrane helix. *Biophys. J.* 85:3097–3105.

[197] Fleming, K. G., C. C. Ren, A. K. Doura, M. E. Eisly, F. J. Kobus, and A. M. Stanley, 2004. Thermodynamics of glycophorin A transmembrane helix dimerization in C14 betaine micelles. *Biophys. Chemist.* 108:43–49.

[198] Finger, C., T. Volkmer, A. Prodöhl, D. E. Otzen, D. M. Engelman, and D. Schneider, 2006. The stability of transmembrane helix interactions measured in a biological membrane. *J. Mol. Biol.* 358:1221–1228.

[199] Lomize, A. L., I. D. Pogozheva, and H. I. Mosberg, 2004. Quantification of helix-helix binding affinities in micelles and lipid bilayers. *Protein Sci.* 13:2600–2612.

[200] Lagüe, P., Z. M. J., and B. Roux, 2000. Lipid-mediated interactions between intrinsic membrane proteins: A theoretical study based on integral equations. *Biophys. J.* 79:2867–2879.

[201] Lagüe, P., M. J. Zuckermann, and B. Roux, 2001. Lipid-mediated interactions between intrinsic membrane proteins: Dependence on protein size and lipid composition. *Biophys. J.* 81:276–284.

[202] May, S., 2000. Theories on structural perturbations of lipid bilayers. *Curr. Opin. Colloid Interface Sci.* 5:244–249.

[203] Wiggins, P., and R. Phillips, 2005. Membrane-protein interactions in mechanosensitive channels. *Biophys. J.* 88:880–902.

[204] Bohinc, K. V., V. Kralj-Iglič, and S. May, 2003. Interaction between two cylindrical inclusions in a symmetric lipid bilayer. *J. Chem. Phys.* 119:7435–7444.

[205] Petrache, H. I., A. Grossfield, K. R. MacKenzie, D. M. Engelman, and T. B. Woolf, 2000. Modulation of glycophorin A transmembrane helix interactions by lipid bilayers: molecular dynamics calculations. *J. Mol. Biol.* 302:727–746.

[206] Deol, S. S., P. J. Bond, C. Domene, and M. S. P. Sansom, 2004. Lipid-protein interactions of integral membrane proteins: a comparative simulation study. *biophys. J.* 87:3737–3749.

[207] Smeijers, A. F., K. Pieterse, A. J. Markvoort, and P. A. J. Hilbers, 2006. Coarse-grained transmembrane proteins: hydrophobic matching, aggregation, and their effect on fusion. *J. Phys. Chem. B* 110:13614–13623.

[208] Crozier, P. S., L. R. Stevens, L. R. Forrest, and T. B. Woolf, 2003. Molecular dynamics simulation of dark-adapted rhodopsin in an explicit membrane bilayer: coupling between local retinal and larger scale conformational change. *J. Mol. Biol.* 333:493–514.

[209] Periole, X., T. Huber, S.-J. Marrink, and T. P. Sakmar, 2007. G-Protein Coupled Receptors Self-Assemble in Dynamics Simulations of Model Bilayers. *J. Am. Chem. Soc.* 129:10126–10132.

[210] de Meyer, F. J.-M., M. Venturoli, and B. Smit, 2008. Molecular simulations of lipid-mediated protein-protein interactions. *Biophys. J.* 95:1851–1865.

[211] Kumar, S., D. Bouzida, R. H. Swendsen, P. A. Kollman, and J. M. Rosenberg, 1992. The weighted histogram analysis method for free-energy calculations on biomolecules. I. The method. *J. Comp. Chem.* 13:1011–1021.

[212] Souaille, M., and B. Roux, 2001. Extension to the weighted histogram analysis method: combining umbrella sampling with free energy calculations. *Comp. Phys. Comm.* 135:40–57.

[213] Roux, B., 2001. The calculation of the potential of mean force using computer simulations. *Comp. Phys. Comm.* 91:275–282.

[214] Hansen, P. L., L. Miao, and J. H. Ipsen, 1998. Fluid lipid bilayers: intermonolayer coupling and its thermodynamic manifestations. *Phys. Rev. E* 58:2311–2324.

[215] Israelachvili, J. N., 1997. Intermolecular & surface forces. Academic Press, San Diego, CA.

[216] Koehorst, R. B. M., R. B. Spruijt, F. J. Vergeldt, and M. A. Hemminga, 2004. Lipid bilayer topology of the transmembrane α-helix of M13 major coat protein and bilayer polarity profile by site-directed fluorescence spectroscopy. *Biophys. J.* 87:1445–1455.

[217] Mortensen, K., W. Pfeiffer, E. Sackmann, and W. Knoll, 1988. Structural properties of a phosphatidylcholine-cholesterol system as studied by small-angle

neutron scattering: Ripple structure and phase diagram. *Biochim. Biophys. Acta* 945:221–245.

[218] Recktenwald, D. J., and H. M. McConnell, 1981. Phase equilibria in binary mixtures of phosphatidylcholine and cholesterol. *Biochemistry* 20:4505–4510.

[219] Dai, J., M. Alwarawrah, and J. Huang, 2010. Instability of Cholesterol Clusters in Lipid Bilayers and The Cholesterol's Umbrella Effect. *J. Phys. Chem. B* 114:840–848.

[220] Róg, T., and Pasenkiewicz-Gierula, 2001. Cholesterol effects on the phospholipid condensation and packing in the bilayer: a molecular simulation study. *FEBS Letters* 502:68–71.

[221] Chiu, S. W., E. Jakobsson, R. J. Mashl, and H. L. Scott, 2002. Cholesterol-induced changes in lipid bilayers: A simulation study. *Biophys. J.* 83:1842–1853.

[222] Niemela, P. S., M. T. Hyvonen, and I. Vattulainen, 2009. Atom-scale molecular interactions in lipid raft mixtures. *Biochim. Biophys. Acta* 1788:122–135.

[223] Pandit, S. A., E. Jakobsson, and H. L. Scott, 2004. Simulation of the early stages of nano-domain formation in mixed bilayers of sphingomyelin, cholesterol, and dioleylphosphatidylcholine. *Biophys. J.* 87:3312–3322.

[224] Cournia, Z., G. M. Ullmann, and J. C. Smith, 2007. Differential effects of cholesterol, ergosterol and lanosterol on a dipalmitoyl phosphatidylcholine membrane: A molecular dynamics simulation study. *J. Phys. Chem. B* 111:1786–1801.

[225] Smondyrev, A. M., and M. L. Berkowitz, 1999. United atom force field for phospholipid membranes: constant pressure molecular dynamics simulation of dipalmitoylphosphatidicholine/water system. *J. Comp. Chem.* 20:531–545.

[226] Smondyrev, A. M., and M. L. Berkowitz, 2001. Molecular dynamics simulation of the structure of dimyristoylphosphatidylcholine bilayers with cholesterol, ergosterol, and lanosterol. *Biophys. J.* 80:1649–1658.

[227] Pasenkiewicz-Gierula, M., R. T., K. Kitamura, and A. Kusumi, 2000. Cholesterol effects on the phosphatidylcholine bilayer polar region: A molecular simulation study. *Biophys. J.* 78:1376–1389.

[228] Róg, T., and M. Pasenkiewicz-Gierula, 2004. Cholesterol-phospholipid hydrophobic interactions: A molecular simulation study. *Biophys. Chem.* 107:151–164.

[229] Berkowitz, M. L., 2009. Detailed molecular dynamics simulations of model biological membranes containing cholesterol. *Biochim. Biophys. Acta* 1788:86–96.

[230] Bennett, W. F. D., J. L. MacCallum, M. J. Hinner, S. J. Marrink, and D. P. Tieleman, 2009. Molecular View of Cholesterol Flip-Flop and Chemical Potential in Different Membrane Environments. *J. Am. Chem. Soc.* 131:12714–12720.

[231] Hofsass, C., E. Lindahl, and O. Edholm, 2003. Molecular dynamics simulations of phospholipid bilayers with cholesterol. *Biophys. J.* 84:102–115.

[232] de Meyer, F., and B. Smit, 2009. Effect of cholesterol on the structure of a phospholipid bilayer. *Proc. Natl. Acad. Sci. USA* 106:3654–3658.

[233] Cao, H., N. Tokutake, and S. L. Regen, 2003. Unraveling the mystery surrounding cholesterol's condensing effect. *J. Am. Chem. Soc.* 125:16182–16183.

[234] Huang, J., 2002. Exploration of molecular interactions in cholesterol supperlattices: Effect of multibody interactions. *Biophys. J.* 83:1014–1025.

[235] Ali, M. R., K. H. Cheng, and J. Huang, 2007. Assess the nature of cholesterol-lipid interactions through the chemical potential of cholesterol in phosphatidylcholine bilayers. *Proc. Natl. Acad. Sci. USA* 104:5372–5377.

[236] Brzozowska, I., and Z. A. Figaszewski, 2002. The equilibrium of phosphatidylcholine-cholesterol in monolayers at the air/water interface. *Colloids and Surfaces B: Biointerfaces* 23:51–58.

[237] Bernsdorff, C., and R. Winter, 2003. Differential properties of the sterols cholesterol, ergosterol, beta-sitosterol, trans-7-dehydrocholesterol, stigmasterol and lanosterol on DPPC bilayer order. *J. Phys. Chem. B* 107:10658–10664.

[238] Gao, W. Y., P. J. Quinn, and Z. W. Yu, 2008. The role of sterol rings and side chain on the structure and phase behaviour of sphingomyelin bilayers. *Molecular Membrane Biology* 25:485–497.

[239] Jo, S., T. Kim, V. G. Iyer, and W. Im, 2008. CHARMM-GUI: A web-based graphical user interface for CHARMM. *J. Comput. Chem.* 29:1859–1865.

[240] Jo, S., J. B. Limm, J. B. Klauda, and W. Im, 2009. CHARMM-GUI membrane builder for mixed bilayers and its application to yeast membranes. *Biophys. J.* 97:50–58.

[241] Klauda, J. B., B. R. Brooks, A. D. MacKerell, R. M. Venable, and R. W. Pastor, 2005. Ab initio study on the torsional surface of alkanes and its effect on molecular simulations of alkanes and a DPPC bilayer. *J. Phys. Chem. B* 109:5300–5311.

[242] Darden, T., D. York, and L. Pederson, 1993. Particle mesh Ewald: An N log(N) method for Ewald sums in large systems. *J. Chem. Phys.* 98:10089–10092.

[243] Méleard, P., C. Gerbeaud, T. Pott, L. Fernandez-Puente, I. Bivas, M. D. Mitov, J. Dufourcq, and P. bothorel, 1997. Bending elasticities of model membranes: Influences of temperature and sterol content. *Biophys. J.* 72:2616–2629.

[244] Needham, D., T. J. McIntosh, and E. Evans, 1988. Thermomechanical and transition properties of dimyristoylphosphatidylcholine/cholesterol bilayers. *Biochemistry* 27:4668–4673.

[245] Orsi, M., D. Y. Haubertin, W. E. Sanderson, and J. W. Essex, 2008. A quantitative coarse-grain model for lipid bilayers. *J. Phys. Chem. B* 112:802–815.

[246] Leathes, J. B., 1925. Croonian lectures on the role of fats in vital phenomena. *The Lancet* 205:853–856.

[247] Lemmich, J., K. Mortensen, J. H. Ipsen, T. Honger, R. Bauer, and O. G. Mouritsen, 1997. The effect of cholesterol in small amounts on lipid-bilayer softness in the region of the main phase transition. *Eur. Biophys. J.* 25:293–304.

[248] Léonard, A., C. Escrive, M. Laguerre, E. Pebay-Peyroula, W. Néri, T. Pott, J. Katsaras, and E. Dufourc, 2001. Location of cholesterol in DMPC membranes. A comparative study by neutron diffraction and molecular mechanics simulation. *Langmuir* 17:2019–2030.

[249] Wilson-Ashworth, H. A., Q. Bahm, J. Erickson, A. Shinkle, M. P. Vu, D. Woodbury, and J. Bell, 2006. Differential detection of phospholipid fluidity, order and spacing by fluorescence spectroscopy of bis-pyrene, prodan, nysatin and merocyanine 540. *Biophys. J.* 91:4091–4101.

[250] Shimschick, E. J., and H. M. McConnell, 1973. Lateral phase separations in binary mixtures of cholesterol and phospholipids. *Biochem. and Biophys. Res. Comm.* 53:446–451.

[251] Lentz, B. R., D. A. Barrow, and M. Hoechli, 1980. Cholesterol-phosphatidylcholine interactions in multilamellar vesicles. *Biochemistry* 19:1943–1954.

[252] McMullen, T. P. W., and R. N. McElhaney, 1995. New aspects of the interaction of cholesterol with dipalmitoylphosphatidylcholine bilayers as revealed by high-sensitivity differential scanning calorimetry. *Biochim. Biophys. Acta* 1234:90–98.

[253] Clarke, J. A., A. J. Heron, J. M. Seddon, and R. V. Law, 2006. The diversity of the liquid ordered (L_o) phase of phosphatidylcholine/cholesterol membranes: A variable temperature multinuclear solid-state NMR and X-ray diffraction study. *Biophys. J.* 90:2383–2393.

[254] Ipsen, J. H., G. Karlström, O. G. Mouritsen, H. Wennerström, and M. J. Zuckermann, 1987. Phase equilibria in the phopshatidylcholine-cholesterol system. *Biochim. Biophys. Acta* 905:162–172.

[255] Radhakrishnan, A., and H. M. McConnell, 1999. Cholesterol-phospholipid complexes in membranes. *J. Am. Chem. Soc.* 121:486–487.

[256] Radhakrishnan, A., T. G. Anderson, and H. M. McConnell, 2000. Condensed complexes, rafts, and the chemical activity of cholesterol in membranes. *Proc. Natl. Acad. Sci. USA* 97:12422–12427.

[257] Ege, C., M. K. Ratajczak, J. Majewski, K. Kjaer, and K. Y. C. Lee, 2006. Evidence for lipid/cholesterol ordering in model lipid membranes. *Biophys. J.:Biophys. Lett.* .

[258] Westh, P., and C. Trandum, 2000. Partitioning of small alcohols into dimyristoylphosphatidylcholine (DMPC) membranes: Volumetric properties. *J. Phys. Chem. B* 104:11334–11341.

[259] Ikonen, E., 2008. Cellular cholesterol trafficking and compartmentalization. *Nat. Rev. Mol. Cell. Biol.* 9:125–138.

[260] Singer, S. J., and G. L. Nicolson, 1972. The fluid mosaic model of the structure of cell membranes. *Science* 175:720–731.

[261] Mouritsen, O. G., and M. M. Sperotto, 1993. Thermodynamics of lipid-protein interactions in lipid membranes. *In* M. Jackson, editor, Thermodynamics of Membrane Receptors and Channels. CRC Press, Inc, Boca Raton, Florida, 127–181.

[262] Jensen, M. Ø., and O. G. Mouritsen, 2004. Lipids do influence protein function - the hydrophobic matching hypothesis revised. *Biochim. Biophys. Acta: Biomembranes* 1666:205–226.

[263] Marcelja, S., 1976. Lipid-mediated protein interactions in membranes. *Biochim. Biophys. Acta* 455:1–7.

[264] Mouritsen, O. G., and M. Bloom, 1984. Mattress model of lipid-protein interactions in membranes. *Biophys. J.* 46:141–153.

[265] Dan, N., P. Pincus, and S. A. Safran, 1993. Membrane-induced interactions between inclusions. *Langmuir* 9:2768–2771.

[266] Kralchevsky, P., V. Paunov, N. Denkov, and K. Nagayama, 1995. Stresses in lipid-membranes and interactions between inclusions. *J. Chem. Soc., Faraday Trans.* 91:3415–3432.

[267] Schmidt, U., G. Guigas, and M. Weiss, 2008. Cluster formation of transmembrane proteins due to hydrophobic mismatching. *Phys. Rev. Lett.* 101:1281041–4.

[268] Psachoulia, E., P. W. Fowler, P. J. Bond, and M. S. P. Sansom, 2008. Helix-helix interactions in membrane proteins: Coarse-grained simulations of glycophorin A helix dimerization. *Biochemistry* 47:10504–10512.

[269] West, B., F. L. H. Brown, and F. Schmid, 2009. Membrane-protein interactions in a generic coarse-grained model for lipid bilayers. *Biophys. J.* 96:101–115.

[270] Janosi, L., A. Prakash, and M. Doxastakis, 2010. Lipid-modulated sequence-specific association of glycophorin A in membranes. *Biophys. J.* 99:284–292.

[271] Sabra, M. C., J. C. M. Uitdehaag, and A. Watts, 1998. General model for lipid-mediated two-dimensional array formation of membrane proteins: application to bacteriorhodopsin. *Biophys. J.* 75:1180–1188.

[272] Gil, T., J. H. Ipsen, O. G. Mouritsen, M. C. Sabra, M. M. Sperotto, and M. J. Zuckermann, 1998. Theoretical analysis of protein organization in lipid membranes. *Biochim. Biophys. Acta* 1376:245–266.

[273] Reynwar, B. J., and M. Deserno, 2008. Membrane composition-mediated protein-protein interactions. *Biointerphases* 3:117–124.

[274] Stüven, E., A. Porat, F. Shimron, E. Fass, D. Kaloyanova, B. Brügger, F. T. Wieland, Z. Elazar, and J. B. Helms, 2003. Intra-golgi protein transport depends on a cholesterol balance in the lipid membrane. *J. Biol. Chem.* 278:53112–53122.

[275] Lundbæk, J. A., O. S. Andersen, T. Werge, and C. Nielsen, 2003. Cholesterol-induced protein sorting: an analysis of energetic feasibility. *Biophys. J.* 84:2080–2089.

[276] Churchward, M. A., T. Rogasevskaia, J. Höfgen, J. Bau, and J. R. Coorsen, 2005. Cholesterol facilitates the native mechanism of Ca-triggered membrane fusion. *J. of Cell Sci.* 118:4833–4848.

[277] Epand, R. M., 2006. Cholesterol and the interation of proteins with membrane domains. *Progress in Lipid Research* 45:279–294.

[278] Brannigan, G., J. Hénin, R. Law, R. Eckenhoff, and M. Klein, 2008. Embedded cholesterol in the nicotinic acetylcholine receptor. *Proc. Natl. Acad. Sci. USA* 105:14418–14423.

[279] Warren, G. B., M. D. Houslay, J. C. Metcalfe, and N. J. M. Birdsall, 1975. Cholesterol is excluded from the phospholipid annulus surrounding an active calcium transport protein. *Nature* 255:684–687.

[280] Poveda, J. A., A. M. Fernandez, J. A. Encinar, and J. M. Gonzalez-Ros, 2008. Protein-promoted membrane domains. *Biochim. Biophys. Acta* 1778:1583–1590.

[281] Marsh, D., 2008. Protein modulation of lipids, and vice versa, in membranes. *Biochim. Biophys. Acta* 1778:1545–1575.

[282] Epand, R. M., S. Maekawa, C. M. Yip, and R. F. Epand, 2001. Protein-induced formation of cholesterol-rich domains. *Biochemistry* 40:10514–10521.

[283] Epand, R. M., B. G. Sayer, and R. F. Epand, 2003. Peptide-induced formation of cholesterol-rich domains. *Biochemistry* 42:14677–14689.

[284] Epand, R. M., 2004. Do proteins facilitate the formation of cholesterol-rich domains? *Biochim. Biophys. Acta* 1666:227–238.

[285] de Meyer, F. J.-M., A. Benjamini, J. Rodgers, Y. Misteli, and B. Smit, 2010. Molecular simulation of the DMPC-cholesterol phase diagram. *J. Phys. Chem. B* 114:10451–10461.

[286] Léonard, A., and E. Dufourc, 1991. Interactions of cholesterol with the membrane lipid matrix. *Biochimie* 73:1295–1302.

[287] Jackson, C., 2009. Mechanisms of transport through the Golgi complex. *J. of Cell Science* 122:443–445.

[288] van Duyl, B. Y., H. Meelldijk, A. J. Verkleij, D. T. S. Rijkers, V. Chupin, B. de Kruijff, and J. A. Killian, 2005. A synergistic effect between cholesterol and tryptophan-flanked transmembrane helices modulates membrane curvature. *Biochemistry* 44:4526–4532.

[289] Rajan, R. S., M. E. Illing, N. F. Bence, and R. R. Kopito, 2001. Specificity in intracellular protein aggregation and inclusion body formation. *Proc. Natl. Acad. Sci. USA* 98:13060–13065.